Fluid inclusions in garnet: migmatitic paragneiss, Algonquin domain, Grenville Province, Ontario

Adam Jeremy Layman

Submitted in Partial Fulfilment of the Requirements
For the Degree of Bachelor of Science, Honours
Department of Earth Sciences
Dalhousie University, Halifax, Nova Scotia
March 2003

Dalhousie University

Department of Earth Sciences
Halifax, Nova Scotia
Canada B3H 3J5
(902) 494-2358
FAX (902) 494-6889

DATE 28 MAY, 2003

AUTHOR ADAM JEREMY LAYMAN

TITLE FLUID INCLUSIONS IN GARNET:
MIGMATITIC PARAGNEISS, ALGONQUIN
DOMAIN, GRENVILLE PROVINCE, ONTARIO

Degree B. Sc Convocation MAY Year 2004

Permission is herewith granted to Dalhousie University to circulate and to have copied for non-commercial purposes, at its discretion, the above title upon the request of individuals or institutions.

THE AUTHOR RESERVES OTHER PUBLICATION RIGHTS, AND NEITHER THE THESIS NOR EXTENSIVE EXTRACTS FROM IT MAY BE PRINTED OR OTHERWISE REPRODUCED WITHOUT THE AUTHOR'S WRITTEN PERMISSION.

THE AUTHOR ATTESTS THAT PERMISSION HAS BEEN OBTAINED FOR THE USE OF ANY COPYRIGHTED MATERIAL APPEARING IN THIS THESIS (OTHER THAN BRIEF EXCERPTS REQUIRING ONLY PROPER ACKNOWLEDGEMENT IN SCHOLARLY WRITING) AND THAT ALL SUCH USE IS CLEARLY ACKNOWLEDGED.

Fluid inclusions in garnet: migmatitic paragneiss, Algonquin domain, Grenville Province, Ontario

Adam Jeremy Layman, Department of Earth Sciences, Dalhousie University, Halifax, Nova Scotia, B3H 3J5 (alayman@dal.ca)

Fluid inclusions in garnet have recently been discovered in migmatitic paragneisses in the polycyclic Algonquin domain (McClintock subdomain), Central Gneiss Belt, Grenville Province, Ontario. The host rocks are metapelitic migmatitic garnet-bearing gneisses; the fluid inclusions occur in garnet. Two kinds of fluid inclusions are recognized: GSI-a, monophase negative crystal-shaped inclusions of pure or near pure CO_2; and GSI-b, two-phase (liquid-vapour), aqueous-carbonic inclusions. Inclusions may represent end members of an evolving fluid. GSI-a inclusions have densities ranging ca. 0.9 – 1.05 g/cm^3. Isochores plotted from GSI-a inclusions give P-T estimates of approximately 6 kbars at 700 °C. An independent P-T estimate from local metapelites gives 726 °C and 7.6 kbars. Monazite age constraints on garnet growth limit the age of the inclusions to sometime after ca. 1474 Ma. The fluid inclusions represent the evolution of fluid in the Algonquin domain trapped at various stages during high-T decompression, *ca.* 1080 Ma. Other evidence of low a_{H_2O} Grenvillian fluids in the region can be found in the migmatites and granulites of the Muskoka domain.

Table of contents **Page**

Table of contents Page

Table of Figures

Table of Figures

Table of Tables

List of Appendices

References

1.0 Introduction

1.1 Fluids in metamorphic rocks

Fluids can play an important role in metamorphism. In low-grade metamorphic rocks, fluids and fluid pressure can be important in grain composition, dissolution and reprecipitation, and rock deformation. In higher-grade rocks, fluid pressure may play an important part in the stability of hydrous or carbonate mineral phases and fluids are common phases of metamorphic reactions (*e.g.*, melting, hydration, dehydration reactions; Winter, 2001). Fluids can also affect melting temperatures (*e.g.*, migmatite genesis).

The fluids present in high grade metamorphic environments are rarely preserved because fluid escapes or evolves during exhumation and uplift. The presence and composition of a fluid phase is generally inferred from the stability of volatile-bearing phases or calculated as part of a reaction. Fluids can, however, be preserved as fluid inclusions (Winter, 2001). Fluid inclusions are fluid trapped by the growth or healing of a mineral phase, and represent the only direct evidence of the presence of a fluid at some point in the mineral's history.

Fluids trapped in inclusions can be either primary or secondary. Secondary fluids were trapped by the annealing of cracks, and contain post-metamorphic fluids. Primary fluids were in equilibrium with the rock at some time during metamorphism, and are trapped as metamorphic minerals (*e.g.*, garnet) grow. Metamorphic fluid composition is generally water-dominated, but

CO_2 may also be a major component, as may CH_4, S, N_2, and dissolved salts (*e.g.*, NaCl; Roedder, 1984; Goldstein and Reynolds, 1994).

The nature or existence of fluids in high-grade metamorphic rocks at peak metamorphism is poorly understood (Roeder, 1984; Winter, 2001). Volatile-bearing phases are commonly reduced in quantity, if present; the volatiles that are present are those that are most difficult to release. Many studies suggest that fluid may be CO_2-rich, and have a low water activity (a_{H_2O}) (Roeder, 1984; Pan *et al*, 1999; Touret, 2001; Van de Berg and Huizenga, 2001).

1.2 Fluids in the Grenville Orogen

The Grenville Province is a belt of high-grade rocks extending from Ontario to Labrador (Fig. 1.1). The Grenville orogen resulted from convergence and crustal thickening at the Laurentian continental margin *ca.* 1080-980 Ma (Davidson, 1984; Jamieson et al, 1992; Culshaw et al, 1994). Analogies between the Grenville orogen and modern orogens (*e.g.*, the Himalayas) make the area and its geologic history a subject of academic interest (Windley, 1986).

Not much is known about fluids in the high-grade metamorphic rocks of the Grenville orogen. Most mention of metamorphic fluids in the Grenville Province refers to retrograde metamorphism in the presence of an aqueous fluid, e.g., granulite facies rocks were retrogressed to amphibolite facies (Culshaw *et al*, 1983). However, it has been suggested that fluids in granulites and migmatites in the Muskoka domain had low a_{H_2O} (Timmermann et al, 2002; Slagstad, 2003). Migmatites in the Muskoka domain are thought to have formed in the presence of a fluid, due to low melting temperatures (Slagstad, 2003).

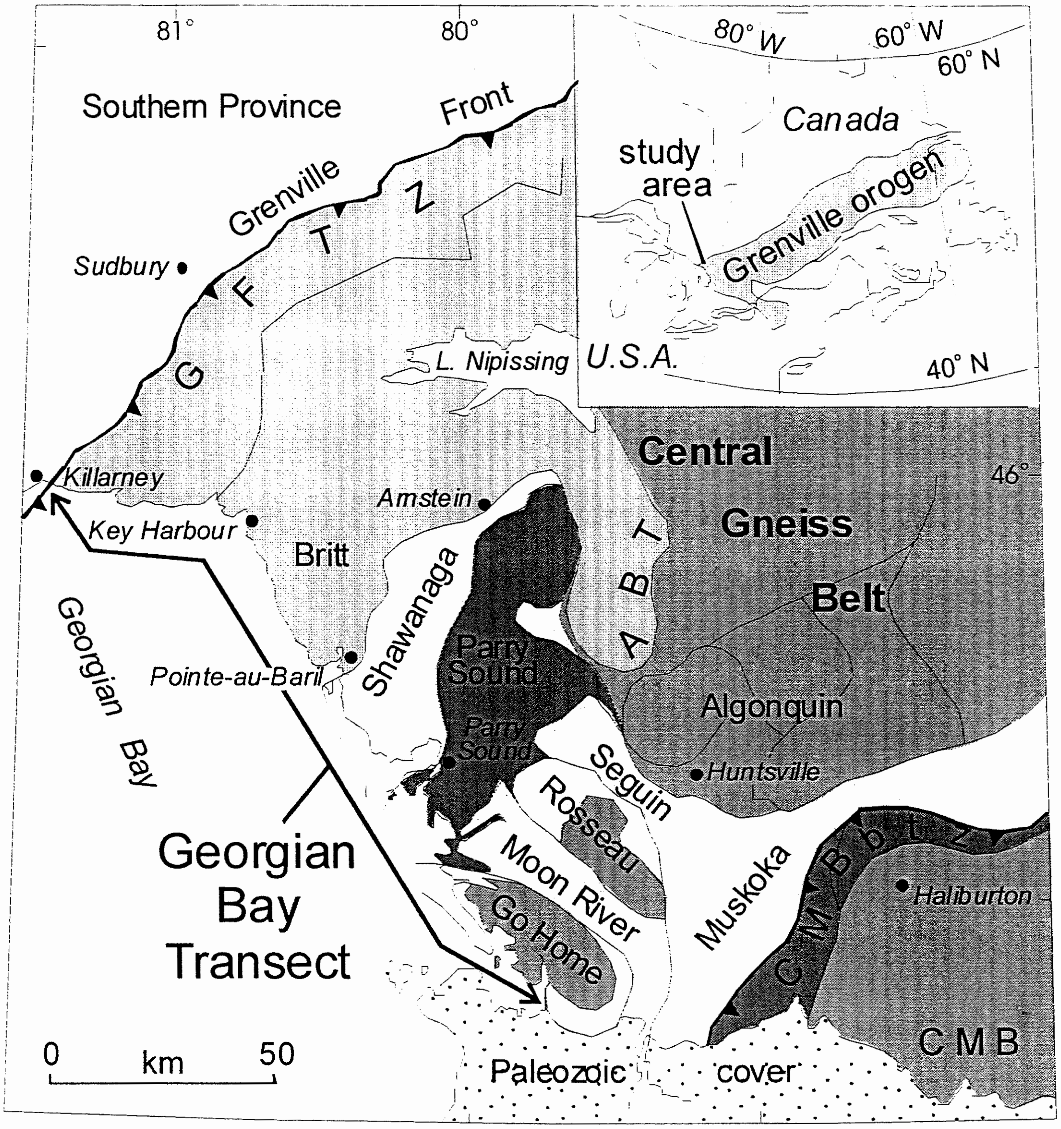

Figure 1.1. Map of the southwestern Grenville Province of eastern Canada, showing domains within the Central Gneiss Belt and important tectonic boundaries. CMB = Central Metasedimentary Belt; CMBbtz = Central Metasedimentary Belt boundary thrust zone; GFTZ = Grenville Front Tectonic Zone; ATB = Allochthon Boundary Thrust. From Timmermann *et al*, 2002.

Granulites are found associated with pegmatites and veins (Timmermann et al, 2002).

1.3 Statement of purpose

Fluids in high grade metamorphic rocks are, in general, poorly understood, though of great importance. What, if any, fluids occur in high P-T regimes? What are the compositions of these fluids, and do these fluids affect metamorphic reactions and processes? This project attempts to address these questions with respect to the Algonquin domain (McClintock subdomain), in the Central Gneiss Belt, in the Grenville Province of Ontario (Fig. 1.1).

Chance discovery of fluid inclusions in garnets in migmatitic gneisses, collected by Rebecca Jamieson from the Algonquin Domain in 2001, initiated strong academic interest. The purpose of this study is to document and describe the fluid inclusions in garnets and to constrain the age and conditions of entrapment as well as possible.

1.4 Methodology - Overview

Migmatitic metapelitic gneiss samples were analyzed petrographically in hand sample and polished thin section. Microprobe x-ray maps were created for chosen garnets, to analyze compositional zoning. Garnets and inclusions in the garnets were analyzed by microprobe to determine composition, for identification purposes, and to accompany compositional mapping.

Metapelites were analyzed by microprobe for thermobarometry, using garnet, biotite, plagioclase, aluminosilicate (sillimanite), and quartz compositions to calculate pressure and temperature. Thermobarometry was compared to fluid inclusion data to determine possible entrapment conditions and to verify, independently, the P-T estimates given by fluid inclusions.

Monazite inclusions in garnets in the samples were used to determine approximate time of garnet growth, and possibly fluid entrapment. Monazites are dated chemically by microprobe analysis using compositional maps and U-Th-Pb ratios.

Fluid inclusions in garnets were analyzed microthermometrically, to determine temperatures of melting (T_m) and homogenization (T_h). Melting and homogenization temperatures can be used to determine fluid composition, phase density, and pressure and temperature of fluid entrapment (Roedder, 1984).

Methods and results are discussed in the following chapters: thermobarometry, chapter 3; fluid inclusion microthermometry, chapter 4; monazite dating, chapter 5. Chapter 2 details the background geology, and field relationships of the samples. Chapter 6 presents the discussion of results and chapter 7 presents the conclusions.

2.0 Geological Setting

2.1 Grenville Province and Central Gneiss Belt

The Grenville Province is a belt of high-grade rocks extending from Ontario to Labrador, formed by northwest directed thrusting along the paleocontinental margin of Laurentia, in the Grenville Orogeny, *ca*. 1190-980 Ma (Culshaw *et al*, 1997). The main Grenvillian event in the study area occurred at *ca*. 1080-980 Ma (Jamieson *et al*, 1992; Culshaw *et al*, 1994). Interest in the Grenville orogen lies in analogies with modern orogens, *e.g.*, the Himalayas, since uplift and erosion have exposed much of the deep crust that is hidden beneath the mountains of similar modern ranges (Windley, 1986).

The southwestern portion of the Grenville Province (Ontario; Fig. 2.1) comprises three tectonic units: the Grenville Front Tectonic Zone (GFTZ), the Central Gneiss Belt (CGB), and the Central Metasedimentary Belt (CMB) (Wynne-Edwards, 1972). The GFTZ is the northwestern boundary of the Grenville Province, a 10-40 km wide shear zone cutting underlying Archean to Paleoproterozoic provinces (Easton, 1992) and comprises various migmatitic orthogneisses and paragneisses, megacrystic granitoids, and pre-Grenvillian (*ca.* 1450 Ma) granulites (Culshaw *et al*, 1997). The pre-Grenvillian Laurentian craton and continental margin have become the CGB, which overlies the GFTZ (Rivers *et al*, 1989). The CMB boundary thrust zone separates the CMB from the CGB (van Breemen and Hanmer, 1986); the CMB comprises remnants of one or more magmatic arcs, which collided with the CGB during the Grenville Orogeny, *ca.* 1100 Ma (Carr *et al*, 2000).

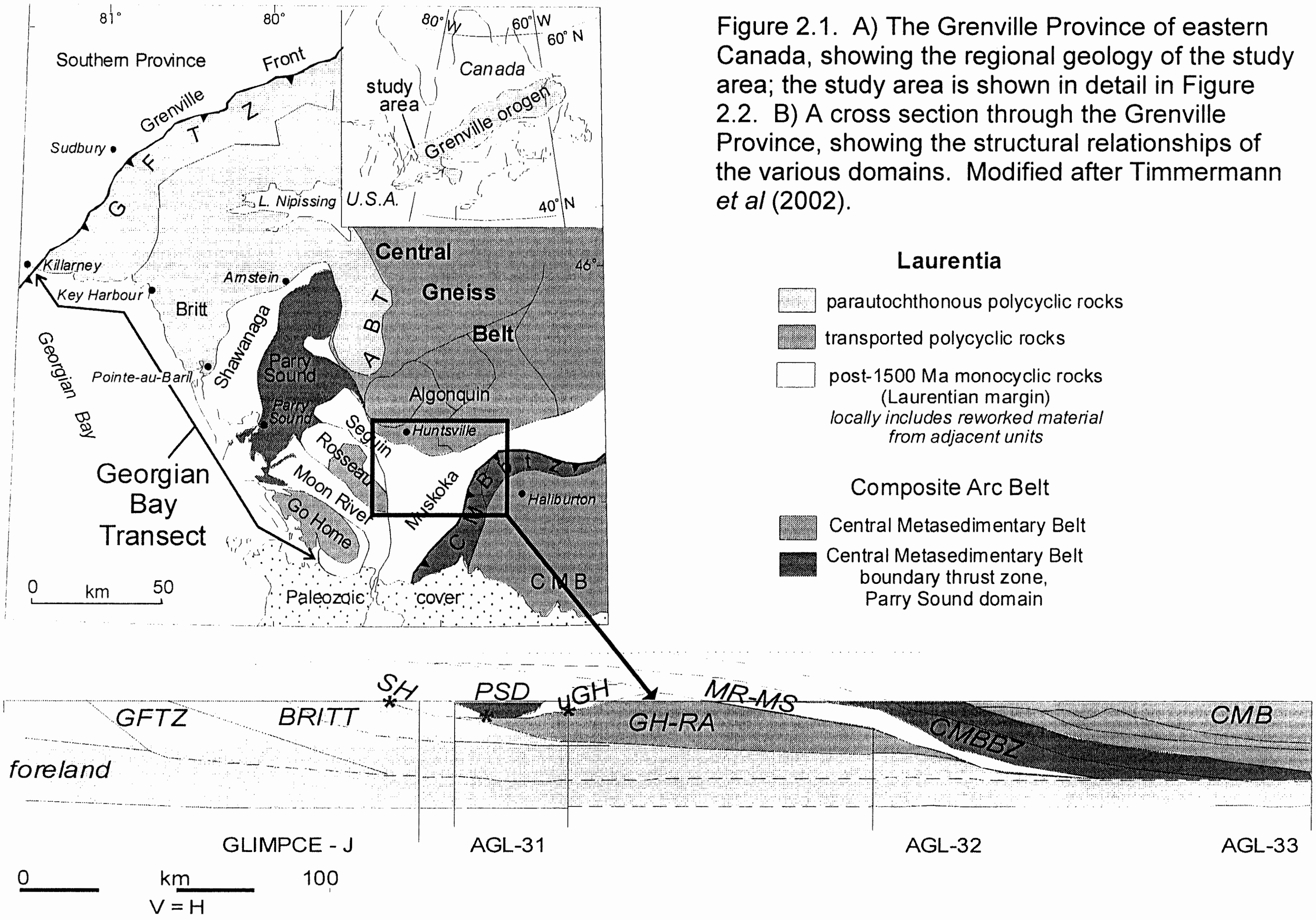

Figure 2.1. A) The Grenville Province of eastern Canada, showing the regional geology of the study area; the study area is shown in detail in Figure 2.2. B) A cross section through the Grenville Province, showing the structural relationships of the various domains. Modified after Timmermann *et al* (2002).

The Central Gneiss Belt represents pre-Grenville Laurentian continental crust and margin (Carr *et al*, 2000). The CGB contains pre-1350 Ma ortho-and-paragneisses and migmatites, which have been subjected to multiple episodes of deformation and metamorphism (*i.e.*, polycyclic; Rivers *et al*, 1989). Rocks are generally upper amphibolite-to-granulite facies (Carr *et al*, 2000). The CGB is divided into several domains, which in the study area include the Algonquin domain and the Muskoka domain (Culshaw *et al*, 1990) (Fig. 2.2).

2.2 Algonquin Domain and McClintock Subdomain

The Algonquin domain comprises the southeastern portion and structurally lowest part of the CGB, and is overlain by the Kawagama zone (Culshaw *et al*, 1983). It consists of pre-1350 Ma ortho-and-paragneisses (Rivers *et al*, 1989), commonly amphibolite to granulite facies (Carr *et al*, 2000). The Algonquin domain is divided into several subdomains, including the Kiosk, Novar, McCraney, Huntsville, and McClintock subdomains, each distinguished by particular gneiss associations (Culshaw *et al*, 1983; Davidson, 1984; Timmermann, 1998).

The McClintock subdomain (Fig. 2.2) comprises metasedimentary gneisses, orthogneisses, and granulites, with some calc-silicate gneiss and marble (Culshaw *et al*, 1983). The McClintock subdomain includes several gneiss assemblages: the Southern Huntsville assemblage, the Birkendale assemblage, and the McClintock assemblage (Timmermann, 1998). Assemblages comprise of pink-to-grey quartzofeldspathic migmatitic orthogneisses, megacrystic granitoids, garnet granulites, and aluminous

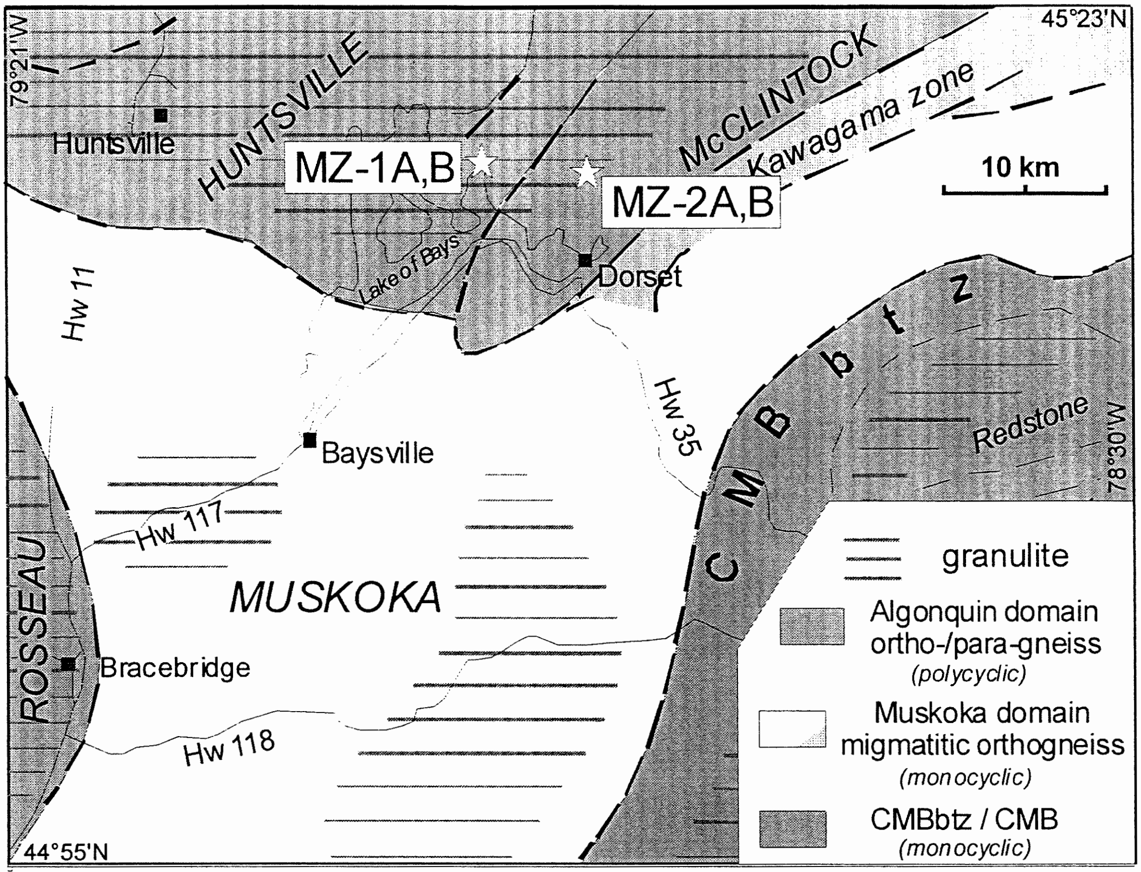

Figure 2.2. Sample locations for samples MZ-1A, MZ-1B and MZ-2A, MZ-2B, showing the Huntsville and McClintock subdomains of the Algonquin Domain, and the Muskoka domain. Modified from Timmermann *et al* (2002).

metapelites (quartz+plagioclase+K-feldspar+garnet+biotite+sillimanite+ graphite). Megacrystic leucocratic granites (K-feldspar+plagioclase+quartz+ biotite+chlorite±garnet) locally intruded the rocks (Timmermann, 1998).

2.3 Field relations of the samples

Samples for this study were collected in 2000 by R.A. Jamieson. Samples were originally collected for the study of monazite in polycyclic paragneiss in the Algonquin domain; fluid inclusion-bearing garnets had not then been recognized. Outcrops showing late stage retrogression or cross-cutting veins were avoided as much as possible.

Samples MZ-1A and MZ-1B were collected near Highway 35 at Birkendale along the shore of the Lake of Bays. A well-known roadcut along Highway 35 (e.g., Davidson and Easton, 1998) exposes shallowly dipping migmatitic pink gneisses, likely metamorphosed felsic igneous rocks. Highly deformed mafic layers are thought to be deformed mafic dikes; one magnificently deformed example is known as the "Birkendale Dragon". Calc-silicate boudins and metapelitic gneisses exposed near the bottom of the roadcut may represent the top of metasedimentary unit from which the samples were taken (Fig. 2.3c; Jamieson, written communication).

The sampled outcrop is a well-layered grey gneiss. Medium-grained biotite-rich and feldspar-rich layers of highly variable thickness define compositional layering. Compositional layering and local subparallel finer-grained shear zones define a strong foliation. Relict coarse-grained feldspars and garnet porphyroclasts as much as 3 cm long suggest that leucocratic layers

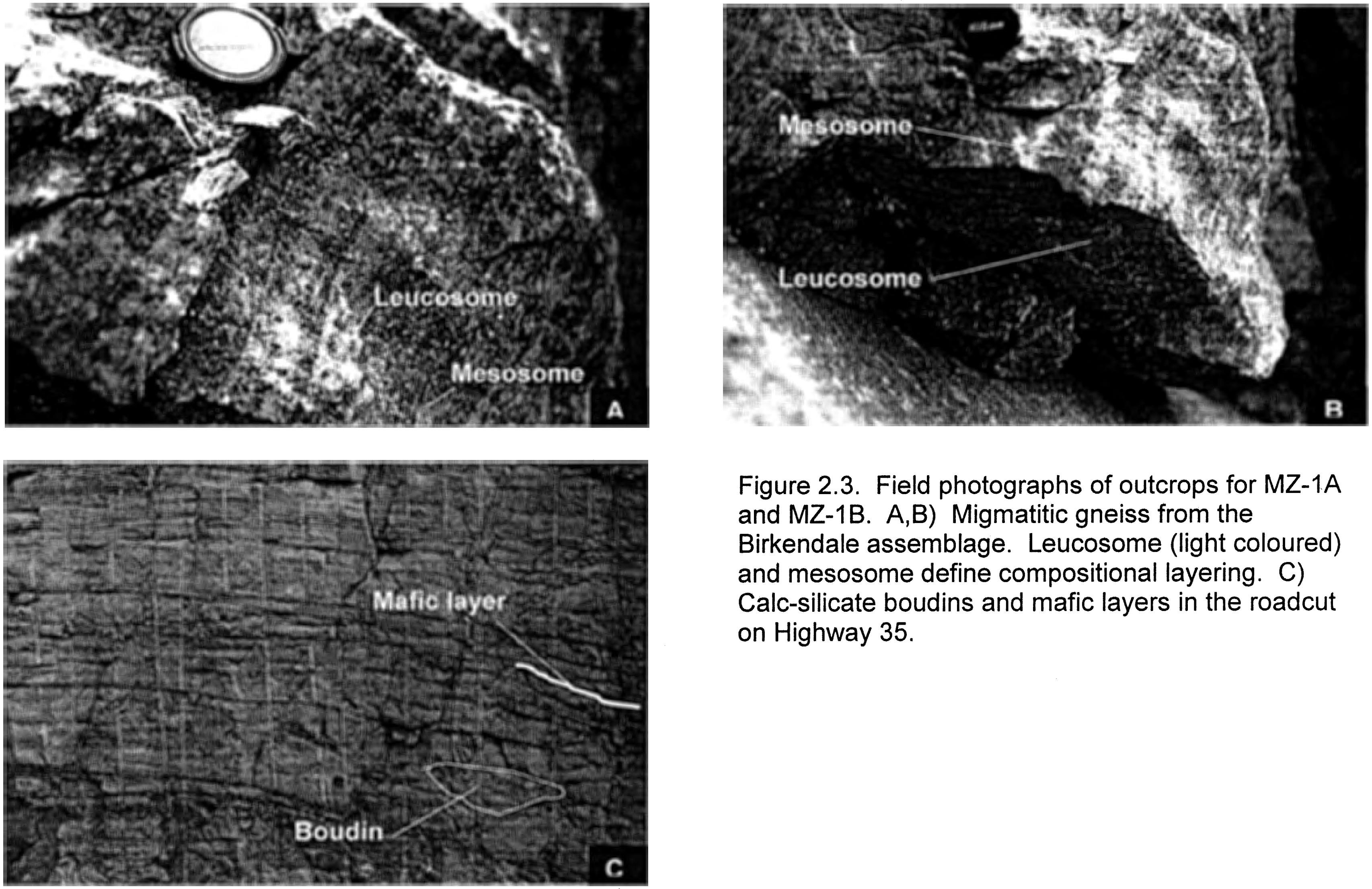

Figure 2.3. Field photographs of outcrops for MZ-1A and MZ-1B. A,B) Migmatitic gneiss from the Birkendale assemblage. Leucosome (light coloured) and mesosome define compositional layering. C) Calc-silicate boudins and mafic layers in the roadcut on Highway 35.

were once coarser-grained. Felsic layers are interpreted to be deformed leucosomes because of inferred originally-coarse grain size, irregular distribution, and petrographic features suggesting that feldspar and garnet crystallized in the presence of a melt. MZ-1A contains a somewhat higher proportion of deformed leucosome, and MZ-1B contains large garnet porphyroclasts (Jamieson, written communication).

Samples MZ-2A and MZ-2B were collected from a roadcut in Highway 35, located 4 km north of the Nordic Inn on the outskirts of Dorset. The outcrop comprises moderately-to-steeply dipping pelitic gneiss on the northeast side and megacrystic orthogneiss on the southwest. The relationship across the contact is uncertain; the contact is concordant with gneissic foliation, and there is no evidence of cross-cutting. The boundary may be tectonic or a highly deformed igneous contact (Jamieson, written communication).

The pelitic gneisses contain medium-to-coarse-grained leucocratic layers, 5-20 cm thick, with coarse-grained lilac-coloured garnets. Sample MZ-2A is from a leucocratic layer. A finer-grained, well-foliated, garnet-sillimanite gneiss is interlayered with the leucocratic layers; sample MZ-2B is from a garnet-sillimanite layer. Garnet-sillimanite gneiss may represent deformed melanosome, although it does not form discrete selvages on leucosome. Rusty discolouring of the garnet-sillimanite gneiss may result from late-stage alteration concentrated in the mica-rich layers (Jamieson, written communication).

The megacrystic orthogneiss is likely part of a 1480-1430 Ma suite of metaplutonic rocks that are widespread throughout the CGB (*e.g.*, Slagstad *et al*, in press; Jamieson, written communication); Timmermann (1998) dated similar rocks nearby at 1489 +24/-13 Ma.

3.0 Petrography

3.1 Sample description

Samples MZ-1A, MZ-1B, and MZ-2A are migmatitic gneisses from the Birkendale gneiss association, McClintock subdomain, Algonquin domain. Sample MZ-2B is from a metapelitic gneiss interlayered with MZ-2A (pers.comm., Jamieson). Field relationships are summarized in chapter 2. Rocks of the Birkendale association are generally upper-amphibolite facies (Timmermann, 1998). Outcrops with late-stage retrogression or cross-cutting veins were avoided as much as possible. None of the samples examined show any signs of cross-cutting veins. Sample MZ-2B may have been retrogressed, but it appears retrogression was concentrated in the metapelitic layers.

3.1.1 MZ-1 samples, Lake of Bays (Fig 2.2)

Sample MZ-1A is a light grey stromatic migmatitic gneiss, weathered orange on some minor faces. Dark grey/black (mesosome) and light grey/white bands (leucosome) define compositional banding. Pink-red garnets and white feldspars are readily visible with the naked eye. The mineral assemblage includes garnet, biotite, quartz, K-feldspar, plagioclase, rutile, and pyrite, with accessory minerals. Samples do not contain veins or retrograde metamorphism (Fig. 3.1).

Porphyroblastic pink-red garnet is present throughout the rock, in both leucosome and mesosome. Garnet is xenoblastic to subidioblastic, with irregular grain boundaries, and varies in size from 0.1-20 mm with an average size

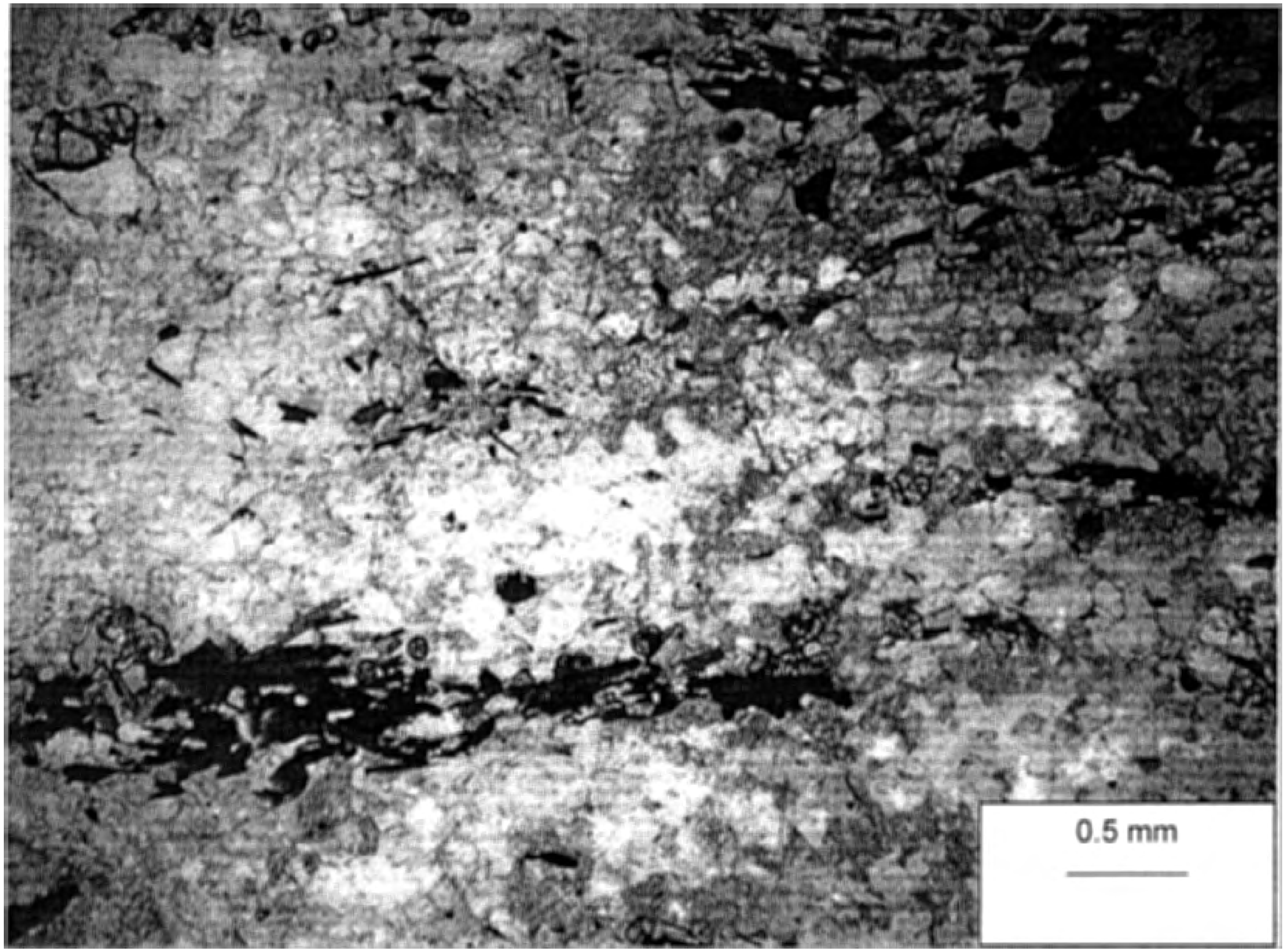

Figure 3.1. Sample MZ-1A. The dark laths are biotite. The small high relief grain in the upper left corner is garnet. The matrix is quartz and feldspars. See text for discussion.

~1 mm. Garnet is typically approximately equant, with some elongated grains, and moderately fractured; fractures are randomly oriented. Garnet is poikiloblastic, and includes K-feldspar, plagioclase, quartz, biotite, rutile, pyrite, monazite, zircon, and fluid inclusions. Rutile inclusions in garnet include micron-scale (breadth) acicular needles aligned along crystallographic planes or larger, subidioblastic, grains.

Red-brown biotite appears black-brown in hand specimen. Abundant biotite defines the mesosome, though minor biotite can be found in the leucosome. Biotite is idioblastic (elongated lath or blade shaped) to xenoblastic (equant) with some sutured grain boundaries. Biotite ranges in size from 0.05-4 mm, with an average grain size ~0.5 mm. Larger biotite grains are more likely to have sutured grain boundaries and xenoblastic appearance. Biotite commonly has radiation halos indicating the inclusion of radioactive minerals, such as zircon or monazite, and also has minor silicate inclusions.

White K-feldspar and plagioclase are indistinguishable in hand sample. In thin section, plagioclase commonly displays distinctive polysynthetic twinning, locally gently bent. Some K-feldspar exhibits perthitic textures. K-feldspar may also be poikilitic, and may have opaque and fluid inclusions. Feldspars are xenoblastic, relatively equant, and range in size from 0.05-2.5 mm, with an average size ~0.7 mm. Larger porphyroblastic grains are common in the leucosome.

Quartz, with feldspars, dominates the mineralogy, both in the mesosome and leucosome. Quartz is xenoblastic and varies in size from 0.05-2 mm, with an average grain size ~0.7 mm. Larger, elongate, porphyroblasts are common in the leucosome. Quartz has poorly defined subgrains in some areas, as indicated by undulose extinction.

Rutile is present in the matrix as subidioblastic grains averaging ~0.3 mm in size and as acicular inclusions in garnet. Pyrite is present in the matrix as xenoblastic, sutured, grains averaging ~0.5 mm in size, and as inclusions in garnet. Accessory minerals present include monazite and zircon.

Leucosome is generally concordant; in the leucosome, felsic minerals are larger and more elongate than in the mesosome. Quartz, K-feldspar, and plagioclase average 1-2 mm, with maximum sizes ~20 mm, in the leucosome. Biotite is minor, if it appears at all. In the mesosome, felsic minerals are more equant and smaller; biotite is larger and common. Garnet does not vary in size or habit from leucosome to mesosome. Commonly, the axes of elongate minerals, including elongated garnets and felsic minerals, are aligned subparallel with the gneissic fabric of the leucosome and mesosome.

Sample MZ-1B is light grey stromatic migmatitic gneiss, weathered orange on some minor faces, similar to sample MZ-1A. Some portions of the rock appear to be more felsic, and have less well defined boundaries between leucosome and mesosome (Fig. 3.2). K-feldspars may have symplectic intergrowths, and perthitic textures are more common.

The more felsic portions of MZ-1B lack well defined mesosome; mesosome is defined by biotite-rich lenses. Biotite-rich lenses are subparallel to the compositional fabric of the more well-defined portions of the sample.

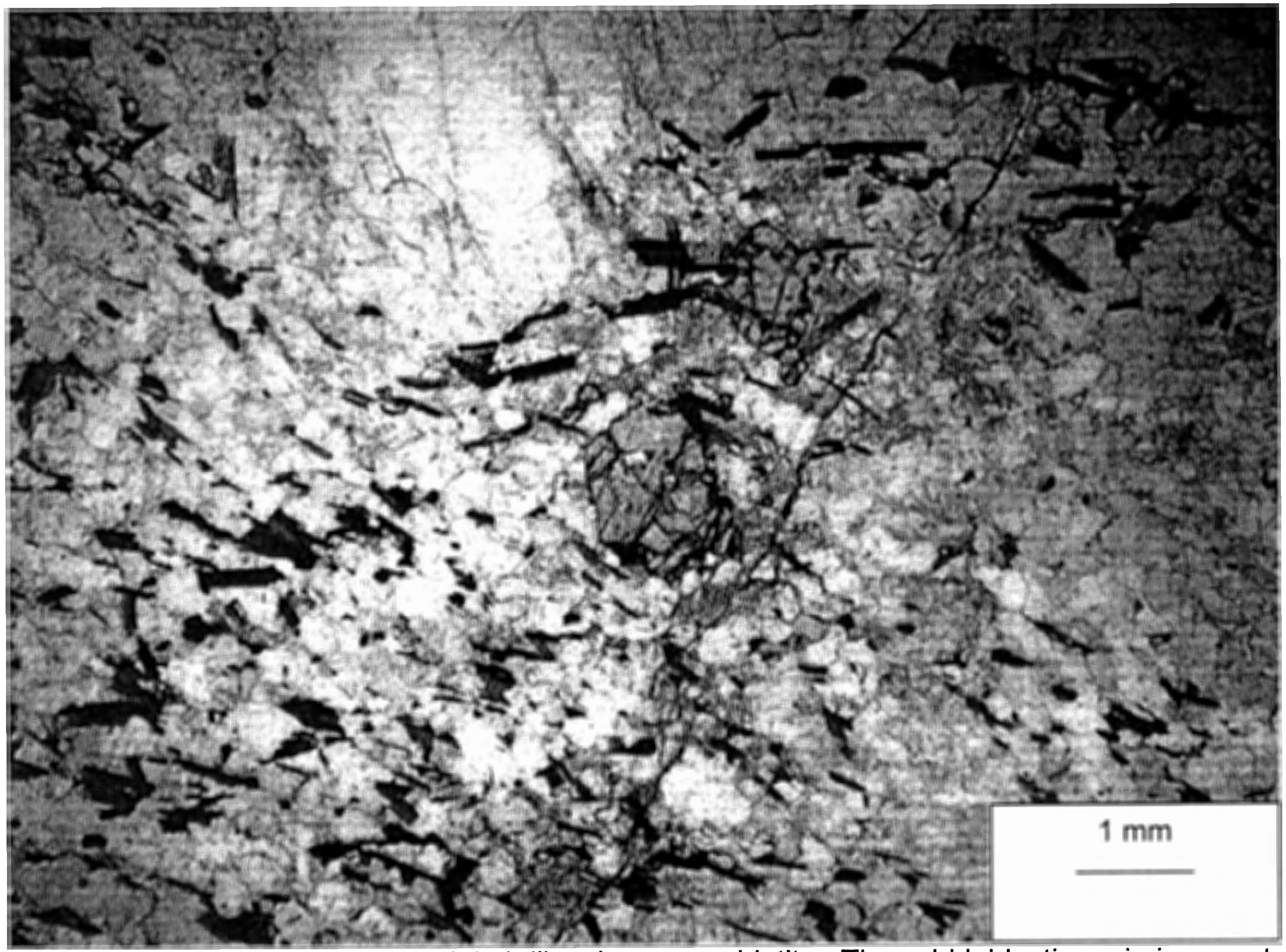

Figure 3.2. Sample MZ-1B. Dark lath like shapes are biotite. The subidoblastic grain is garnet. Above and to the left of the garnet is K-feldspar. The matrix is quartz and feldspars. See discussion in text.

3.1.2 MZ-2 samples, Highway 35 roadcut (Fig. 2.2)

Sample MZ-2A is a grey patchy migmatitic gneiss, weathered orange-brown on exposed faces. Sample MZ-2A is similar to sample MZ-1B, containing more felsic material than MZ-1A and poorly defined mesosomes. Typically, MZ-2A feldspars and quartz are larger than feldspars and quartz in either MZ-1A or MZ-1B, ~0.9 mm on average (Fig. 3.3).

Sample MZ-2B is a metapelitic garnet-sillimanite gneiss, weathered dark brown-orange on weathered faces, and interlayered with sample MZ-2A on a decimetre scale. The fresh face appears dark brown with pale off-white bands. The compositional layering is defined by rare, narrow, concordant, felsic bands. White feldspar is readily apparent, but only in felsic bands. The mineral assemblage present includes biotite, sillimanite, garnet, K-feldspar, plagioclase, pyrite, ilmenite, rutile, and accessory minerals (Fig. 3.4).

Garnet is not visible in hand specimen. In thin section, garnet is xenoblastic to subidioblastic, with irregular grain boundaries. Garnet ranges in size from <0.1 -0.7 mm, with an average size of ~0.4 mm. Garnet is equant to elongate, and moderately fractured. Garnet is poikiloblastic, and contains K-feldspar, plagioclase, quartz, rutile, pyrite, ilmenite, monazite and zircon. Rutile inclusions in garnet range micron-scale (breadth) acicular needles aligned along crystallographic planes or larger, subidioblastic, grains.

Biotite is black brown in hand sample, and red-brown to brown-yellow in thin section. Biotite is idioblastic (elongated lath or blade shaped) to xenoblastic with irregular grain boundaries. Biotite ranges in size from 0.05-1 mm, with an

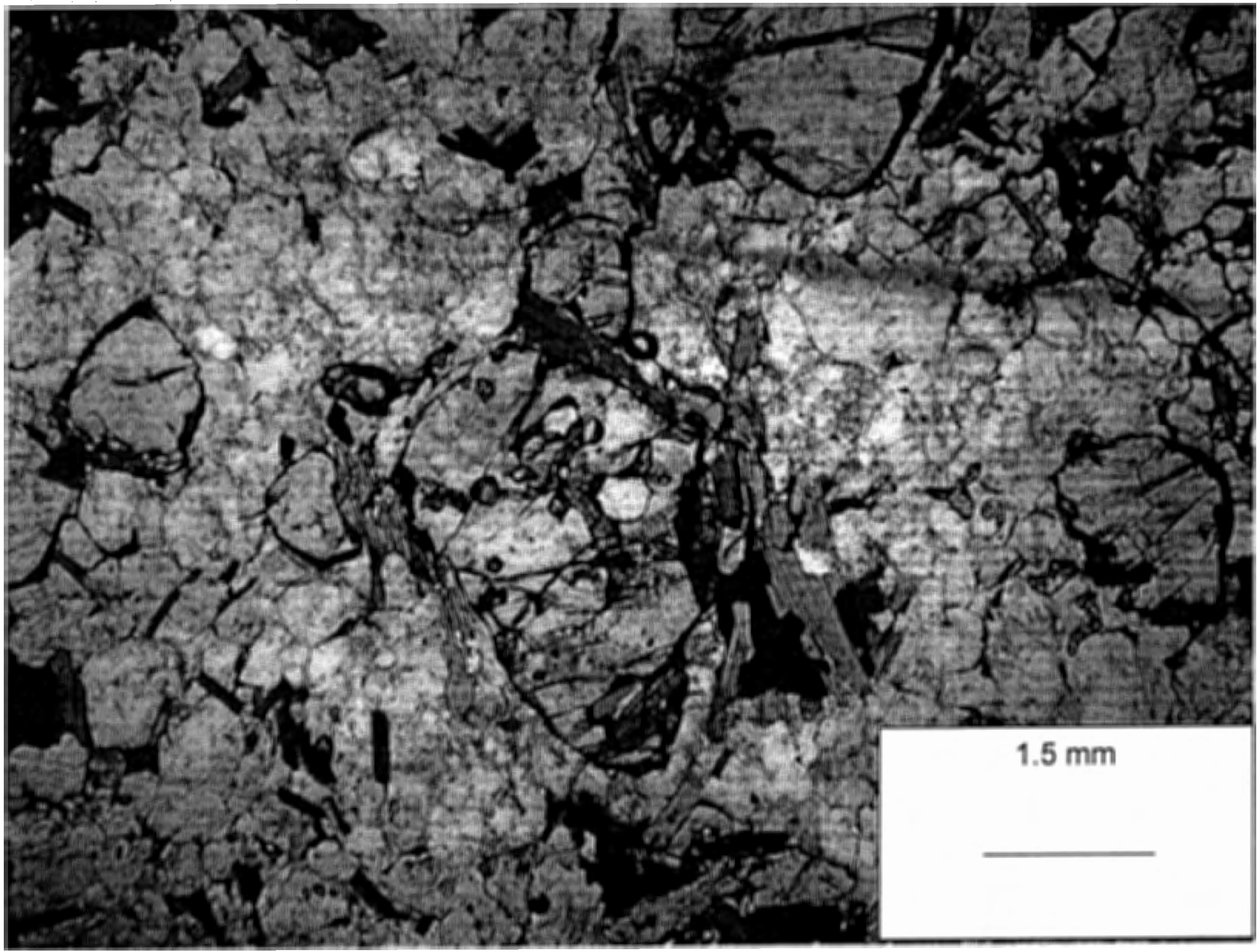

Figure 3.3. Sample MZ-2A. The large inclusion-rich grain is garnet. Dark to light coloured laths are biotite. The matriz is quartz and feldspars.

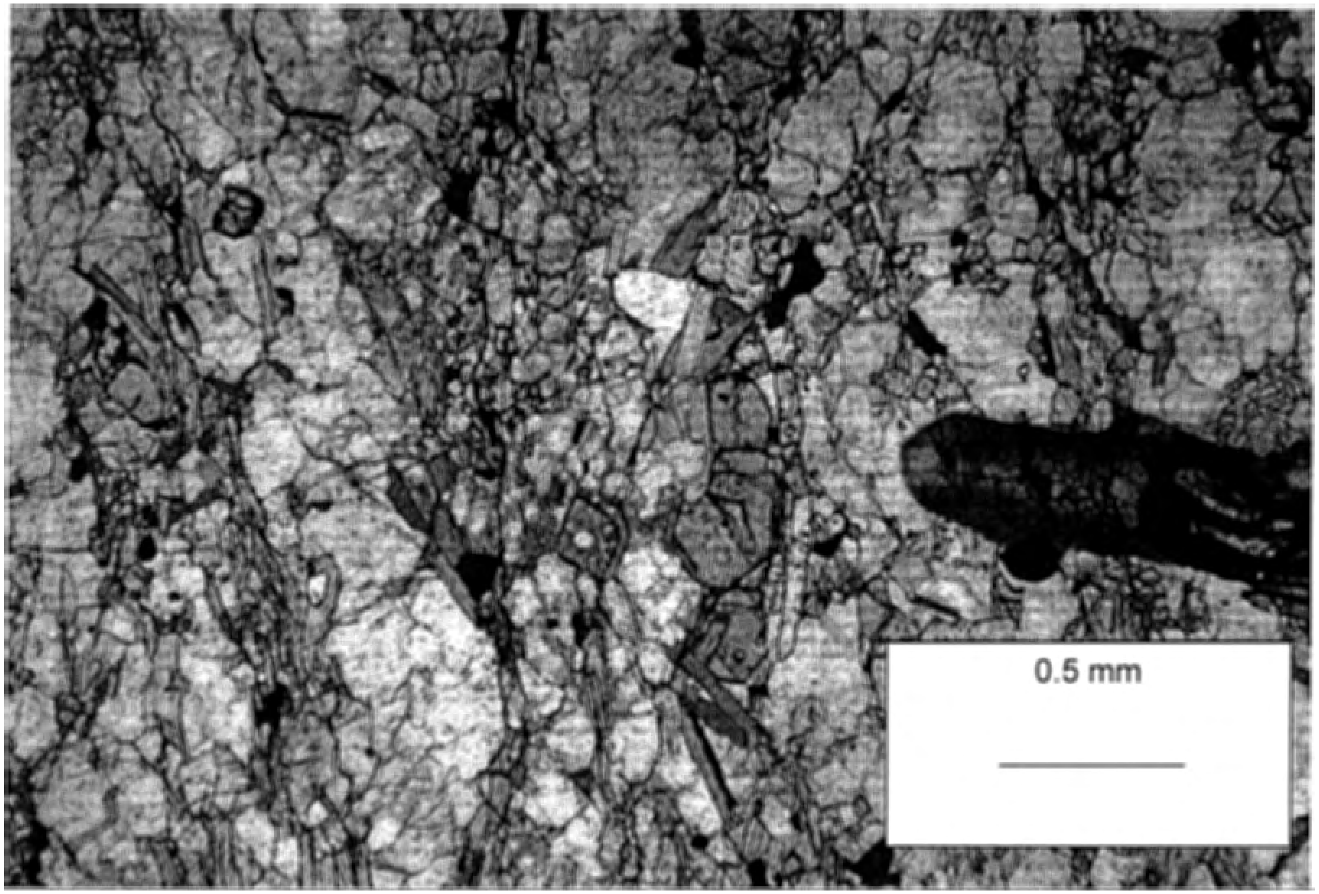

Figure 3.4. Sample MZ-2B. Biotite and sillimanite define the foliation. Elongate garnet is the high relief grain in the centre of the frame. The matrix is quartz and feldspar. The semi-transparent black mark on the right is an ink mark used to relocate the grain for microprobe work.

average grain size ~0.4 mm. Larger grains are more xenoblastic and have more irregular grain boundaries. Biotite commonly has radiation halos indicating the inclusion of radioactive minerals, such as zircon or monazite, and also has minor silicate and rutile inclusions.

Sillimanite is idioblastic to subidioblastic; near-square cross-sections through sillimanite show distinct oblong-shaped cores of aluminosilicate. Length-oriented grains are bladed. Sillimanite ranges in size from <0.1-1.5 mm, with an average grain size of ~0.4 mm. Sillimanite is moderately fractured, typically across the long axis.

Off-white K-feldspar and plagioclase are indistinguishable in hand sample. In thin section, plagioclase commonly displays distinctive polysynthetic twinning, locally gently bent. Perthitic K-feldspar grains are common. K-feldspar can also be poikilitic, and has opaque and fluid inclusions. Feldspars are xenoblastic, relatively equant, and range in size from <0.1-9 mm, with an average size ~0.9 mm. Larger porphyroblastic grains in felsic bands are typically oblate.

Quartz, with feldspars, dominates the felsic bands, and plays a major role in the matrix. Quartz is xenoblastic and varies in size from 0.1-4 mm, with an average grain size ~0.8 mm. Larger porphyroblasts in felsic bands are generally oblate.

Rutile is present in the matrix as subidioblastic grains averaging ~0.3 mm in size and as acicular inclusions in garnet. Pyrite is present in the matrix as xenoblastic, sutured, grains averaging ~0.5 mm in size, to as large as 3 mm and as inclusions in garnet. Ilmenite is present in the matrix and as inclusions in garnet; ilmenite grains in the matrix are typically ~0.3 mm. Accessory minerals present include monazite and zircon.

Biotite and sillimanite define a schistosity, seen in thin section as parallel elongated minerals, including quartz and feldspar. Gneissosity, defined by felsic and mafic bands, is parallel to the schistosity, and elongate minerals in the felsic bands are typically aligned parallel to the fabric as well.

3.2 Microprobe analysis

Selected garnets from samples MZ-1A, MZ-1B, and MZ-2A were compositionally mapped by electron microprobe, to analyse zoning patterns. The microprobe is a JEOL JXA-8200 electron microprobe at Dalhousie University, Halifax, Nova Scotia. The JEOL JXA-8200 has five wavelength dispersive spectrometers (WDS). The WDS is capable of analyzing elements from boron to uranium. The instrument produces high quality (1280x1024) secondary and backscattered images as well as high resolution X-ray maps. For elemental analysis, the instrument is usually operated at 15Kv with 20na of probe current. Counting time for major elements is 20 seconds on WDS. The matrix correction program used is ZAF from JEOL. Geological samples, oxides and metals are used as standards (pers. comm., MacKay).

3.2.1 Garnet composition

Garnet is an orthosilicate with the general structural formula $[Fe,Mg,Ca,Mn]_3Al_2Si_3O_{12}$. In metamorphic rocks, garnet zoning may reflect changes in P-T conditions and other aspects of metamorphic history.

The complete suite of compositional maps and accompanying BSE images is included in Appendix C. Representative maps are discussed below, and are shown in Figures 3.5 and 3.6. Major element analyses for selected garnets and analyzed inclusions are given in Appendix A; trends in the major elements are discussed below.

Figure 3.5a is an X-ray map of Fe in garnet MZ-1A-0.2, showing no detectable trend in almandine content. The darker grey minerals below the garnet grain are biotites; black represents quartz and feldspars, which have no appreciable Fe content. Figure 3.5b is an X-ray map of Mg in garnet MZ-1A-0.2 showing the decrease in Mg content towards adjacent biotite. Mg from garnet and Fe from biotite exchange as the rock cools from peak metamorphic conditions (Spear, 1993).

Figure 3.6a is a Ca map of garnet MZ-1A-0.3, showing a decrease in Ca concentration from core to rim. Plagioclase (high Ca) is abundant in the matrix. Figure 3.6b is the accompanying BSE, showing the boundaries of the garnet. Ca is partitioned between plagioclase and garnet as a function of P-T. Ca-poor rims in garnet indicate a decrease in pressure after peak metamorphic conditions (Spear, 1993).

Major element analyses were obtained for garnets in samples MZ-1A, MZ-1B, MZ-2A, and one garnet selected for P-T work from MZ-2B. Appendix B contains photomicrographs of the garnets and their petrographic settings. BSE and compositional maps for all garnets are compiled in Appendix C. Figure 3.7 plots compositions from 125 points in garnet from MZ-1A, MZ-1B, MZ-2A, and

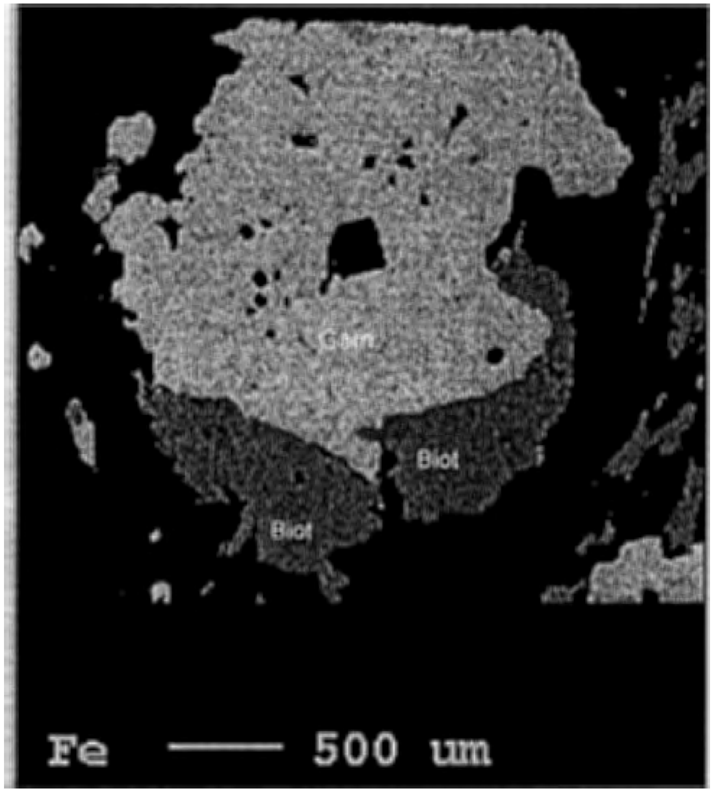

Figure 3.5a. Fe X-ray compositional map of garnet MZ-1A-0.2. Large light grey grain is garnet, darker grey grains below are biotite. Dark areas are matrix quartz and feldspar.

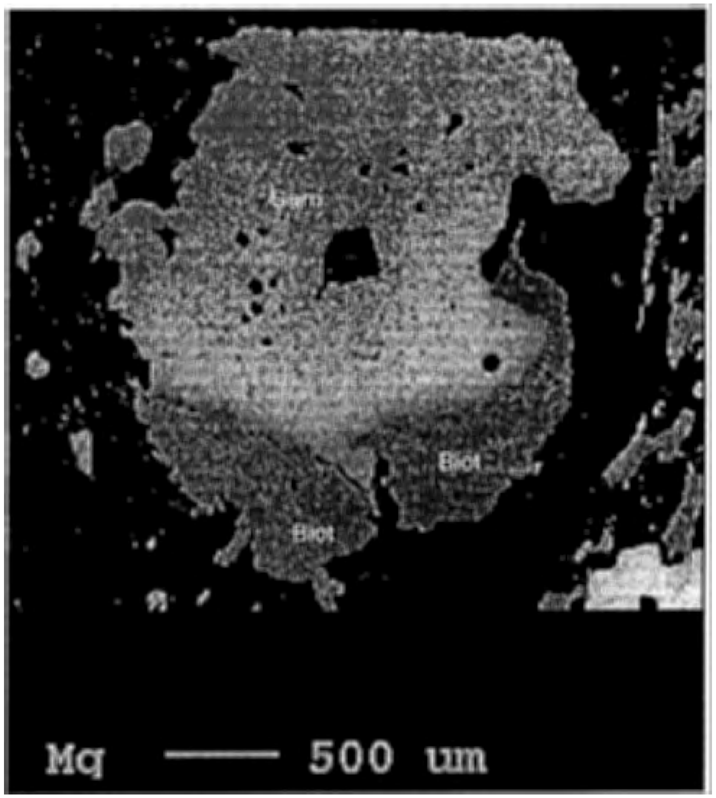

Figure 3.5b. A Mg compositional map of garnet MZ-1A-0.2. Large light grey grain is garnet, darker grey grains below are biotite. Note Mg zoning. Narrow dark rims on garnet reflect Mg-depletion (Fe-enrichment) related to retrograde exchange with biotite.

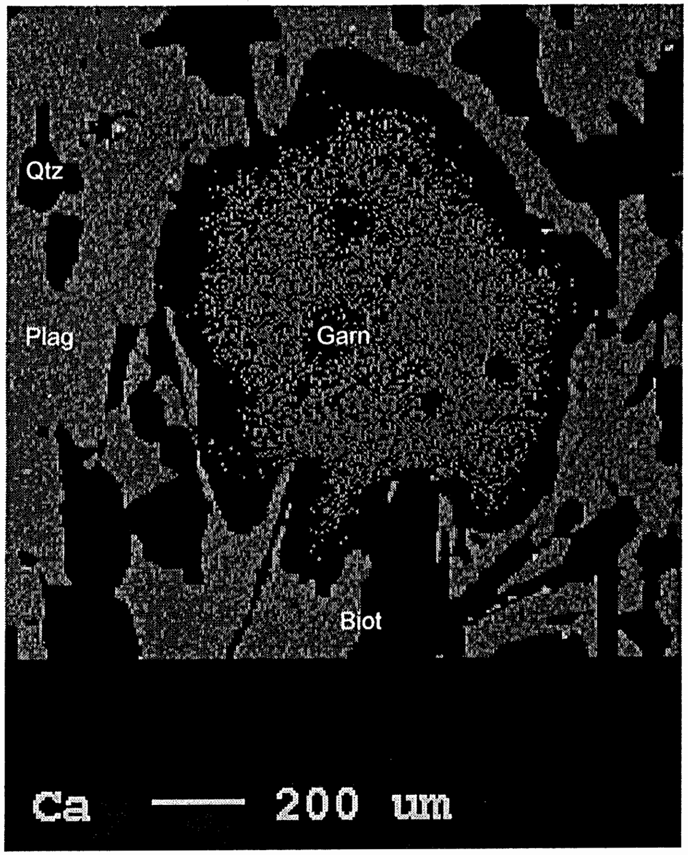

Figure 3.6a. Ca X-ray compositional map of garnet MZ-1A-0.3. Note Ca zoning with very low Ca rims; this likely represents a pressure decrease during the equilibration of garnet with its matrix.

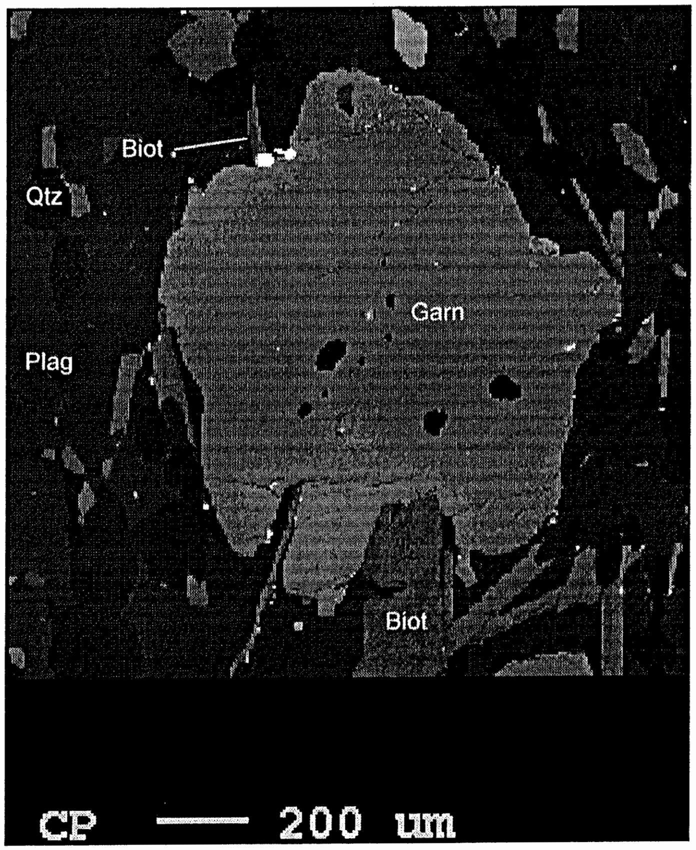

Figure 3.6b. BSE image of garnet MZ-1A-0.3, showing the grain boundaries of the garnet in Figure 3.6a. Lighter grey patches rims represent Mg depletion (Fe-enrichment) owing to retrograde exchange with matrix biotite.

Figure 3.7

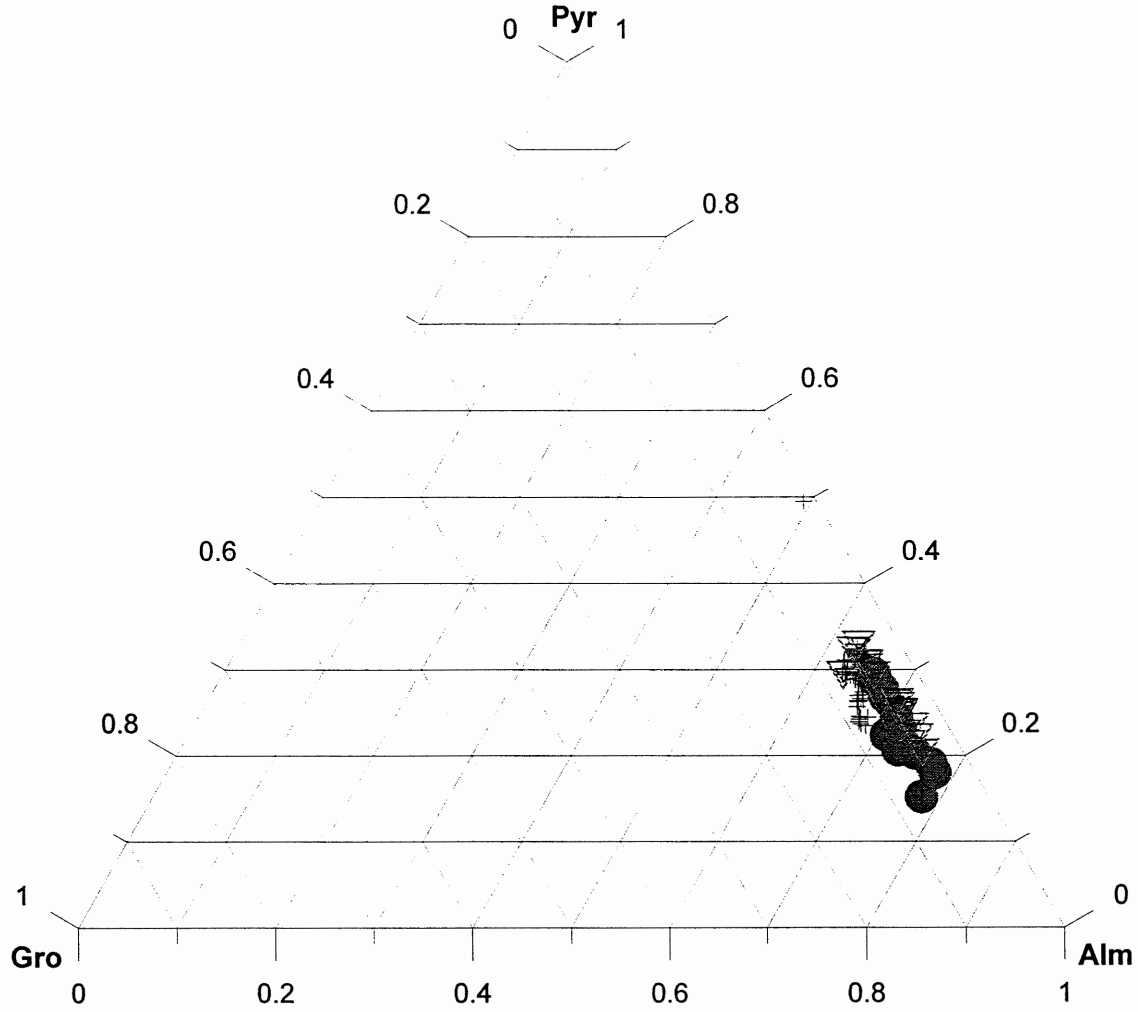

Figure 3.7. Garnet composition plotted as mole fraction almandine (Alm), pyrope (Pyr), and grossular (Gro). Garnet cores are represented by +, rims by ▽, and rims adjacent to biotite by ●.

MZ-2A. Garnet cores are generally similar in composition. Rim composition varies; rims adjacent to biotite have lower Mg and higher Fe values. Rims not adjacent to biotite also have variable Mg. Figure 3.8 shows the trends apparent in the chemical data; Fe increased towards the rim, Mg decreases. Average garnet core composition is $Alm_{64}Pyr_{29}Gro_6Sps_1$ ($Fe_{1.92}Mg_{0.87}Ca_{0.18}Mn_{0.03}Al_2Si_3O_{12}$). Average rim composition where garnet is not adjacent to a biotite is $Alm_{69}Pyr_{25}Gro_5Sps_1$. Average rim composition where garnet is directly in contact with biotite is $Alm_{71}Pyr_{23}Gro_5Sps_1$.

3.3 Thermobarometry

Thermobarometry was used to determine possible entrapment conditions for fluid inclusions, and for comparison with fluid inclusion isochores.

3.3.1 Previous work

Previous P-T work on metapelites (garnet + biotite + sillimanite + plagioclase + quartz + K-feldspar) in the McClintock domain has produced estimates of 7.2 ± 1.6 kbar and 730 ± 55 °C (Timmermann, 1998). An apparent retrograde anti-clockwise P-T path for the Birkendale gneiss association was interpreted as an artifact of differing closure temperatures of net-transfer and exchange reactions; this theory is supported by the presence of sillimanite rather than kyanite as the stable aluminosilicate. The P-T path for the Birkendale gneiss association is thought to be one of decompression followed by cooling, similar to that of other nearby units (Timmermann, 1998).

Figure 3 8

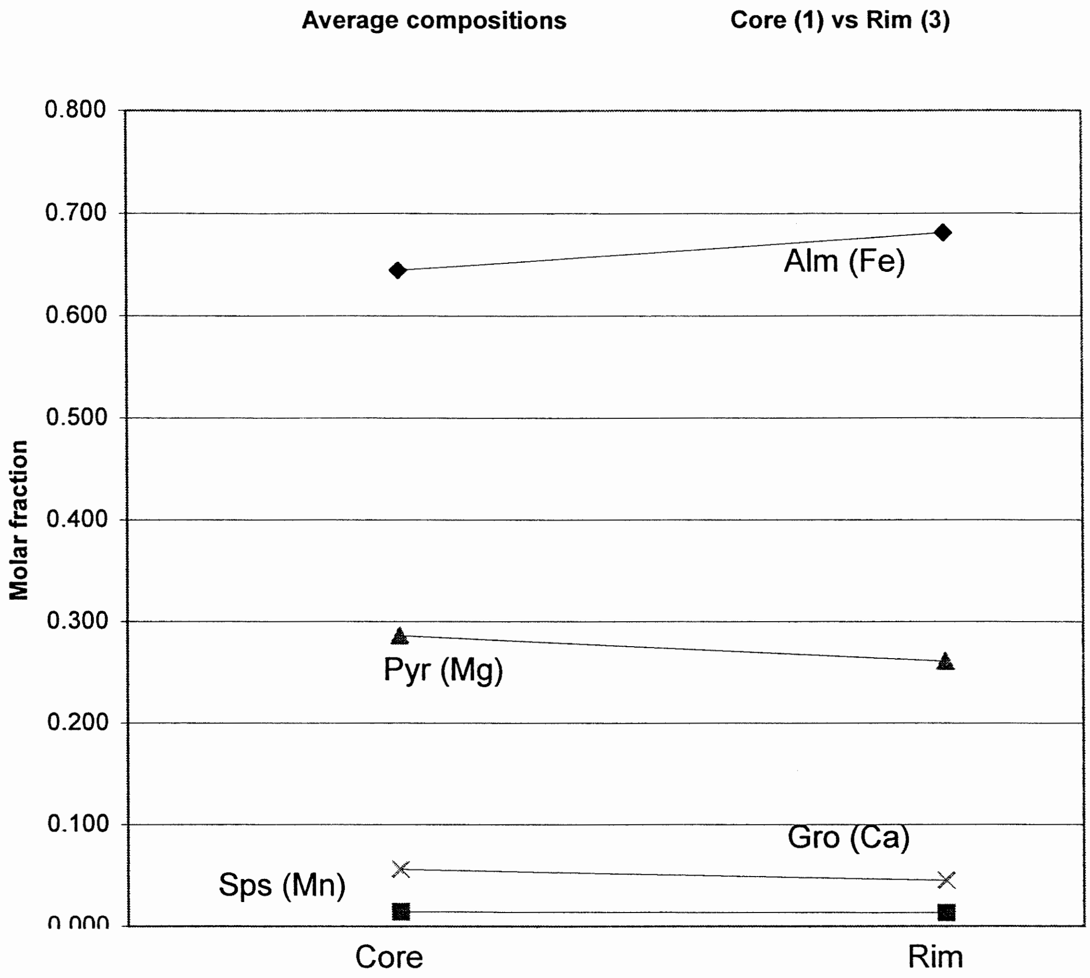

Figure 3.8. Average compositions of cores and rims from selected garnets, showing chemical zoning trends; rim analyses in biotite-adjacent Mg anomalies are not included.. Alm (Fe) increases in the rim, while Pyrope (Mg) and Gross (Ca) decrease approaching the rim.

3.3.2 Methods

Sample MZ-2B was used to calculate metamorphic pressure and temperature using the garnet-biotite exchange thermometer and the Garnet-aluminosilicate-silica-plagioclase (GASP) barometer. The garnet composition used in the calculations is averaged from core and non-biotite adjacent rim measurements. Plagioclase and biotite are averaged from all readings taken (plagioclase, MZ-2B pt 34 through MZ-2B pt 40; biotite, MZ-2B pt 30 and MZ-2B pt 31). The presence of sillimanite and quartz implies that the activities of silica and alumina are unity (a_{SiO_2}, $a_{Al_2SiO_5} = 1$).

The garnet-biotite exchange thermometer is based on the reaction:

$$\underset{\text{almandine}}{Fe_3Al_2Si_3O_{12}} + \underset{\text{phlogopite}}{KMg_3AlSi_3O_{10}(OH)_2} = \underset{\text{pyrope}}{Mg_3Al_2Si_3O_{12}} + \underset{\text{annite}}{KFe_3AlSi_3O_{10}(OH)_2} \qquad \text{Eq. 3.1}$$

Molar fractions calculated from *e.g.* microprobe analysis are used to calculate the distribution coefficient for the reaction, K_D:

$$K_D = \frac{X_{ann} \bullet X_{pyr}}{X_{alm} \bullet X_{phl}} \qquad \text{Eq. 3.2}$$

, which relates to T and P via the equation:

$$52{,}112 - 19.51\,T + 0.238\,P + 3RT\ln(K_D) = 0 \qquad \text{Eq. 3.3}$$

(Ferry and Spear, 1978)

in which T is the temperature (°K) and P is the pressure (bars). The effects of pressure are minimal, and so the reaction is a good thermometer (Spear, 1993).

The distribution of Fe and Mg between co-existing garnet and biotite is therefore a function of temperature. As temperature drops, Eq. 3.1 proceeds to the right. Cations are exchanged; biotite prefers Mg, and exchanges Fe for the Mg in garnet (Spear, 1993). Garnet-biotite exchange becomes more efficient as temperature drops, but is limited by slow diffusion rates in garnet. Diffusion in biotite is quite rapid on geological time scales (Spear, 1993). The retrograde exchange of Mg for Fe is applicable to the Mg deficiencies seen at garnet-biotite contacts, where garnets have been depleted on the rims but the cores retain higher concentrations, and biotite shows no zonation.

The GASP geobarometer is based on the net-transfer reaction:

$$\underset{\text{anorthite}}{3\,CaAl_2Si_2O_8} = \underset{\text{grossular}}{Ca_3Al_2Si_3O_{12}} + \underset{\text{sillimanite}}{2\,Al_2SiO_5} + \underset{\text{quartz}}{SiO_2} \qquad \text{Eq. 3.4}$$

The calculated molar fractions of the various phases are used to calculate the equilibrium constant, K_{eq}:

$$K_{eq} = \left[\frac{X_{gro}}{X_{an}}\right]^3 \qquad \text{Eq. 3.5}$$

which relates to T and P via the equation:

$$11675 - 32.815\,T + 1.301\,(P-1) + RT\ln K_{eq} = 0 \qquad \text{Eq. 3.6}$$

(Ghent, 1976).

The GASP reaction is sensitive to both pressure and temperature, and defines the upper pressure limit of anorthite stability. High Ca garnet and low Ca plagioclase are stable at high pressures and low temperatures, low Ca garnet and high Ca plagioclase are stable at low pressure and high temperatures (Spear, 1993).

3.3.3 Results

P-T conditions were calculated from points 1-4, 6,8,9,11-15 (garnet), 30, 31 (biotite), and 34-40 (plagioclase) in sample MZ-2B (See Appendix C) using TWQ 2.02 (Berman and Aranovich, 1996), and are presented in Figure 3.9. Points 21 and 26 are quartz and sillimanite (Al_2SiO_5), respectively. Temperature is calculated as 726 ± 25 °C, pressure as 7.6 ± 1 kbar. Errors are nominal; with only two equations the intersection is mathematically perfect, so errors have been assumed based on average errors for pressure and temperature.

3.4 Discussion

Variations in Fe and Mg content towards the rim suggests that garnet has undergone retrograde diffusion with biotite during cooling. Decrease in Ca content of garnet suggests garnet has undergone retrograde diffusion with plagioclase as pressure dropped. Results are in agreement with the suggested P-T path of Timmermann (1998).

Figure 3.9

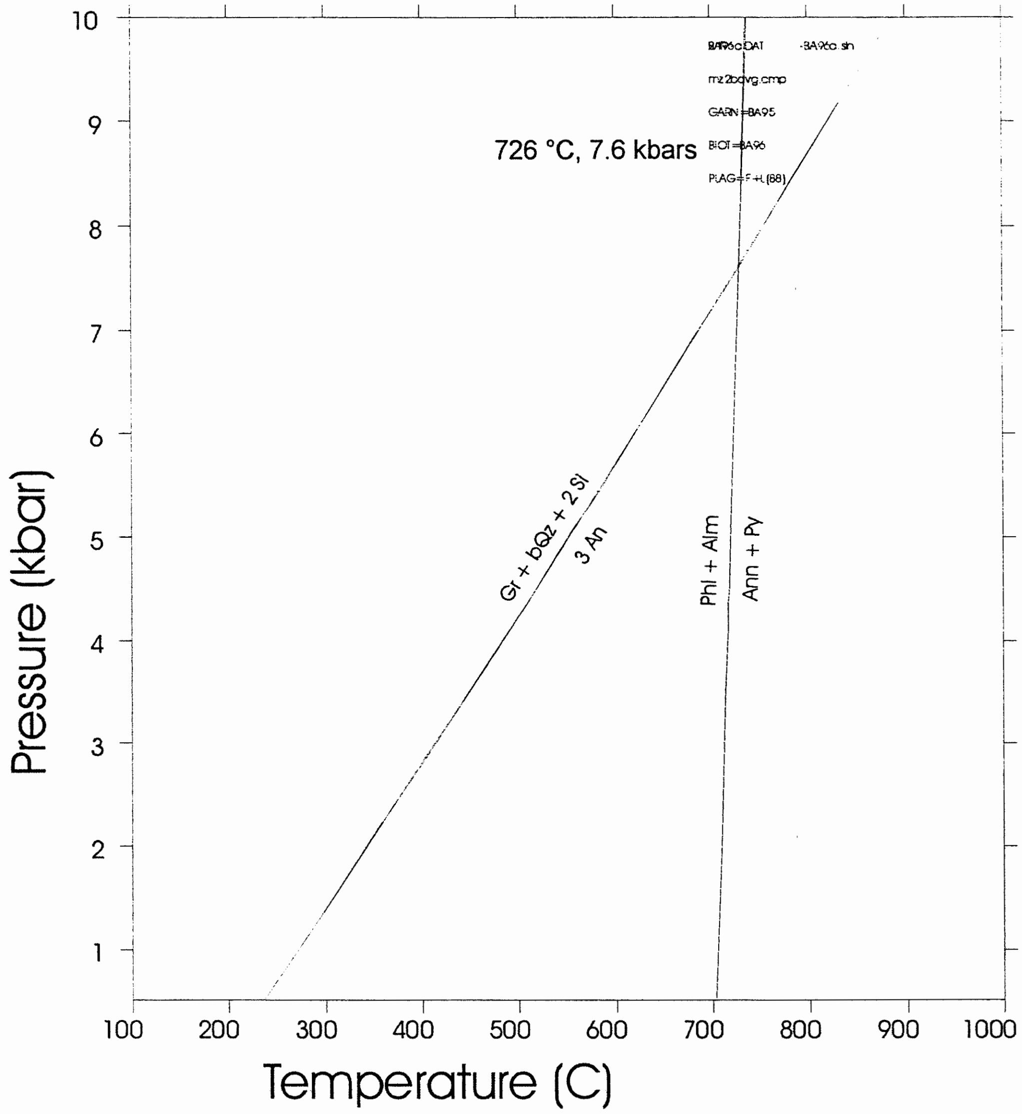

Figure 3.9. P-T, calculated using TWQ2.02 (Berman and Aranovich, 1996). Intersection is at 726 °C, 7.6 kbars. See Appendix D for electron microprobe analyses.

4.0 Fluid Inclusion Microthermometry

4.1 Fluid inclusions

4.1.1 Fluid inclusion entrapment

Minerals commonly grow in the presence of one or more fluids (Roedder, 1984). These fluids may be liquid, gas, or supercritical fluid, depending on the conditions of crystallization. Fluid composition can vary, and may include volatiles (e.g., H_2O, CO_2, CH_4, etc) and solutes (e.g., NaCl, Cu, Ag, Au) (Roedder, 1984; Touret, 2001). Composite fluids containing two or more of the above components are common (Roedder, 1984; Touret, 2001).

Crystals growing in a fluid-present medium may entrap the surrounding fluid (Roedder, 1984; Goldstein and Reynolds, 1994). The inclusions of entrapped fluid are **fluid inclusions**. Fluid inclusions provide invaluable information about what fluids were present at the time of crystal growth, and can also provide information about pressure and temperature conditions at the time of crystal growth (Roedder, 1984; Goldstein and Reynolds, 1994; Touret, 2001). Fluid inclusions are generally the only direct record of these fluids (Roedder, 1984; Touret, 2001).

Three classes of fluid inclusions are recognized: primary, secondary, and pseudo-secondary (Roedder, 1984; Goldstein and Reynolds, 1994). The distinction between classes is made mainly on shape and grouping of the inclusions (Roedder, 1984). Primary fluid inclusions are those trapped during the initial period of mineral growth (Fig. 4.1; Roedder, 1984; Goldstein and Reynolds, 1994). Primary inclusions are generally found along growth planes (Goldstein

Figure 4.1

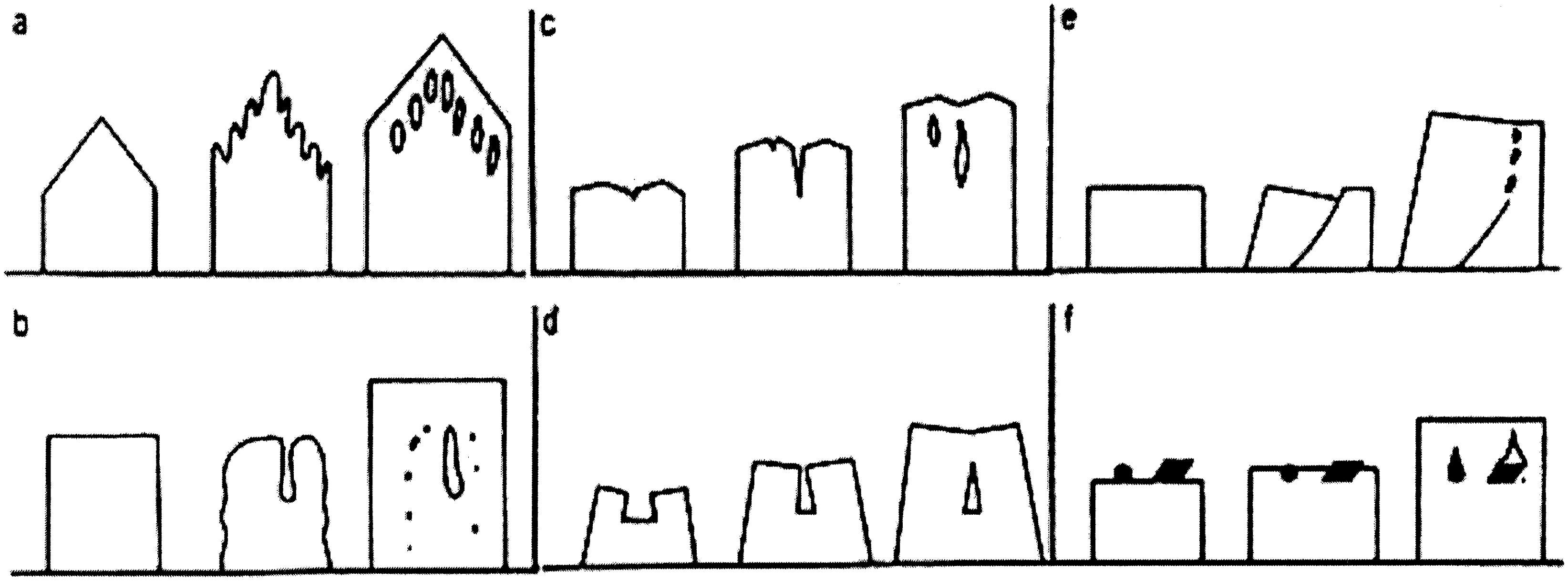

Figure 4.1. Methods of primary fluid inclusion entrapment. A) Dendritic growth covered by later growth. B) Partial dissolution of growing surface covered by later growth. C) Inclusions trapped between growth spirals. D) Subparallel growth of crystal blocks. E) Fracturing during growth phase trapped as growth continues. F) Growth is obstructed by foreign objects, fluid included with foreign object. From Roedder (1984).
When the overgrowing crystal is a second growth phase, rather than continued growth, inclusions are pseudo-secondary (Roedder, 1984).

and Reynolds, 1994) though they can also be isolated individual inclusions with negative crystal shapes (Roedder, 1984). Secondary inclusions are generally found along fracture planes (Fig. 4.2; Roedder, 1984). Fluid filling a fracture in the host mineral is entrapped as the fracture heals and crystal regrows (Roedder, 1984). Pseudo-secondary inclusions are secondary inclusions where the original grain hosting the secondary inclusions has been overgrown by a second growth phase (Roedder, 1984). Pseudo-secondary inclusions, like primary inclusions, record the presence of fluid before or during the younger growth phase (Goldstein and Reynolds, 1994).

Some authors (*e.g.*, Touret, 2001) have found the primary-secondary terminology potentially misleading, as it refers to inclusion genesis, and prefer to refer to fluid inclusions with purely textural and compositional terms, making no assumptions about the order or method of entrapment. Touret (2001) proposed a terminology based on the grouping of inclusions of similar composition and texture, assuming that inclusions of similar composition in a similar setting are contemporary. He referred to these groups as **Groups of Synchronous Inclusions** (**GSI**'s). Using Touret's (2001) terminology, the inclusions in Figure 1a (oblong, fluid X) could be differentiated from the inclusions in Figure 1d (triangular, fluid X).

4.1.2 Microthermometry

The interpretation of data provided by fluid inclusions is based on two assumptions: first, that the inclusion has not changed volume since the time of entrapment (the system is isochoric); second, that the system is chemically

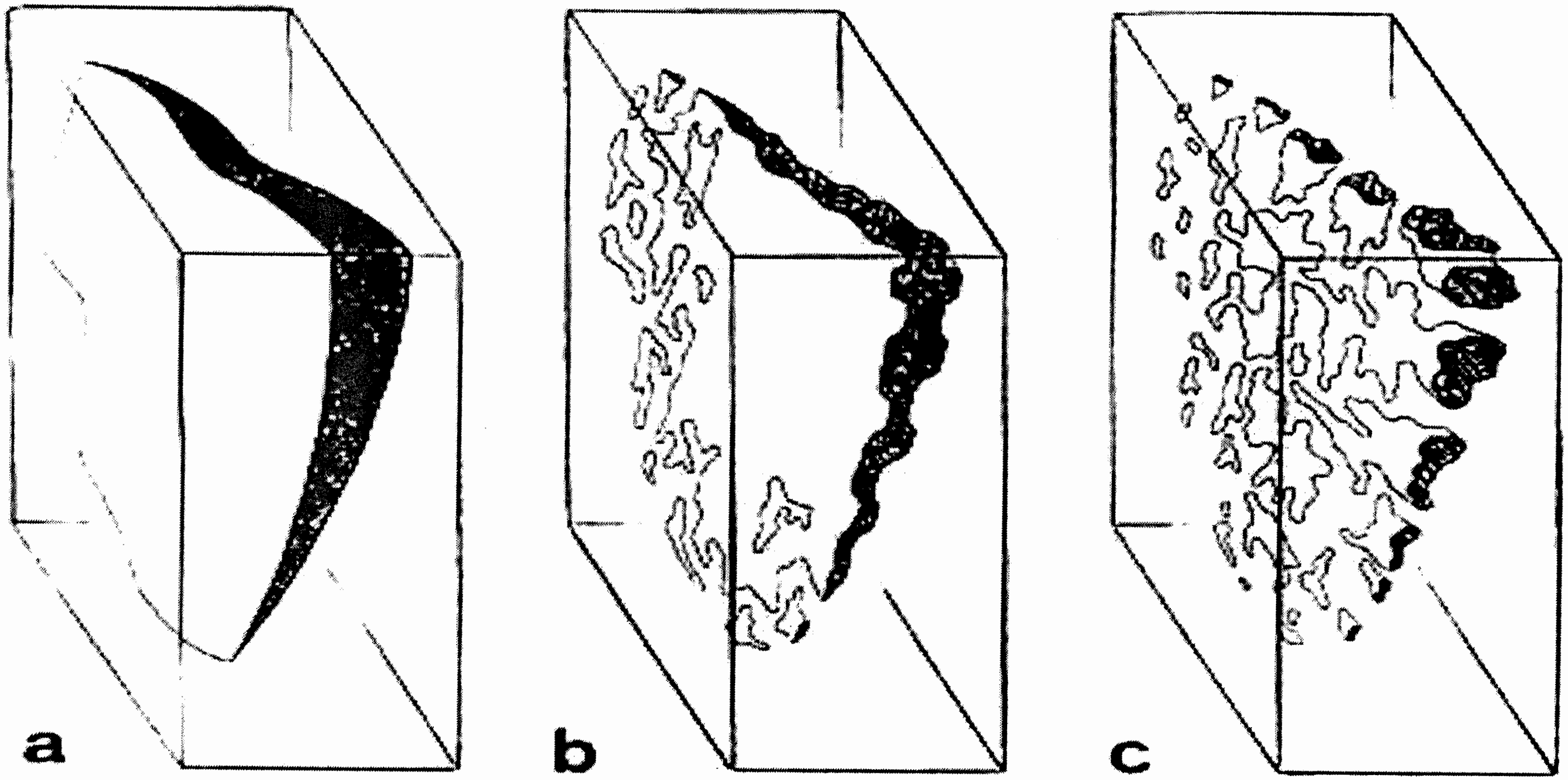

Figure 4.2. Secondary inclusion entrapment. A) Fracture in a crystal is filled with fluid. B), C) Annealing along the fracture traps fluid. From Roedder (1984).

closed (isoplethic) (Roedder, 1984; Goldstein and Reynolds, 1994; Touret, 2001). If so, fluid inclusions offer information about the environment and conditions of fluid entrapment (Roedder, 1984).

It is assumed, unless otherwise determined, that at the time of entrapment, the fluid present in an inclusion had a certain mass and a specific volume determined by the fluid inclusion itself, and therefore a certain density (Touret, 2001). It is also assumed (unless evidence to the contrary is presented) that the fluid was a homogeneous phase at the time of entrapment, either a single phase fluid or homogeneous composite fluid; even if the fluid has become multiple phases since entrapment, if the system was closed the relative proportions of fluid components remain equal (Roedder, 1984). The system is thereby isochoric and isoplethic. A closed system fluid inclusion records the fluid pressure and temperature at the time of entrapment (Roedder, 1984). The inclusion has been "frozen" on a particular path in pressure-temperature space, determined by the conditions of entrapment (Touret, 2001). So long as the system remains isoplethic and isochoric, the fluid in the inclusion will follow the same P-T path on heating and cooling (Touret, 2001).

In the laboratory, a sampled fluid inclusion is heated and cooled, and the temperatures of various phase changes are recorded. Microthermometric data include temperature of freezing/melting (T_m) of a certain phase and the temperature of homogenisation (T_h) for certain phases (*i.e.*, liquid-vapour homogenization, immiscible fluid homogenization) (Roedder, 1984; Goldstein and Reynolds, 1994). T_m and T_h data are the bases of microthermometric studies. Heating and cooling the fluid in the inclusion forces the fluid along the predetermined P-T path, allowing various temperatures of observable phase changes or homogenizations to be measured (Roedder, 1984).

T_m, or the temperature of melting (solid-to-liquid phase changes), is used to determine fluid compositions (Roedder, 1984; Goldstein and Reynolds, 1994). The fluid inclusion is cooled until the liquid inside is frozen to a solid, then heated slowly. The temperature at which the fluid melts is noted (T_m). Every fluid has a distinct melting point, and T_m is used to determine the fluid composition (*e.g.*, pure CO_2 melts -56.6 °C; Touret, 2001). Even the melting point of multiple phase inclusions can be distinctive (*e.g.*, H_2O with 23 wt% NaCl melts ~21.2 °C; Goldstein and Reynolds, 1994). Temperature is not noted for the freezing of the liquid phase because liquids can exist metastably into the solid temperature range (Goldstein and Reynolds, 1994).

T_h, or the temperature of homogenization, can be measured for every homogenization of fluid phases (generally liquid and/or vapour). In pure phases, the temperature of homogenization is called the critical point, and represents the point at which vapour and liquid become indistinguishable (*i.e.*, a supercritical fluid; Diamond, 2001). Composite H_2O-CO_2 fluids, for example, have three possible phase homogenizations: liquid and vapour CO_2 becoming a carbonic supercritical fluid, liquid and vapour H_2O becoming an aqueous supercritical fluid, and the homogenization of the aqueous and carbonic phases to a single homogeneous phase (Diamond, 2001). For purely carbonic inclusions T_h is used to determine the density of the inclusion; the temperature at which the liquid and vapour phases homogenize must lie on an isochore (line of equal density) with the pressure of entrapment (Fig. 4.3; Roedder, 1984). Using an independent thermometer, the pressure of entrapment can be calculated (Roedder, 1984). For brine (saline aqueous fluid) inclusions, T_h can be used to determine the salinity and density of the aqueous phase (Roedder, 1984).

4.1.3 Post-entrapment changes

Once entrapped, the fluid inclusion may be preserved until the crystal is broken and the fluid permitted to escape. There are, however, several ways an inclusion or the enclosed fluid may be modified after entrapment. Post-entrapment changes to fluid inclusions or the fluids contained therein violate the assumptions one must make to interpret fluid inclusion data (Roedder, 1984). Some post-entrapment changes are inconsequential, and can be ignored. Some changes are more significant, and render data collected from inclusions suspect (Roedder, 1984).

The most common form of post-entrapment change to a fluid inclusion is crystallization from within the fluid (Roedder, 1984). Crystallization of the host mineral is generally invisible, and ignored; the fluid is saturated with respect to the host material and precipitates onto the inclusion wall during cooling (Roedder, 1984). Other daughter minerals may also form; for example, NaCl-rich aqueous inclusions commonly have daughter crystals of halite (Roedder, 1984). In many cases, the daughter crystals precipitate from solution as the fluid cools because most compounds are more soluble in hotter solvents, and can be

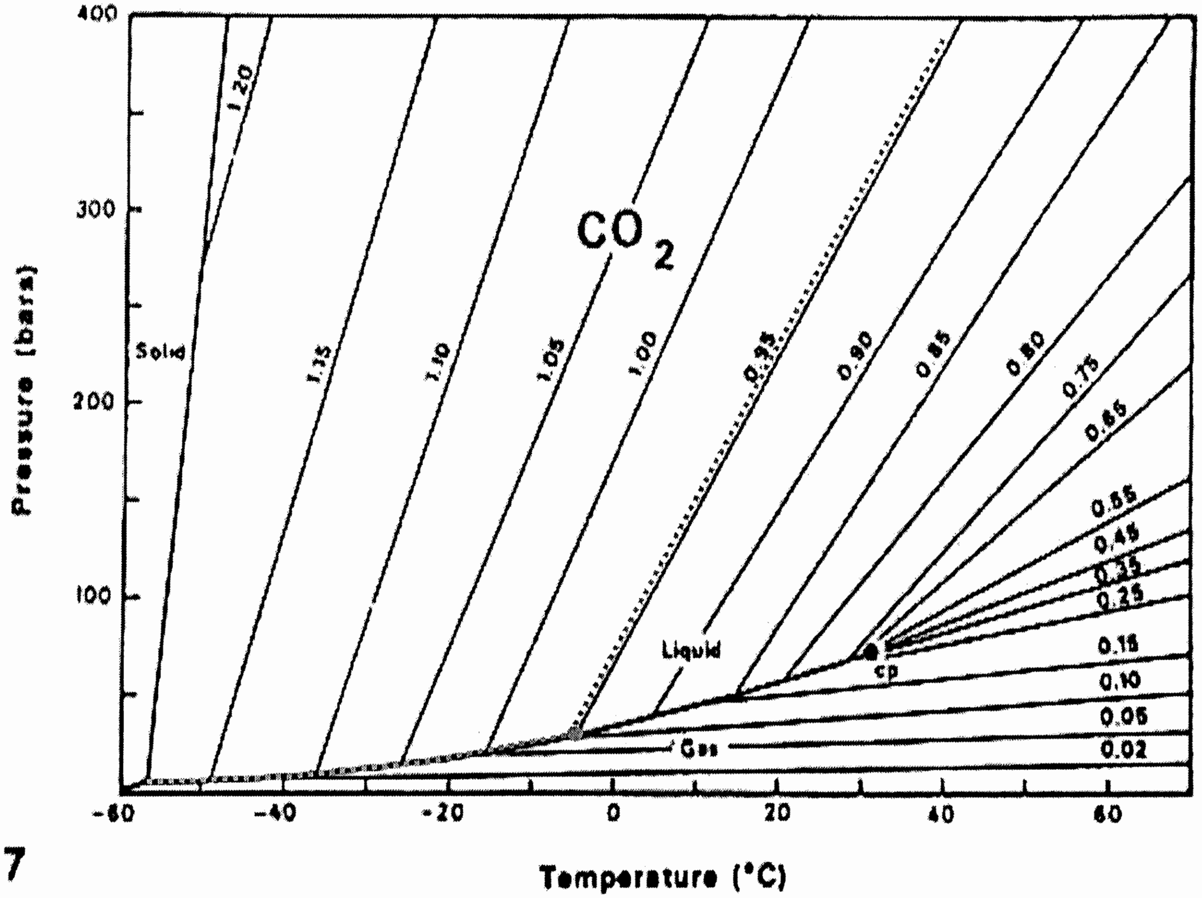

7

Figure 4.3. Carbon dioxide (CO_2) isochores, i.e., lines of equal density in P-T space. The temperature at which the fluid homogenizes and the phase to which it homogenizes indicate the fluid density, e.g., if a fluid homogenizes at -5 °C to the liquid phase, the CO_2 density is ~ 0.95 g/cm^3. The dashed grey line represents the fluid in a fluid inclusion; once the fluid homogenizes (leaves the LIQ-VAP boundary), it follows the isochore for its particular density. Densities given are in g/cm^3. From Roedder (1984).

redissolved by heating (Roedder, 1984). Like the entrapped fluid phases, daughter mineral solubility can be used to measure fluid composition and density (*e.g.*, the temperature at which all NaCl dissolves into an H_2O fluid can be used to determine the weight percentage NaCl and the density of the fluid; Roedder, 1984).

Volume changes to fluid inclusions are common and problematic (Roedder, 1984). Some reversible volume changes, such as thermal expansion or contraction of the host mineral or daughter products during heating or cooling, and precipitation of daughter minerals, are of small importance (Roedder, 1984). More problematic are irreversible changes in volume caused by overpressure within the inclusion which leads to greater fluid pressure within the inclusion which fractures or deforms the surrounding host grain, or phase changes in the host mineral that increase the inclusion volume (Roedder, 1984). Many types of irreversible volume change alter the density, thereby invalidating the isochoric assumption needed to interpret fluid inclusions (Touret, 2001).

Necking describes fluid inclusion volume change as a function of grain dissolution and recrystallization, common to secondary fluid inclusions (Roedder, 1984). Necking results from dissolution/precipitation and minor associated deformation of the host mineral, whereby a relatively large fluid inclusion with high surface energy (randomly shaped) becomes several smaller fluid inclusions with negative crystal shapes (Fig. 4.4; Roedder, 1984). Necking of a homogeneous fluid is generally not a concern, as every new, smaller inclusion will have the same composition and density (Roedder, 1984). Problems arise

Figure 4.4

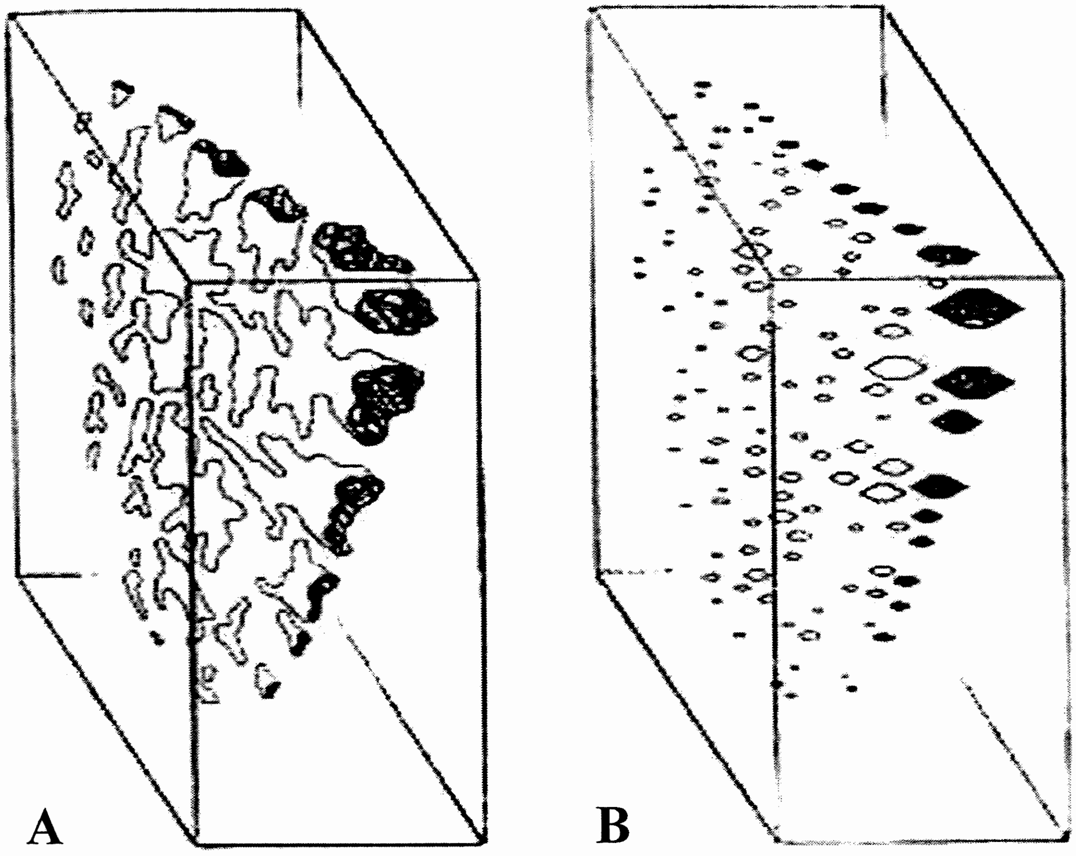

Figure 4.4. Necking fluid inclusions. High surface energy inclusions (A) dissolve and reprecipitate the host mineral, and lower surface energy by adopting negative crystal shapes (B). From Roedder (1984).

when fluid inclusions containing multiple phases neck; the new inclusions will have varying ratios of each of the phases from the heterogeneous mixture, depending on what phases are present during necking, inclusion orientation, and the size of the new inclusions (Fig. 4.5; Roedder, 1984).

Chemical changes to fluid inclusions may be just as important as physical changes. Leakage of the entrapped fluid or its components, or diffusion of external fluid into the inclusion, can alter the chemistry (the system is no longer isoplethic) and density (the system is no longer isochoric; Roedder, 1984). Aqueous inclusions in quartz may leak H_2O, either via small dislocations in the crystal lattice or diffusion through the host mineral, and the resulting water loss can have an effect on the composition of the fluid (X_{H_2O} becomes less in composite fluids, or salinity increases) and the density (less material in the inclusion results in lower density; Roedder, 1984).

In general, important post-entrapment changes to inclusions are those that violate the assumptions necessary for fluid inclusion interpretation. Fluid leakage, irreversible deformations of the inclusion, and necking of multiple phase inclusions violate the isochoric and isoplethic assumptions.

4.2 Fluid inclusions in metamorphic rocks

The presence of fluid inclusions in high-grade metamorphic rocks presents a rare opportunity to examine the fluids present during a metamorphic episode. It is suggested that few, if any, fluid inclusions are pre-metamorphic, due to recrystallization (Roedder, 1984). Higher grade metamorphic rocks also have

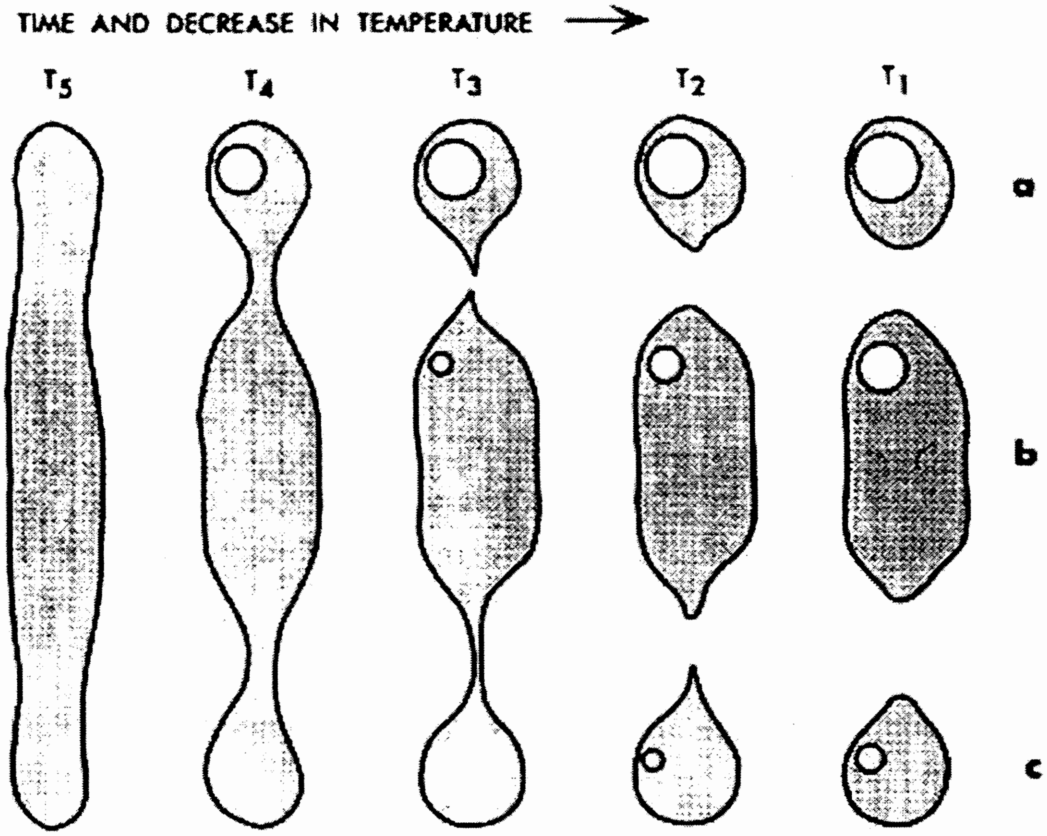

Figure 4.5. Inclusions necking during phase separation. As the inclusion cools through time (proceeding to the left in the diagram) multiple phases evolve. Necking down during the evolution of the new phase causes the necked inclusions to be have different fluid ratios, both from other inclusions necked at the same time and from the original inclusion. No inclusion (of a, b, and c) will return a proper homogenization temperature. From Roedder (1984).

fewer volatile constituents, compared to other rock types, since devolatization has, by this level of metamorphism, already progressed (Roedder, 1984).

Many researchers, notably Roedder (1984) and Touret (2001), agree that the majority of fluids occurring in high-grade (granulite and equivalent facies) metamorphic environments are dominantly CO_2+H_2O fluids with relatively low H_2O activities (commonly, $X_{H_2O}<0.85$; Diamond, 2001), as evident from fluid inclusion studies (Touret, 2001). Granulite facies rocks commonly have inclusions of pure or nearly pure CO_2 (Roedder, 1984; Touret, 2001).

4.2.1 Fluid inclusions in garnet

Fluid inclusion studies have generally concentrated on quartz, calcite, halite, and other diagenetic minerals (Roedder, 1984; Goldstein and Reynolds, 1994). In metamorphic rocks, quartz is by far the most common host mineral studied. Fluid inclusions in garnet have been recognized (i.e., De Maesschalck *et al*, 1991), but there have been few studies on its properties as a host mineral (*e.g.*, does fluid leakage occur, and if so, at what rate?). For simplicity, and in the absence of data, possible post-entrapment changes for fluid inclusions in quartz are considered to be analogous to those in garnet.

4.3 CO_2-H_2O systematics

Mixed volatile fluids comprising CO_2-H_2O are common in high-grade metamorphic rocks (Touret, 2001). The mixing of these two fluids complicates the phase relations of the compounds. Both end-member systems have four phases: a low-T solid phase, a moderate-T liquid phase, a low-P vapour phase, and a high-T supercritical fluid (Fig. 4.6); Table 4.1 details the abbreviations used

Table 4.1

Table 4.1. Phase abbreviations used in text, figures, and Table 4.1. After Diamond (2001).

Abbreviation	**Composition, state**
SOLcar	CO_2, solid
ICE	H_2O, solid
CLA	$CO_2 \bullet 5.75H_2O$, solid
LIQcar	CO_2, liquid
LIQaq	H_2O, liquid
VAP	CO_2-H_2O, vapour
VAPcar	CO_2, vapour
VAPaq	H_2O, vapour
SCF	CO_2-H_2O, supercritical fluid
SCFcar	CO_2, supercritical fluid
SCFaq	H_2O, supercritical fluid

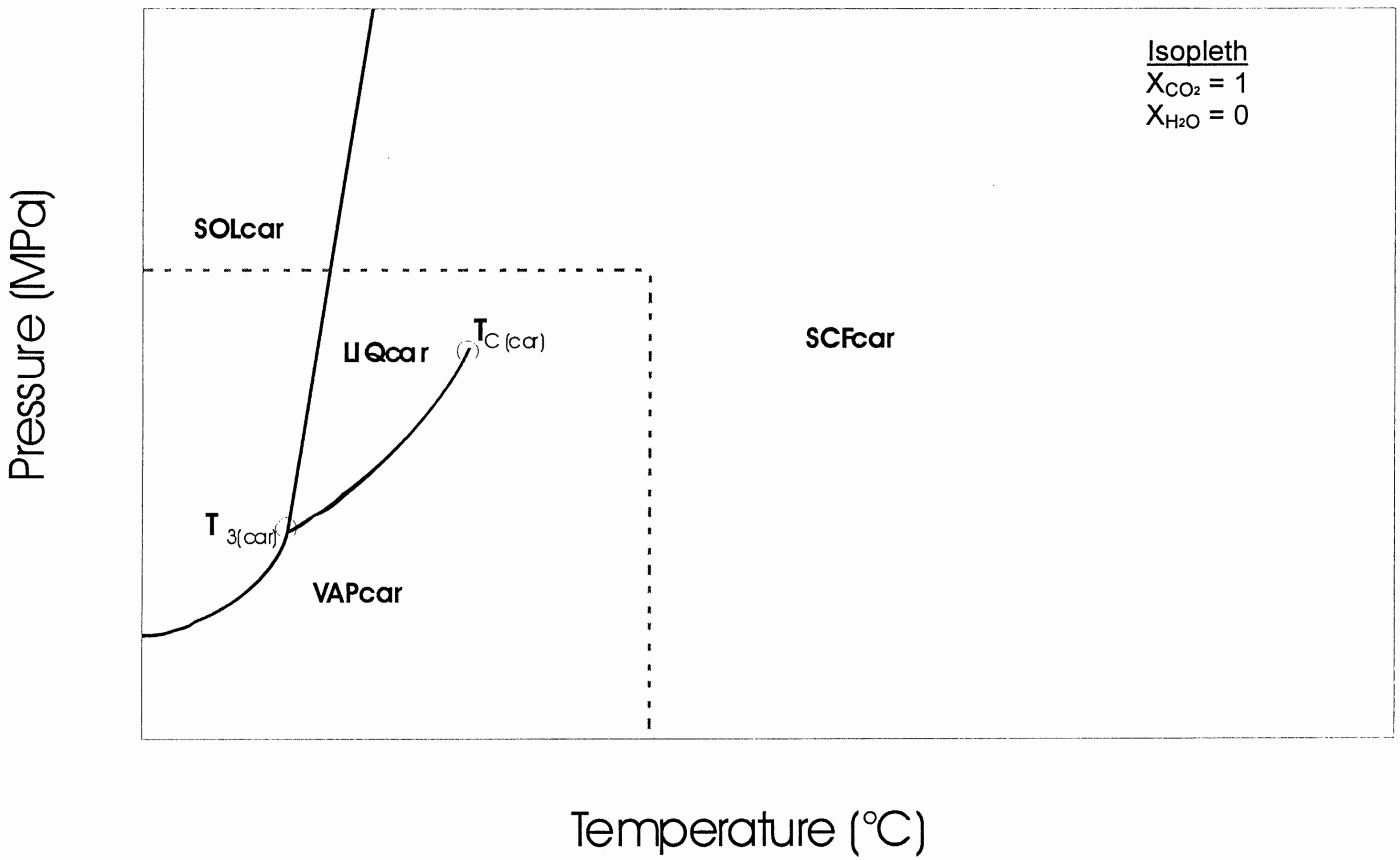

Figure 4.6. P-T phase diagram for the pure phase CO_2, showing the four stable phases and their respective fields and boundaries. The drawing is not to scale; the dashed line represents the expanded area of the diagram. Abbreviations used are detailed in Table 4.2. After Diamond (2001).

in Figure 4.6 and throughout this chapter. The solid phases exist on the low-T side of the triple point eutectic (Fig. 4.6). Beyond the critical point (Fig. 4.6), the liquid and vapour phases become indistinguishable, and behave as a supercritical fluid with gaseous and liquid characteristics (Diamond, 2001).

In the composite system, two new phases are added to the CO_2-H_2O system. The first new phase is the low-temperature clathrate. The clathrate is a solid carbon dioxide hydrate ($CO_2 \bullet 5.75H_2O$) and forms at temperatures slightly above those of ice and CO_2(solid) formation (Fig. 4.7; Diamond, 2001). The second new field is the two-phase fluid resulting from the immiscibility of the two fluids. Below the critical temperature of water (Fig. 4.7) CO_2, generally a supercritical fluid (much of the immiscibility field is beyond the CO_2 critical point) and liquid H_2O are immiscible, *i.e.*, relatively insoluble in one another (Diamond, 2001). Although the vapour phases mix completely (Fig. 4.7) liquid water does not dissolve much CO_2, nor does much liquid H_2O mix with the CO_2 fluid, giving rise to two immiscible fluids (Fig. 4.7; Diamond, 2001).

P-T conditions for the entrapment of fluid inclusions for high-grade metamorphic rocks (*i.e.*, granulite facies) are generally well beyond the critical values for both phases, within the supercritical fluid field on all relevant phase diagrams (Diamond, 2001; Touret, 2001). Determining the isochore (line of equal density in P-T space) can be easily accomplished using the lower-T phase changes (Diamond, 2001; pers. comm., Kontak) described in section 4.3.2.

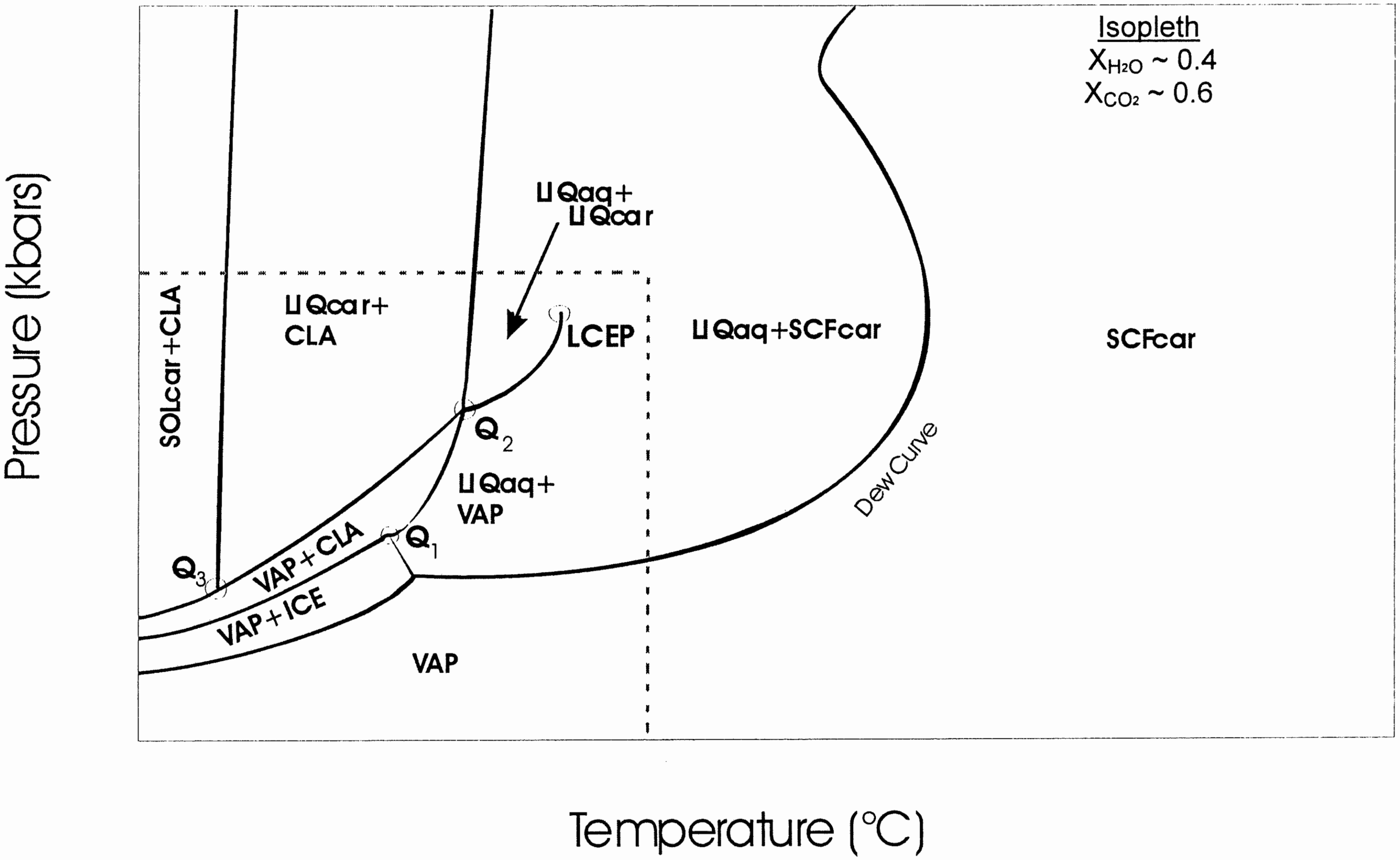

Figure 4.7. An isopleth in the CO_2-H_2O system. Note the presence of clathrate (CLA = CO_2•5.75H2O, solid) on the left hand (low-T) side of the graph. Drawing is not to scale; the dashed line represents the expanded portion of the diagram. Abbreviations used are detailed in Table 4.2. After Diamond (2001).

4.3.1 CO_2-H_2O systematics at high P-T

P-T conditions for the entrapment of fluid inclusions are generally well beyond all critical values for the H_2O-CO_2 system (Diamond, 2001). At high P-T conditions entrapped fluids should therefore be homogeneous (Bakker and Diamond, 2000; Diamond, 2001).

4.3.2 CO_2-H_2O systematics during cooling

Phase changes at T below those corresponding to likely temperature of entrapment for inclusions in high-grade metamorphic rocks are the basis of fluid inclusion microthermometry. The CO_2-H_2O system is described in terms of three elements defining a three dimensional P-T-X space. The complex phase relationships in the composite system (X_{CO_2}, $X_{H_2O} \neq 1$) were simplified by Diamond (2001) into four subsets, each compositional range defined by a representative isoplethic (constant composition) plane. Figure 4.8 shows Diamond's (2001) subsets, with given X_{H_2O} (X_{CO_2}) ranges.

Isoplethic P-T graphs are used to demonstrate phase relations for the various systems (Diamond, 2001). Isochores, or lines of equal density, run through P-T space for a given composition, intersecting phase boundaries at distinct P-T coordinates (Diamond, 2001). The temperature at which a phase boundary is crossed can be diagnostic of composition, e.g., in the case of purely carbonic inclusions, the homogenization temperature and whether the fluid homogenizes to either the liquid or vapour phase gives the density of the inclusions (Fig. 4.3; Diamond, 2001).

Excluding pure end-members of the compositional axis (*e.g.*, X_{H_2O}=1, X_{CO_2}=1) Diamond (2001) identified four model isopleths: high X_{H_2O}, low X_{CO_2}; very high X_{H_2O}, very low X_{CO_2}; low X_{H_2O}, high X_{CO_2}; very low X_{H_2O}, very high X_{CO_2} (Fig. 4.8 a, b, c, d respectively). The pure CO_2 phase is shown in Figure 4.8e. Several key points are common to two or more of the four models, and are detailed in Table 4.2, with pressure and temperature values and stable phases. The following discussion of phase relationships is based on Diamond (2001).

Figure 4.8a demonstrates the high X_{H_2O}, low X_{CO_2} range ($0.852 \le X_{H_2O} \le 0.985$, $0.015 \le X_{CO_2} \le 0.148$), common in low-to-moderate grade metamorphic rocks (Diamond, 2001). An arbitrary, purely qualitative, isochore has been drawn (in light grey) through the isopleth for the purposes of comparison with other isopleths (after Diamond, 2001). Fluid immiscibility dominates the phase relations. The bubble and dew curves are the upper and lower limits of the immiscibility field; fluid crossing (in P-T space) into the immiscible fluid field across these lines causes a bubble of CO_2 to emerge or aqueous fluid to dew (condense) on the inclusion wall, respectively. Following the sample isochore (*e.g.*, a fluid inclusion with a density defining the isochore) from low temperature, the inclusion starts at point 6, following the phase boundary VAP+ICE=CLA+ICE (see Table 4.2 for abbreviations) to point 5. At point 5, the ice melts (ICE=LIQaq), and follows the CLA+LIQaq=LIQaq+VAP phase boundary to point 4. At point 4, clathrate melts, forming a carbonic liquid bubble, which generally surrounds the vapour bubble. The fluid follows the LIQcar+VAPcar phase

Table 4.2. P-T data for selected points in the H_2O-CO_2 models of Diamond (2001). Modified after Diamond, 2001. Abbreviations for phases are detailed in Table 4.2.

Phase element	Symbol†	Phase assemblage	T (°C)	P (MPa)
CO_2 triple point*	$T_{3(car)}$	SOLcar+LIQcar+VAPcar	-56.56	0.518
CO_2 critical point*	$T_{c(car)}$	LIQcar+VAPcar=SCFcar	31.06	7.383
H_2O triple point*	$T_{3(aq)}$	SOLaq+LIQaq+VAPaq	0.01	0.0006
H_2O critical point*	$T_{c(aq)}$	LIQaq+VAPaq+SCFaq	373.95	22.06
Quadruple point 1**	Q_1	VAP+CLA+LIQaq+ICE	-1.48	1.034
Quadruple point 2**	Q_2	VAP+LIQcar+LIQaq+CLA	10	4.51
Quadruple point 3**	Q_3	SOLcar+VAP+LIQcar+CLA	-56.59	0.518
Lower critical end point**	LCEP	LIQcar+LIQaq+VAP=SCFcar+LIQaq	31.05	7.39
Composite critical point**	T_c	LIQaq+VAPaq+SCFcar=SCF	~373.95	22.06

* Points restricted to pure phases.

** Points restricted to composite phases.

† Symbols are those used in Figure 8.

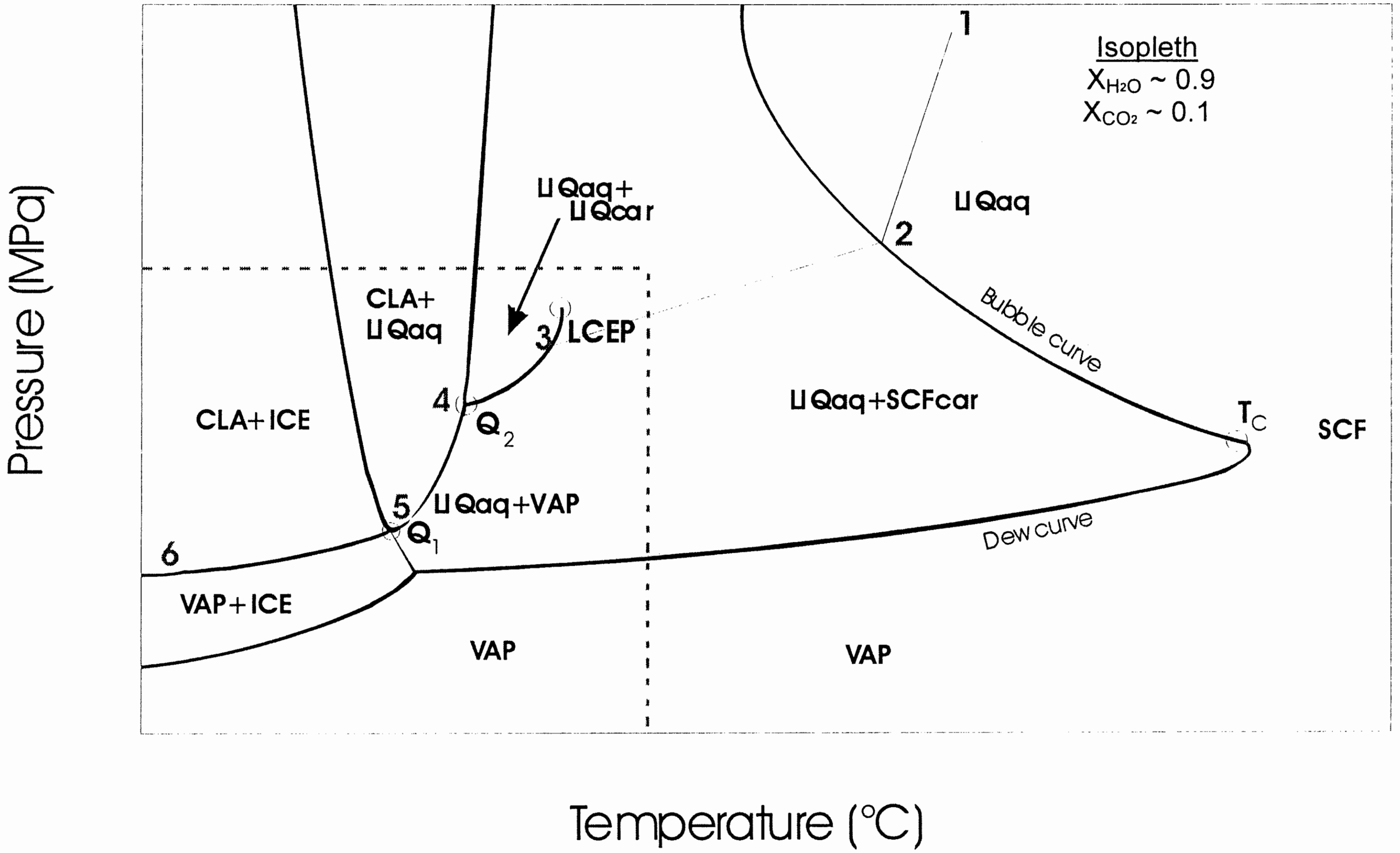

Figure 4.8a. An isopleth in the CO_2-H_2O system, representative of compositions $0.852 < X_{H_2O} < 0.985$. The example isochore is shown in light grey (see details in text). Drawing is not to scale; the dashed line represents the expanded area of the diagram. Abbreviations used are detailed in Table 4.2. After Diamond (2001).

boundary to point 3; point 3 represents the carbonic homogenization temperature, and therefore the carbonic fluid density for this particular isochore.

The carbonic liquid vapourizes to join the vapour bubble; a denser fluid than the sample isochore may homogenize to the liquid phase, depending on where exactly the isochore intersects the LIQcar=VAPcar boundary. Denser inclusions intersect the boundary from the liquid region, and will homogenize to the liquid phase during reheating; less dense inclusions intersect the boundary from the vapour side, and homogenize to the vapour phase (Fig. 4.3). The fluid traverses the immiscible fluids field from point 3 to point 2, until intersection with the bubble curve at point 2, where the aqueous fluid dissolves the carbonic fluid. Point 1 represents a possible entrapment point for the fluid, though entrapment at any point along the isochore and above point 2 will result in a fluid inclusion following the sample isochore.

Figure 4.8b demonstrates the very high X_{H_2O}, very low X_{CO_2} range ($0.985 < X_{H_2O} < 1$, $0 < X_{CO_2} < 0.015$). Carbonic liquid never occurs in the very high X_{H_2O} range; CO_2 is present only in the vapour phase. The immiscible fluid field is reduced to a slim field where both aqueous fluid and vapour phases are stable. The sample isochore, starting at very low temperature, starts in the VAP+ICE stability field, until the ice melts at point 3. The fluid traverses the immiscibility field to point 2, at which point the aqueous fluid dissolves the vapour phase. Point 1 represents a possible entrapment point for the fluid, though entrapment at any point along the isochore and above point 2 will result in a fluid inclusion following the sample isochore.

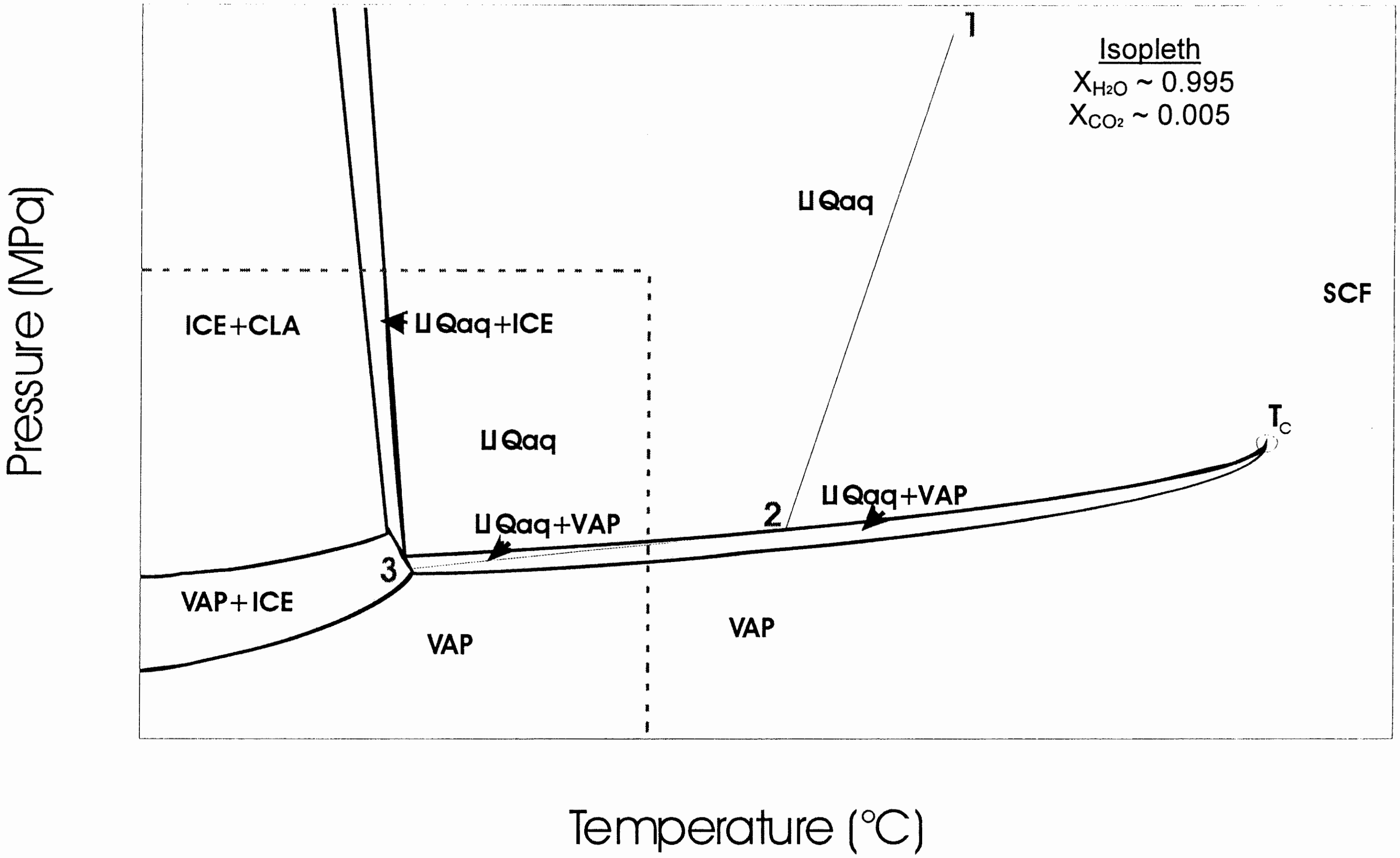

Figure 4.8b. An isopleth in the CO_2-H_2O system, representative of compositions $0.985 < X_{H_2O} < 1$. The example isochore is shown in light grey (see details in text). Drawing is not to scale; the dashed line represents the expanded area of the diagram. Abbreviations used are detailed in Table 4.2. After Diamond (2001).

Figure 4.8c demonstrates the low X_{H_2O}, high X_{CO_2} range ($0.002 < X_{H_2O} < 0.852$, $0.148 < X_{CO_2} < 0.998$), common in moderate-to-high grade metamorphic rocks (Diamond, 2001). The large range of compositions covered by the low X_{H_2O} model allows for considerable variability in the size and shape of the immiscibility field. The most prominent feature of the phase diagram is the increased importance of carbonic phases. Only at phase boundaries are any aqueous phases other than the vapour phase stable with the clathrate. Aqueous liquid may not exist outside the immiscible fluid field, depending on the exact fluid composition; the low temperature liquid is carbonic, and freezes to solid CO_2. Following the sample isochore, the fluid starts on the SOLcar+CLA=VAP+CLA phase boundary. As temperature is increased, the carbonic solid melts to liquid CO_2 at point 5, and follows the LIQcar+CLA=VAP+CLA phase boundary to point 4. At point 4, the clathrate melts, creating a carbonic bubble which separates into liquid and vapour bubbles, leaving three phases in the inclusion (aqueous liquid, carbonic liquid, and vapour). The fluid follows the LIQaq+LIQcar=LIQaq+VAP phase boundary to point 3, where the vapour and carbonic liquid phases homogenize. The fluid crosses the immiscibility field, to homogenize at point 2. Point 1 represents a possible entrapment point for the fluid, though entrapment at any point along the isochore and above point 2 will result in a fluid inclusion following the sample isochore.

Figure 4.8d demonstrates the very low X_{H_2O}, very high X_{CO_2} range ($0 < X_{H_2O} < 0.002$, $0.998 < X_{CO_2} < 1$), common in high-grade metamorphic rocks (Diamond, 2001). The very low X_{H_2O} range of compositions is essentially

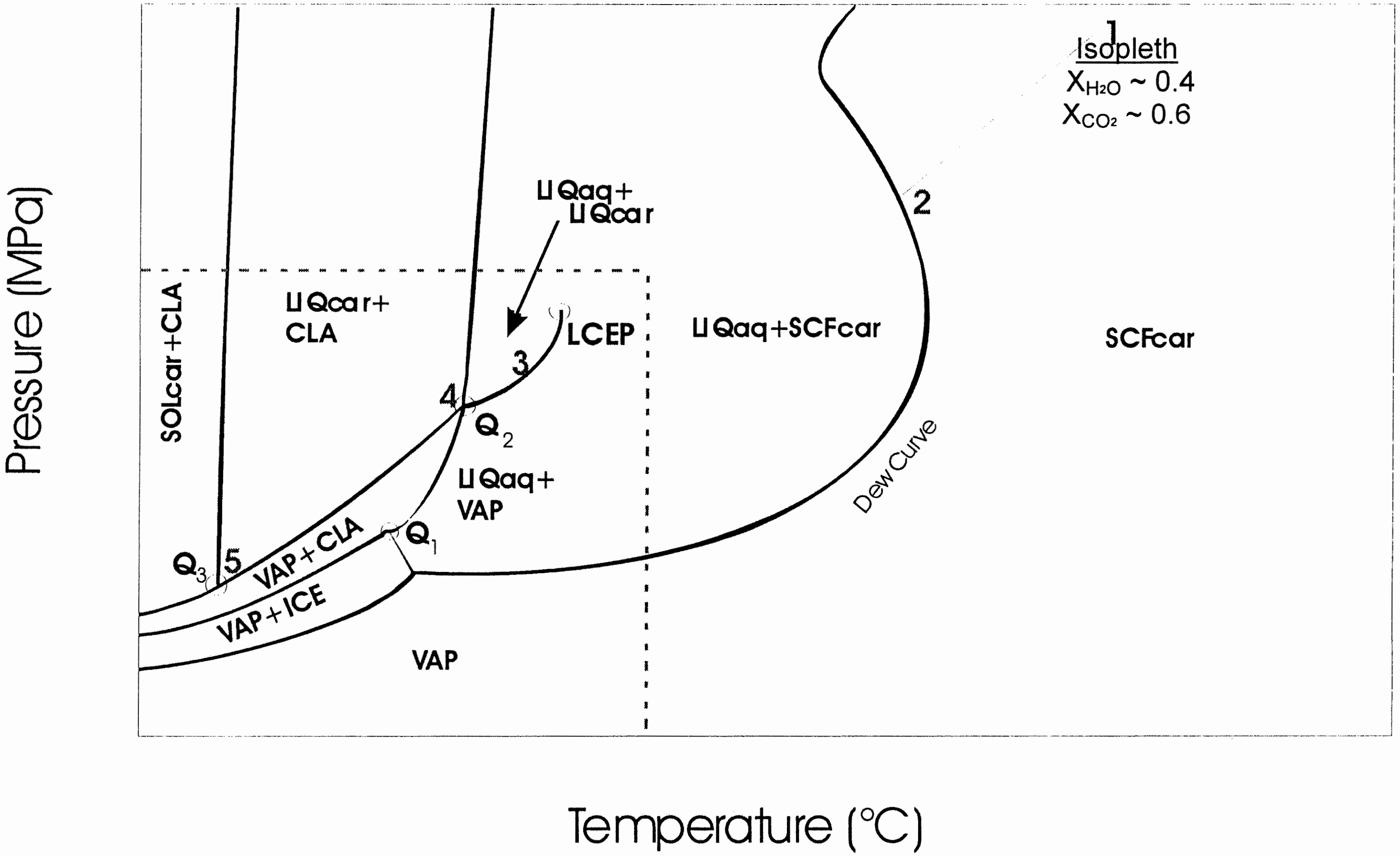

Figure 4.8c. An isopleth in the CO_2-H_2O system, representative of compositions $0.002 < X_{H_2O} < 0.852$. The example isochore is shown in light grey (see details in text). Drawing is not to scale; the dashed line represents the expanded area of the diagram. Abbreviations used are detailed in Table 4.2. After Diamond (2001).

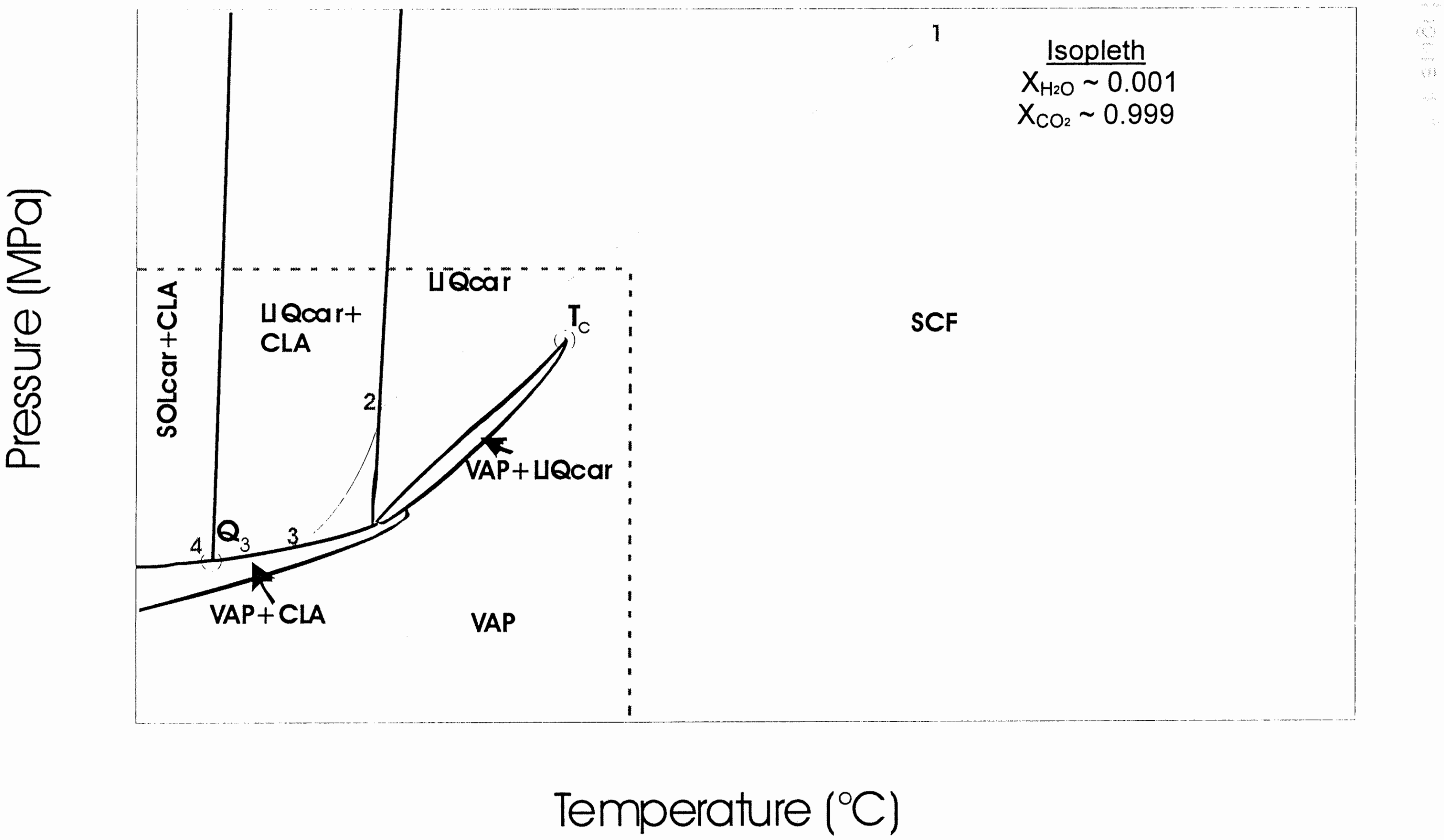

Figure 4.8d. An isopleth in the CO_2-H_2O system, representative of compositions $0 < X_{H_2O} < 0.002$. The example isochore is shown in light grey (see details in text). Drawing is not to scale; the dashed line represents the expanded area of the diagram. Abbreviations used are detailed in Table 4.2. After Diamond (2001).

equivalent to the pure CO_2 phase, and all phase relationships shown are essentially theoretical (Diamond, 2001).

Figure 4.8e demonstrates the pure CO_2 phase diagram ($X_{H_2O}=0$, $X_{CO_2}=1$), and is representative of all compositions with $X_{H_2O} < 0.002$ (Diamond, 2001). The triple point, at which liquid, solid, and vapour phases are stable, occurs at -56.56 °C, 0.518 MPa (Diamond, 2001). The sample isochore starts in the solid-vapour phase boundary, and proceeds to point 3 (the triple point) on heating. Upon melting, two phases emerge, a liquid and a vapour; the fluid follows the phase boundary LIQcar=VAPcar to point 2, where the fluid homogenizes, on the sample isochore, to the liquid phase. Point 1 represents a possible entrapment point for the fluid, though entrapment at any point along the isochore and above point 2 will result in a fluid inclusion following the sample isochore.

4.4 Fluid inclusion petrography

Because of ambiguity inherent in the primary-secondary terminology (names imply genesis, but are mainly texturally derived), Touret (2001) suggested the term Groups of Synchronous Inclusions (**GSI**'s) for describing fluid inclusions. GSI's are based on compositional and textural features, and attempt to describe populations of inclusions, without implying genesis or order of entrapment (Touret, 2001). For descriptive purposes, the terminology of Touret (2001) is used for fluid inclusion petrography. Interpretation of genesis, with evidence, may warrant a return to the standard terminology.

Samples MZ-1A, MZ-1B and MZ-2A were analyzed petrographically, using a binocular microscope in transmitted light. Appendix H contains selected fluid

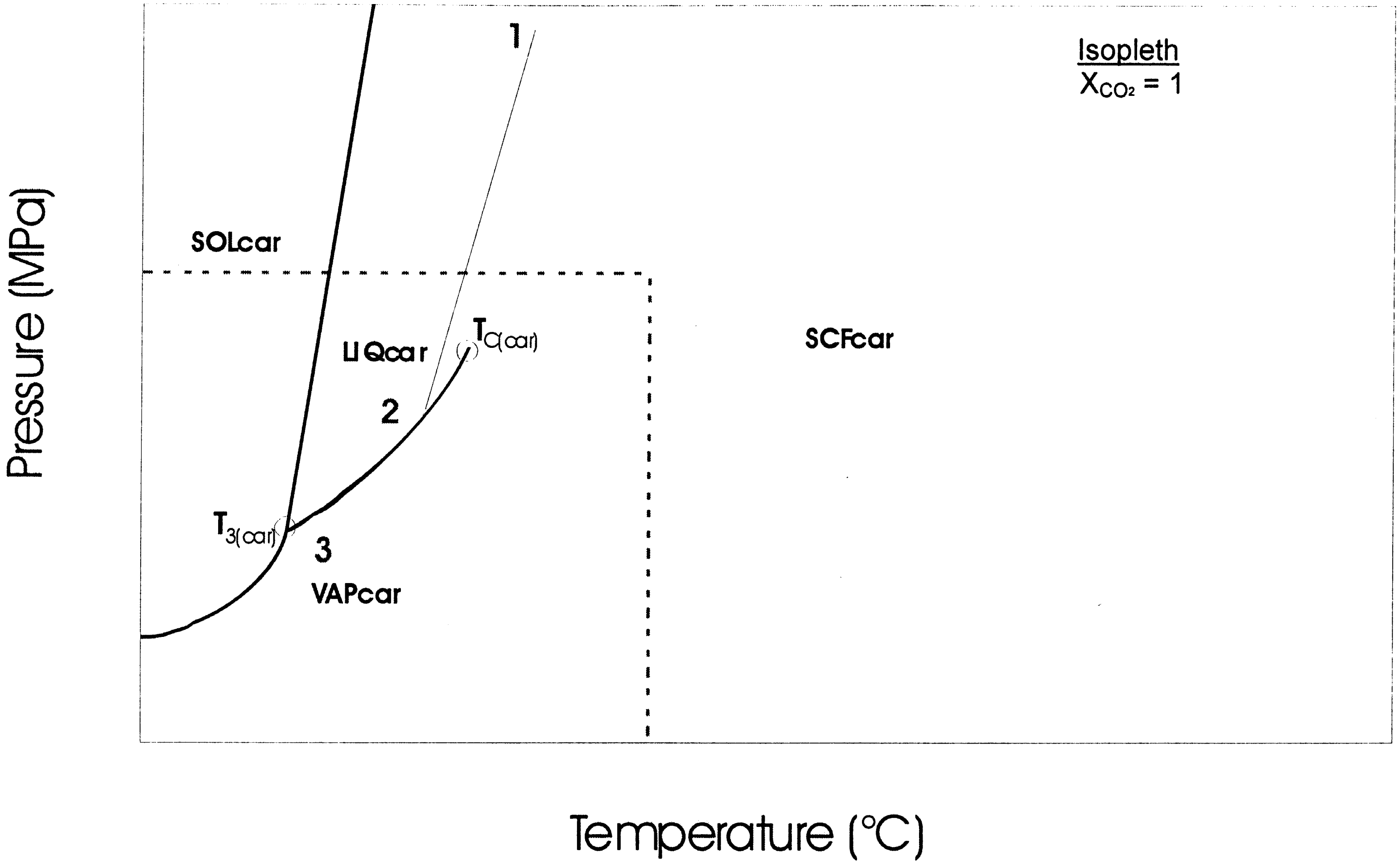

Figure 4.8e. P-T phase relations for pure CO_2. The example isochore is shown in light grey (see details in text). Drawing is not to scale; the dashed line represents the expanded area of the diagram. Abbreviations used are detailed in Table 4.2. After Diamond (2001).

inclusion photos, with sample numbers and general descriptions. Host rocks are garnetiferous migmatitic gneisses, containing garnet, biotite, K-feldspar, plagioclase and quartz (Fig. 4.9). Two GSI's were recognized in garnet in petrographic analysis, and are described below: GSI-a, and GSI-b.

GSI-a comprises single phase, negative crystal-shaped fluid inclusions (Fig. 4.10). GSI-a fluid inclusions are generally in planar clusters or arrays, and range in size from <2 - ~60 μm along the long axis. Average fluid inclusion size is <10 μm. Planes show no discernible orientation or pattern and dip shallowly to steeply from the plane of the polished section. Some planes appear to be curviplanar in habit. Fluid inclusion arrays also contain small, highly birefringent, mineral grains of unknown composition; commonly, a fluid inclusion wets a mineral grain. Larger (>20 μm) fluid inclusions wet large silicate grains. Melting temperatures (presented in section 4.5) indicate that GSI-a fluid inclusions are virtually pure CO_2. Rare single phase CO_2 inclusions have elongate, necked, shapes (Fig. 4.10c).

GSI-b comprises two phase (liquid and vapour), elongated to negative crystal-shaped fluid inclusions (Fig. 4.11). GSI-b fluid inclusions generally form planar arrays, and range in size from <5 - >200 μm along the long axis, with an average size of 15-20 μm. Planes show no discernible orientation or pattern and dip shallowly to steeply from the plane of the polished section. Fluid inclusion arrays also contain small mineral grains of unknown composition which the fluid inclusions commonly wet. Grains appear similar to the grains found in GSI-a

Figure 4.9

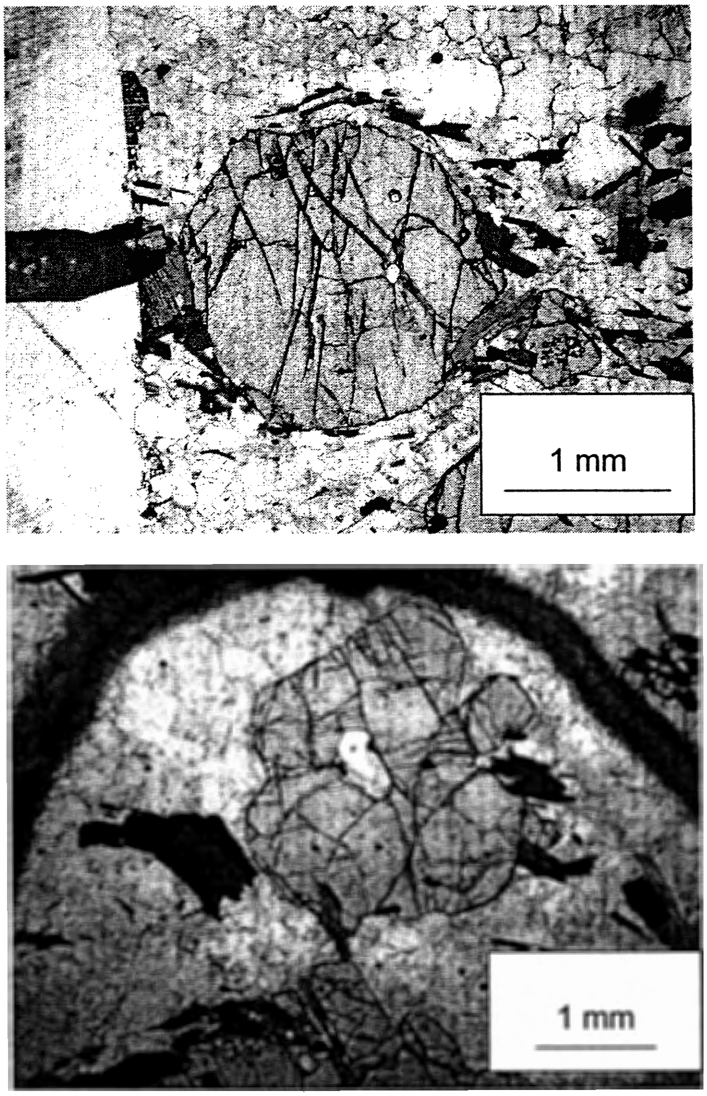

Figure 4.9. Examples of migmatitic host rocks and garnets. Above, MZ-1A; below, MZ-2A. Dark laths are biotite, matriz is quartz and feldspars. The black semi-transparent marks (on the left in the upper photo, and the hemi-circle in the lower photo) are black ink marks used to relocate grains.

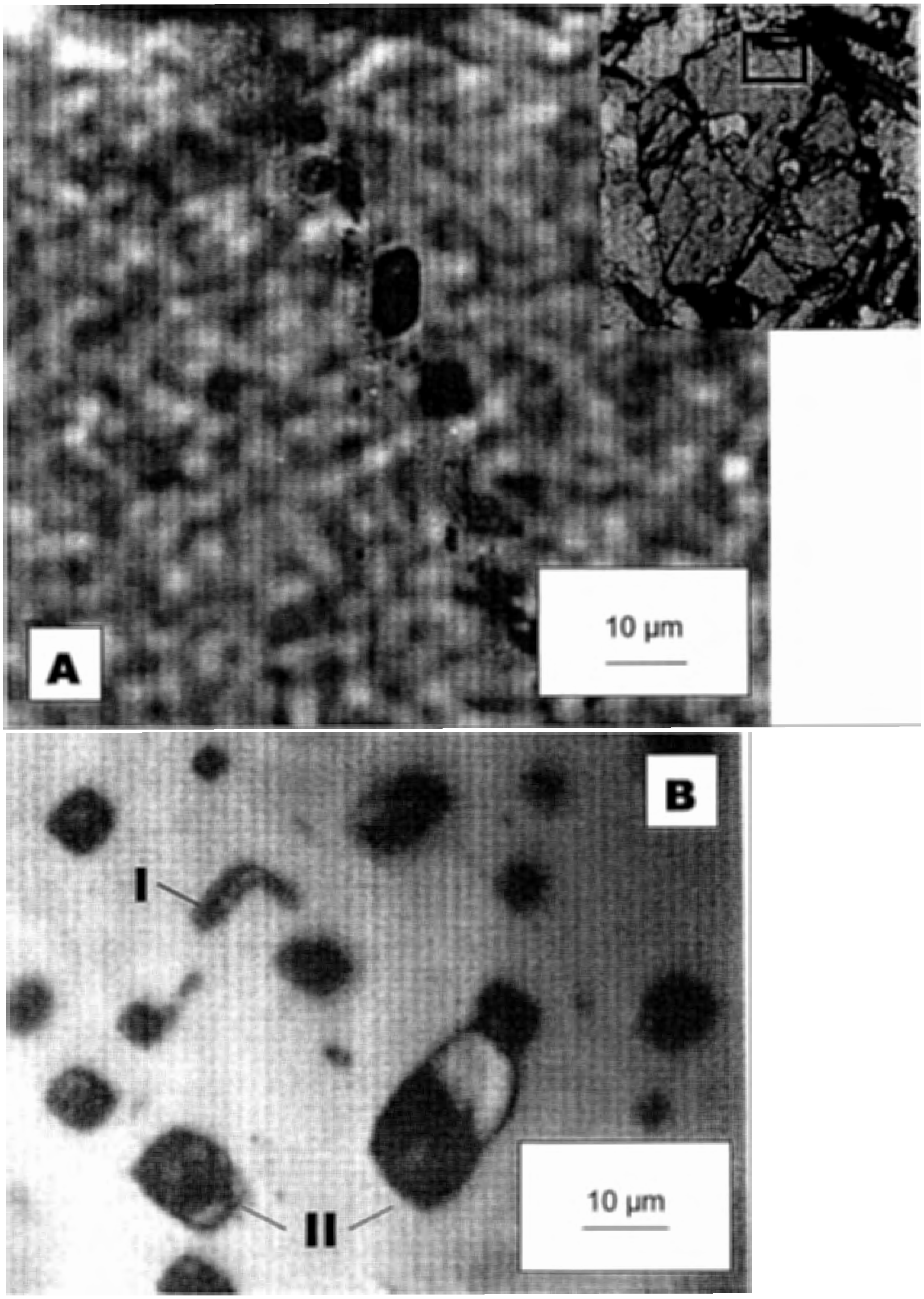

Figure 4.10. GSI-a type fluid inclusions in garnet; both photos are from sample MZ-1A. A) A planar array of GSI-a inclusions in garnet; inset is host garnet grain, grain is 0.7 mm across. B) GSI-a inclusions showing several textural features: I – necked non-negative crystal shaped, II – wetting solid inclusions. Photo (B) by Dan Kontak.

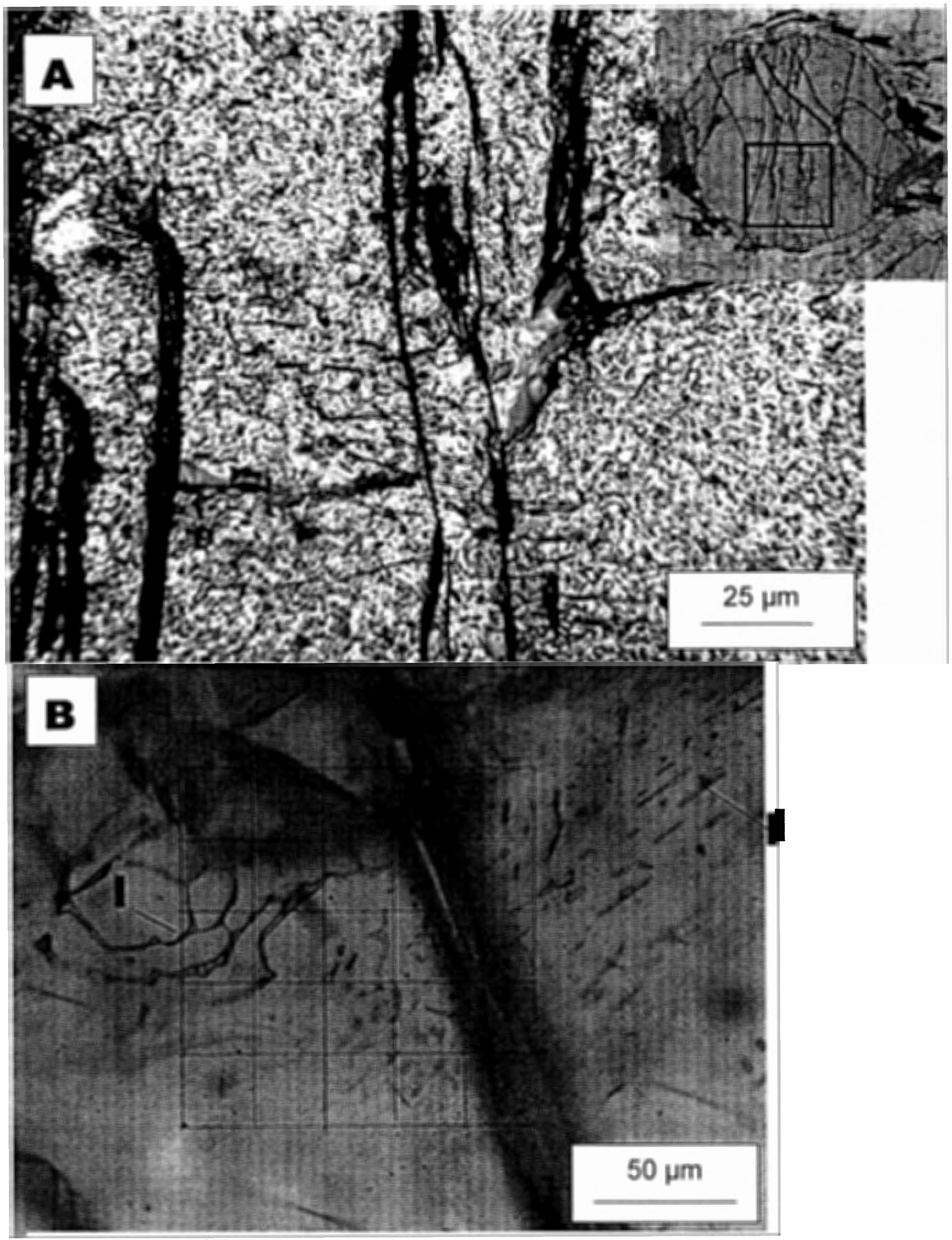

Figure 4.11. GSI-b type fluid inclusions in garnet; both photos are from sample MZ-1A. A) A planar array of GSI-b inclusions in garnet; inset is host garnet grain, grain is 2 mm across. B) GSI-b inclusions showing several textural features: I – elongate, branching inclusions, II – necked,

several interconnected arms. Negative crystal-shaped fluid inclusions and longer branching inclusions seem to have a gradational relationship in some places; *i.e.*, elongate inclusions appear to fine into negative crystal-shaped inclusions. GSI-b fluid inclusions have, based on visual estimates, variable liquid vapour ratios. Melting temperatures indicate that the vapour phase is virtually pure CO_2 (Tm= -56.6 °C) and the liquid phase is aqueous.

In relation to the host mineral, both GSI-a and GSI-b type fluid inclusions are randomly oriented. Garnet lacks growth zoning; both GSI-a and GSI-b are present in the core and the rim of host garnet crystals. Intersections of planes of GSI-a and GSI-b were not found; fractures cut both GSI-a and GSI-b planes. Several GSI-a planes intersect in sample MZ-1A.

4.5 Microthermometry results

GSI-a fluid inclusions in sample MZ-1A were analyzed microthermometrically, using a U.S. Geological Survey gas-flow heating-freezing stage (FLUID INC.) at the Nova Scotia Department of Natural Resources (Kontak, 1998). Selected inclusions were >20 μm in size. Results are tabulated in Table 4.3; a range of high-density CO_2 inclusions shown as isochores in Figure 4.12. Homogenization temperatures range from -22 to +6 °C (always to the liquid phase), corresponding to CO_2 densities *ca.* 1.03 - 0.89 g/cm^3. The phase relations seen in these inclusions fit the pure CO2 end member phase diagram (Fig. 8e).

Figure 4.12

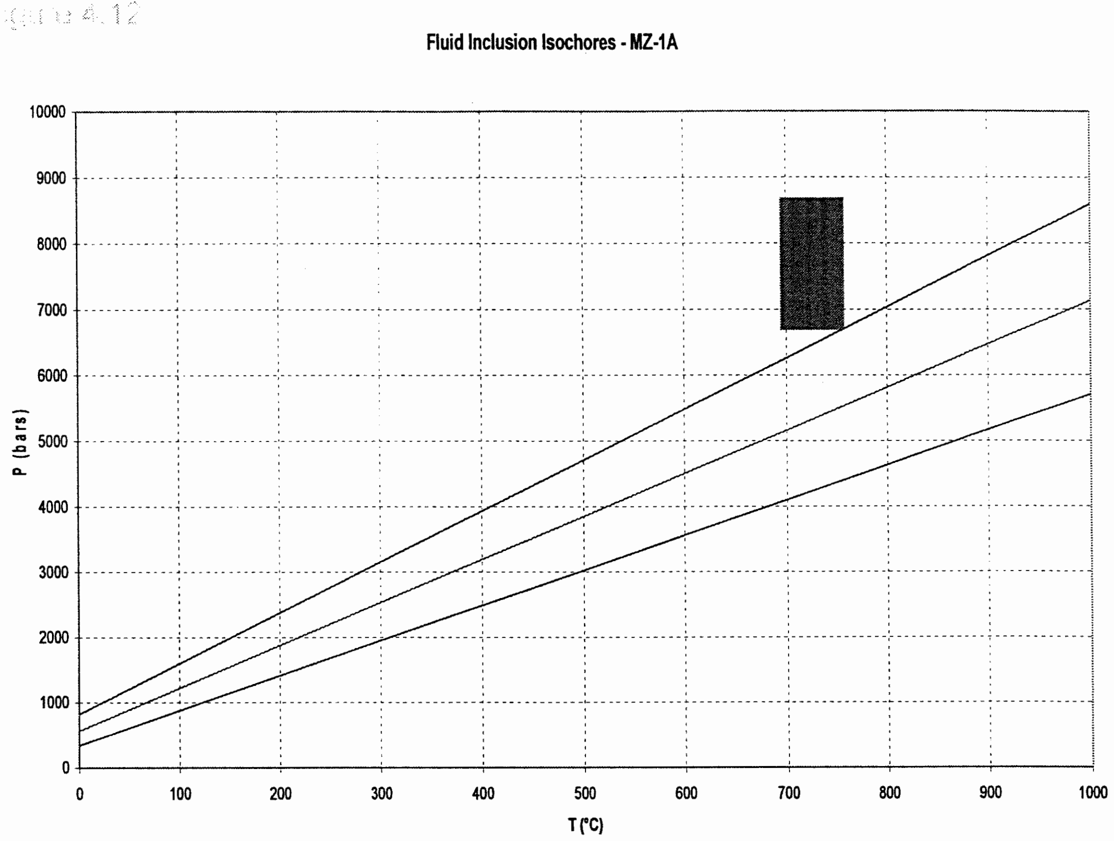

Figure 4.12. Calculated isochores for CO_2, GSI-a inclusions. The upper line represents the densest inclusions: T_h=-22 °C, density *ca.* 1.03 g/cm^3. The middle line represents moderate inclusions: T_h=-8, density *ca.* 96 g/cm^3. The lower line represents the least dense inclusions: T_h=+6, density *ca.* 0.89 g/cm^3. The grey box represents the calculated P-T conditions for sample MZ-2B, with assumed errors

Table 4.3. Microthermometric results for GSI-a fluid inclusions in MZ-1A

Isochore points

T_h (°C)	-22	-19	-11	-9	-8	-5	-2	0	3	6
P (at 400 °C)	3930	3768	3319	3242	3191	3038	2876	2786	2636	2486
P (at 600 °C)	5484	5269	4676	4573	4504	4300	4084	3963	3761	3559

Increases in melting temperature are indicative of impurities in the fluid. These inclusions may fit the very high CO_2 member of the CO_2-H_2O composite fluid system (Fig. 8d).

GSI-b type inclusions in sample MZ-1B were frozen, and carbonic phases melted *ca.* -56 °C. Aqueous phases melted *ca.* -22 °C. Variable liquid-vapour ratios required more measurements than were possible in the given time frame of this study. These inclusions fit the low H_2O member of the CO_2-H_2O composite fluid system (Fig. 8c).

4.6 Laser Raman Analysis

Laser Raman analyses were performed by Dr. Dan Marshall at Simon Fraser University utilizing a red (632.8 nm) laser as an excitation source. The laser beam interacted with the sample via an Olympus 100X long working distance objective and the scattered light was collected using a Dilor LabRam Raman spectrometer. The scattered light was then detected using a two-dimensional cryogenically cooled detector (CCD; D. Marshall, written communication).

The microscope used to target the samples and to collect the scattered Raman light was an Olympus® model BX50 petrographic reflected and transmitted light microscope equipped with a motor driven x-y stage. The microscope was equipped with 10X, 50X, 100X and long working distance objectives. The lower power objectives were used to target the fluid inclusions for analyses with all analyses being performed with the 100X. Multiple scans of different fluid inclusions indicated that this lens yields the maximum signal peak to background ratios for fluid inclusions analyses (D. Marshall, written communication).

All analyses were performed in non-confocal (normal) mode as numerous scans of test fluid inclusions indicated that this yielded optimum signal to background ratios, as the fluid inclusions were always larger than the 2 micron sample depth that can be obtained with the system in confocal mode. To avoid any heterogeneities that may be present within a fluid inclusion analyses were performed on the maximum depth of the phase of interest within the fluid inclusion (D. Marshall, written communication).

The software used to collect the Raman Spectra was the Dilor® software running on a PC compatible computer. Counting times for the individual spectra varied from between 8 and 30 minutes, depending on the size and depth of the target fluid inclusions (D. Marshall, written communication).

4.6.1 Results

Laser Raman spectroscopy was performed on a GSI-a inclusion. Peaks in the spectroscopic analysis indicate that the fluid is pure CO_2.

4.7 Discussion

Both GSI-a and GSI-b type fluid inclusions are, in the terminology of Roedder (1984) and Goldstein and Reynolds (1994), secondary fluid inclusions. Both GSI-a and GSI-b are variably necked planes, formed by fluid influx into fractures in garnet.

Solid inclusions of unknown composition are entrapped within the fluid inclusion planes of both types. Both types of inclusions wet the solid inclusions.

The solid inclusions were likely entrapped at the same time as the wetting fluid. Entrapment of the solid phases in the fracture with the fluid indicates that the solid phase was in equilibrium with the metamorphic assemblage when garnet recrystallized.

The presence of the solid inclusions, in equilibrium with the rocks when garnet recrystallized to trap the fluid, and the secondary nature of both sets of inclusions suggests that the two types of fluid inclusions have a shared origin. The presence of two distinct fluid types and the difference in the amount of necking suggest that the inclusions represent two distinct fluids.

The P-T conditions of entrapment for CO_2 fluid inclusions may fall along the P-T path as outlined by Timmermann (1998; Figure 4.13). As the rocks cooled from peak metamorphism, garnets annealed, trapping the equilibrium fluid assemblage. The low a_{H_2O} of the fluid may be one reason for the lack of late-stage retrograde metamorphism in the rocks.

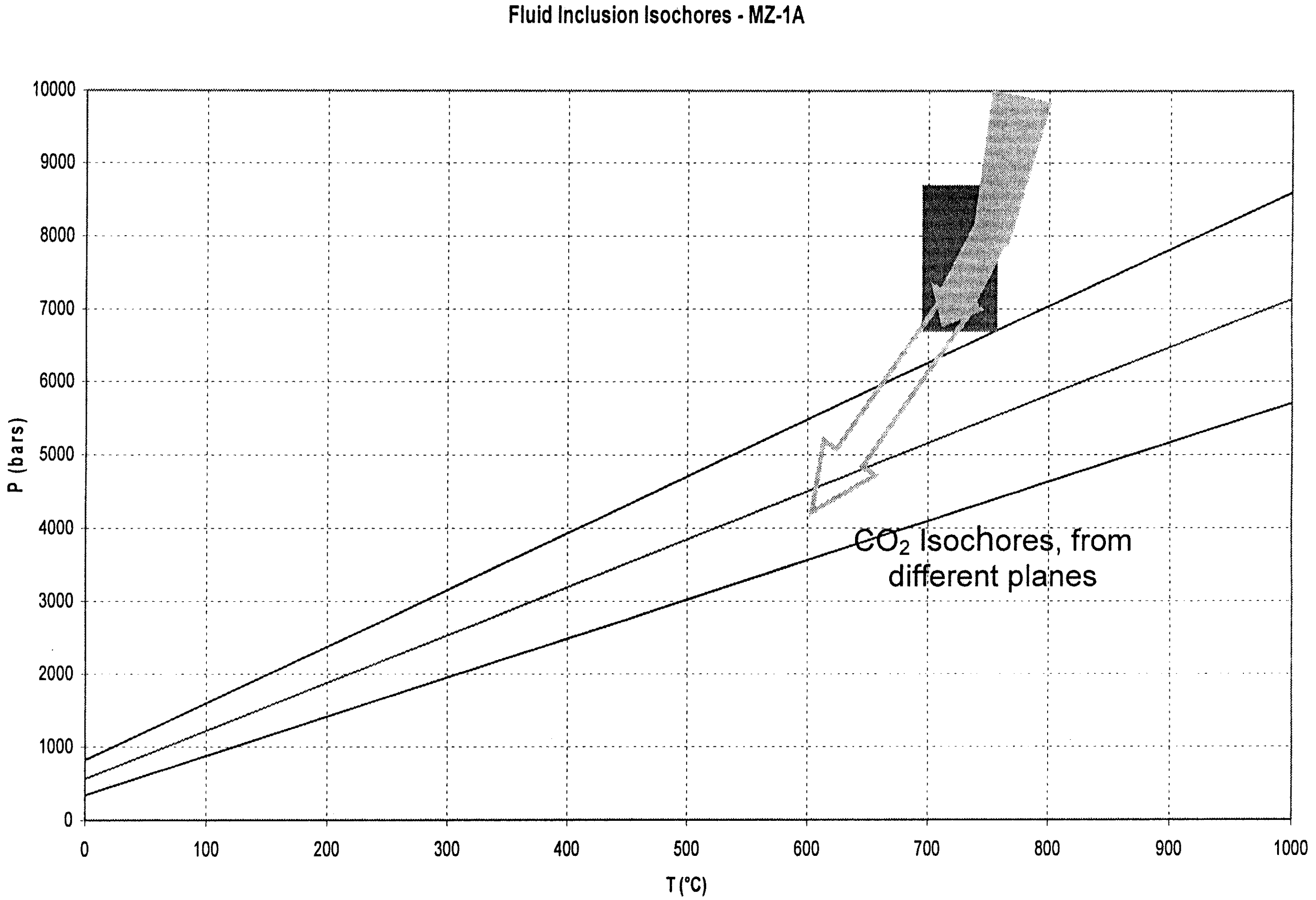

Figure 4.13. P-T path. Timmermann's (1998) suggested P-T path for the Birkendale assemblage, with CO_2 isochores from fluid inclusions in garnets.

5.0 Geochronology

Monazite dating was performed to constrain ages on garnet growth and possible fluid inclusion entrapment. Monazite was selected for the in situ, non-destructive, aspect of the technique. Figure 5.1 shows a compilation of ages for the Central Gneiss Belt, showing the polycyclic nature of rocks within the CGB. Large portions of the CGB have experienced two or more episodes of metamorphism, with the latest being the Grenvillian Orogeny.

5.1 Previous Work

The Ottawan stage of the Grenville Orogeny has been dated from 1080 to 980 Ma (Jamieson *et al*, 1992; Culshaw *et al*, 1997; Carr *et al*, 2000). In general, tectonic and metamorphic ages reflect a younging trend to the northwest, towards the GFTZ (Jamieson *et al*, 1992; Culshaw *et al*, 1997). A suite of plutonic and metamorphic ages is recorded within the rocks of the Algonquin domain, reflecting multiple events of metamorphism, *i.e.*, polycyclic.

Previous work in the Algonquin domain has recognized two distinct metamorphic events: *ca.* 1450 Ma and *ca.* 1040 Ma (*e.g.*, van Breemen and Davidson, 1990; Nadeau and van Breemen, 1998; Timmermann, 1998). Plutonism was common during the *ca.* 1450 Ma event (Nadeau and van Breemen, 1998; Timmermann, 1998). Late syn-thrusting and extensional shear accompanied the *ca.* 1040 event (Nadeau, 1990). Nadeau (1990) also identified a 1715 +123/-71 Ma plutonic event in the Huntsville subdomain.

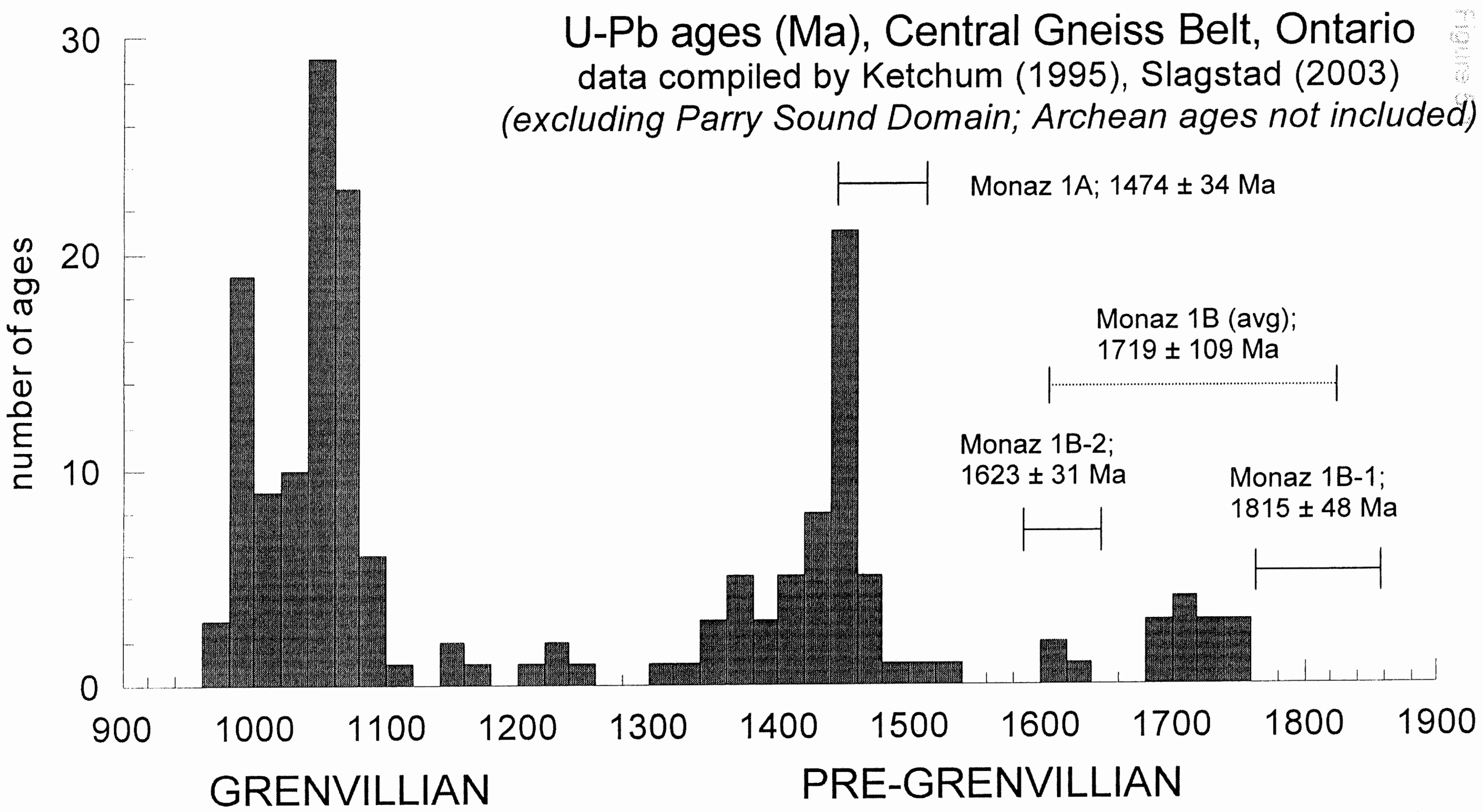

Figure 5.1. A compilation of ages from the CGB, Grenville Province, shown in gray. Age data from Monaz 1A and Monaz 1B is given above the histogram. Modified after R.A. Jamieson (pers.comm.).

5.2 Monazite microprobe dating methodology

5.2.1 Monazite [(Ce, Th, REE)PO_4] as a geochronometer

Monazite is a phosphate mineral [(Ce, Th, REE)PO_4] common as an accessory phase in igneous and metamorphic rocks (Williams and Jercinovic, 2002). Monazite is also common as detrital material in beach sands and sedimentary/metasedimentary rocks (Deer *et al*, 1992). Due to relatively high concentrations of Th (*ca.* 3-15 wt%) and U (*ca.* 100 ppm – 5 wt%) and its relative abundance as an accessory mineral, monazite has become a candidate for chemical U-Th-Pb dating, especially for high-grade metamorphic rocks (Montel *et al*, 1996; Foster *et al*, 2000).

Both U and Th have radioactive isotopes (^{235}U, ^{238}U, and ^{232}Th) that decay (via decay chains) to Pb daughter products (^{207}Pb, ^{206}Pb, and ^{208}Pb, respectively; Steiger and Wasserburg, 1966), as follows:

$$^{235}U \longrightarrow {}^{207}Pb + 7\alpha + 4\beta \qquad \text{Eq. 5.1a}$$

$$^{238}U \longrightarrow {}^{206}Pb + 8\alpha + 6\beta \qquad \text{Eq. 5.1b}$$

$$^{232}Th \longrightarrow {}^{208}Pb + 6\alpha + 5\beta \qquad \text{Eq. 5.1c}$$

(Faul, 1966)

The radioactive decay of these isotopes occurs along a natural time scale given, mathematically, as the decay constant (Fowler, 1990). Each radioactive isotope has its own particular decay constant.

Two assumptions are necessary for chemical age calculations: 1) that there is no source of daughter material except as a decay product from the parent material (for U-Th-Pb dating, inherited Pb is called ‘common Pb’), 2) that there have been no other changes (outside radioactive decay) to the parent-daughter ratios, *i.e.*, the system is closed (Montel et al, 1996).

U-Th-Pb ages are generally calculated from ratios determined by isotopic analyses (Fowler, 1990). Monazite dating by electron microprobe does not measure isotopic concentrations. Rather, radioactive parent isotopic concentrations are assumed to be at the levels of crustal abundances, and the daughter Pb is proportioned in the calculations (see Appendix G; Montel *et al*, 1996). Common Pb occurrence in monazite is negligible (<1 ppm; Parrish, 1990), and diffusion rates in monazite are believed to be quite low (the system is essentially closed to diffusive Pb loss; Parrish, 1990; Montel *et al*, 1996).

Monazite ages (as with most radiometric dates) may represent either the crystallization age or cooling age for a given grain (Cliff, 1985). If the mineral formed below the closure temperature for monazite (*e.g.*, the temperature below which diffusion no longer removes the daughter product from the mineral), and has not gone above that temperature during history of the grain, the calculated age is a crystallization or growth age (Cliff, 1985). Cooling ages represent the time at which a grain formed at $T > T_C$ cooled through its closure temperature (Dodson, 1973).

Monazites are commonly chemically and/or chronologically zoned. Older cores may be overgrown by younger overgrowths. Younger rims are typically embayed, and show some chemical difference from the older core. One of the main advantages of spot-dating techniques, such as SHRIMP (Sensitive High

Resolution Ion MicroProbe) and monazite dating via electron microprobe, is the ability to date specific micron-scale points within a zoned grain.

Another advantage to in situ dating via electron microprobe, compared to dating methods requiring the removal of the grain, *i.e.*, TIMS (Thermal Isotopic Mass Spectrometry), lies in the nondestructive aspect of the method. Both petrographic features, such as grain location or relations to surrounding grains, and the datable material itself are preserved. These factors allow for reproducibility of dating for comparison and confirmation, as well as later comparison to other petrological features, *e.g.*, fluid inclusions.

5.2.2 Monazite dating methods

Samples used for monazite dating had been previously prepared as doubly polished thin sections ~75 µm thick for fluid inclusion work. For the purposes of monazite dating, the samples were given double carbon coatings. The microprobe used was a JOEL JXA-8200 at Dalhousie University, Halifax, Nova Scotia. For monazite dating, 200 na of beam current and a 600 second count time are used for trace element analysis (U, Th, Pb, Y). Other instrument conditions are the same as those for normal analysis.

Monazite grains were identified first during microprobe analyses of inclusions in garnets, and confirmed with a petrographic microscope. Two monazite grains included in garnets were selected for analysis, one in the core of garnet MZ-1B-0.4, the other in the rim of garnet MZ-1A-0.3 (Fig. 5.2), and the locations noted so that they could be relocated.

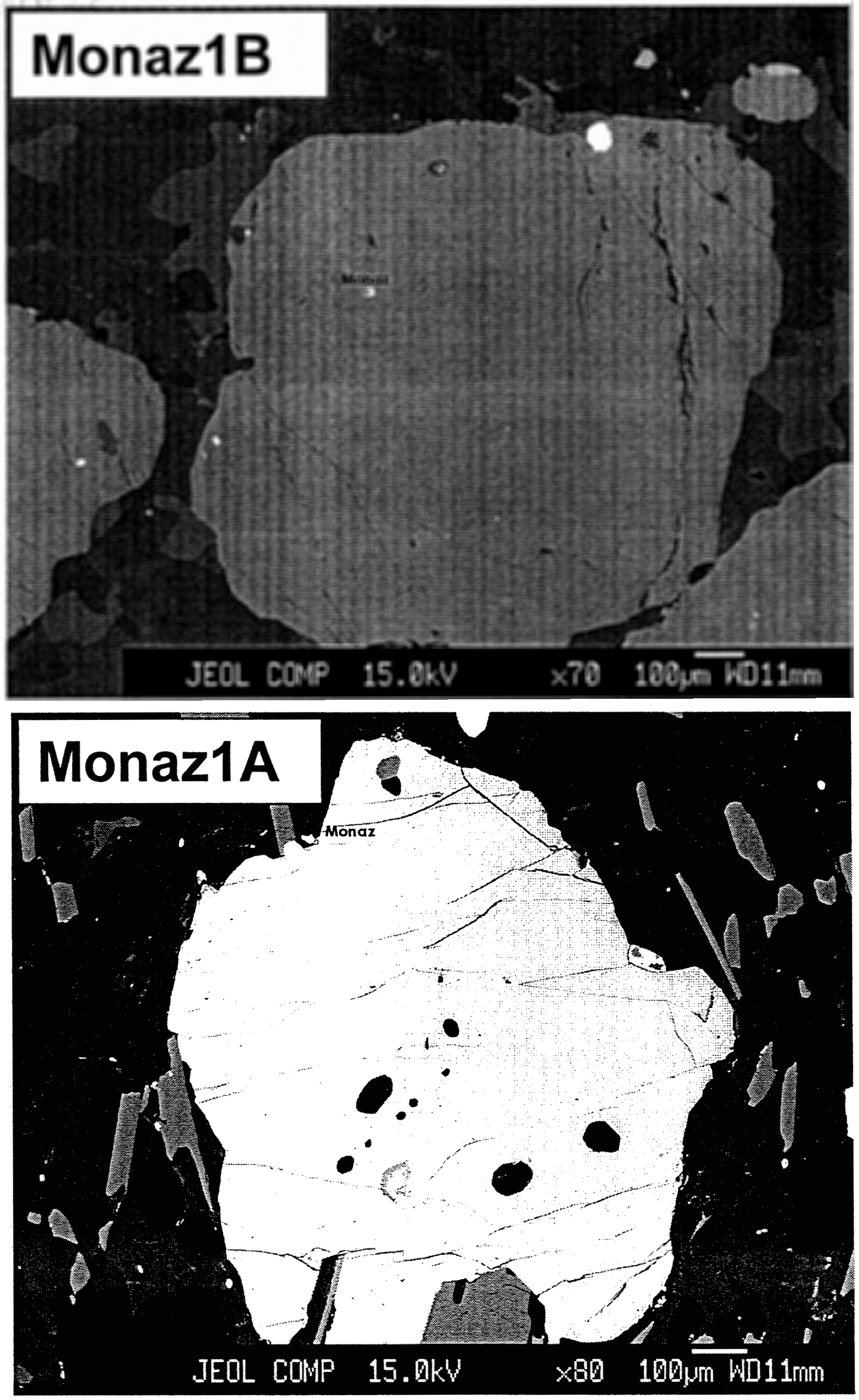

Figure 5.2. BSE images of garnets hosting dated monazite grains. Monaz1B is in sample MZ-1B, and Monaz1A is in sample MZ-1A. Note that Monaz1A is partially in contact with the matrix, but is enclosed on three sides by garnet.

High contrast backscatter electron (BSE) images were taken for both monazite grains. Heavy element zoning is readily visible. X-ray maps for U, Th, Y, and Pb were obtained from the monazite grains, and major element analyses were obtained from each chemical domain.

Chemical domains were identified using the chemical maps and BSE's. Trace element analyses U, Th, Y, and Pb were obtained for each identified domain. Ages are calculated iteratively, using the equations of Montel *et al* (1996):

$$\mathrm{Pb} = \frac{\mathrm{Th}}{232} \bullet [e^{(\lambda 232 * t)}-1] \bullet 208 + \frac{U * 0.9928}{238.04} \bullet [e^{(\lambda 238 * t)}-1] \bullet 206 + \frac{U * 0.0072}{235} \bullet [e^{(\lambda 235 * t)}-1] \bullet 207 \qquad \text{Eq. 5.1}$$

where Th and U are the measured quantities of those elements in parts per million (ppm), λ^{232}, λ^{238}, λ^{235} are the decay constants for Th^{232}, U^{238}, and U^{235}, respectively, and t is age in years. U^{238} and U^{235} are assumed to have the same relative proportion as in the crust (99.28% and 0.72%, respectively). In practice, the calculation is done by first estimating the age, then calculating the amount of Pb that would be in the sample, if the sample were that age, and comparing the estimate to the measured Pb value. The procedure is repeated until Pb (calculated) is equal to Pb (measured), narrowing the age through trial and error. Appendix G contains a sample calculation using some data from sample Monaz 1B. It should be noted that $Pb_{measured}$ is corrected, based on Y, because of peak overlap effects.

5.3 Monazite age results

Two monazite grains were selected for analysis: a grain in the core of garnet MZ-1B-0.4 (**Monaz 1B**, Table 5.1a, Figure 5.3), and a grain in the rim of garnet MZ-1A-0.3 (**Monaz 1A**, Table 5.1b, Figure 5.4). Two grains were selected to relate to fluid inclusions. Garnets in sample MZ-1A-0 have large, grain wetting, GSI-a type fluid inclusions, although not in the same garnet that contains the analyzed monazite grain. Sample MZ-1B-0.4 contains GSI-b type fluid inclusions.

Monaz 1B is 25 µm in size, and included in the core of a garnet crystal (Fig. 5.4). Figure 5.3 presents X-ray maps for Th, U, Y, and Pb. Y is zoned to the rim of the crystal. Averaged over the grain, the calculated age for Monaz 1B is 1719 ± 109 Ma. Spot dating allows recognition of two age domains (Fig. 5.4): for points 1-4, in the core, the calculated age is 1814 ± 48 Ma; for points 5-8, in the high-Y anomaly in the rim, the calculated age is 1623 ± 31 Ma.

Monaz 1A is 17 µm is size, and is included in the outermost rim of a garnet crystal; the grain is in contact with the matrix on one side (Fig. 5.2). Figure 5.4 presents X-ray maps for Th, U, Y, and Pb. Th, U, and Pb are similarly zoned to the rim, consistent with the heavy element zoning in the BSE image. A large high-Y anomaly is present in the rim, with a second minor anomaly near the core. The heavy element zonation parallels the contact with the matrix. The calculated age for this grain is 1474 ± 34 Ma. No chronological zoning is apparent.

Table 5.1. Chemical dating results from Monaz 1B. Ages calculated using the iterative equations of Montel et al (1996); Appendix C contains a sample calculation. Pb (cor) represents a correction in the measured amount of Pb; because of peak interference, some Pb is in reality Y. The Y correction is calculated by subtracting 0.18% of the measured Y from the measured Pb. Pb(calc) is the calculated amount of Pb based on the age; age is determined by matching Pb(calc) to Pb(cor).

Decay Constants		**Analytical parameters:**	
Th^{232}	4.95E-11	acquisition time:	**600 sec.**
U^{238}	1.55E-10	bias (sp3):	**1955 V**
U^{235}	9.85E-10	other:	**Y on TAP sp1**

Point	Grain/zone	Y	Th	U	Pb	Pb (cor)	Pb(calc)	Age (Ma)
Monaz 1B								
1		8155	22370	4432	3157	3142	3143	**1756**
2		8240	17653	2217	2265	2250	2250	**1870**
3		7256	20838	1873	2372	2359	2359	**1830**
4		7825	18994	2400	2346	2332	2332	**1805**
5		2378	33587	5410	3899	3895	3895	**1590**
6		2506	33624	5550	4026	4021	4022	**1622**
7		11473	27346	6640	3981	3960	3959	**1664**
8		10473	31432	6580	4141	4122	4122	**1617**

Average age= 1719 Ma ± 109

Point 1-4 Age (avg)= 1815 Ma ± 48 Monaz 1B-1

Point 5-8 Age (avg)= 1623 Ma ± 31 Monaz 1B-2

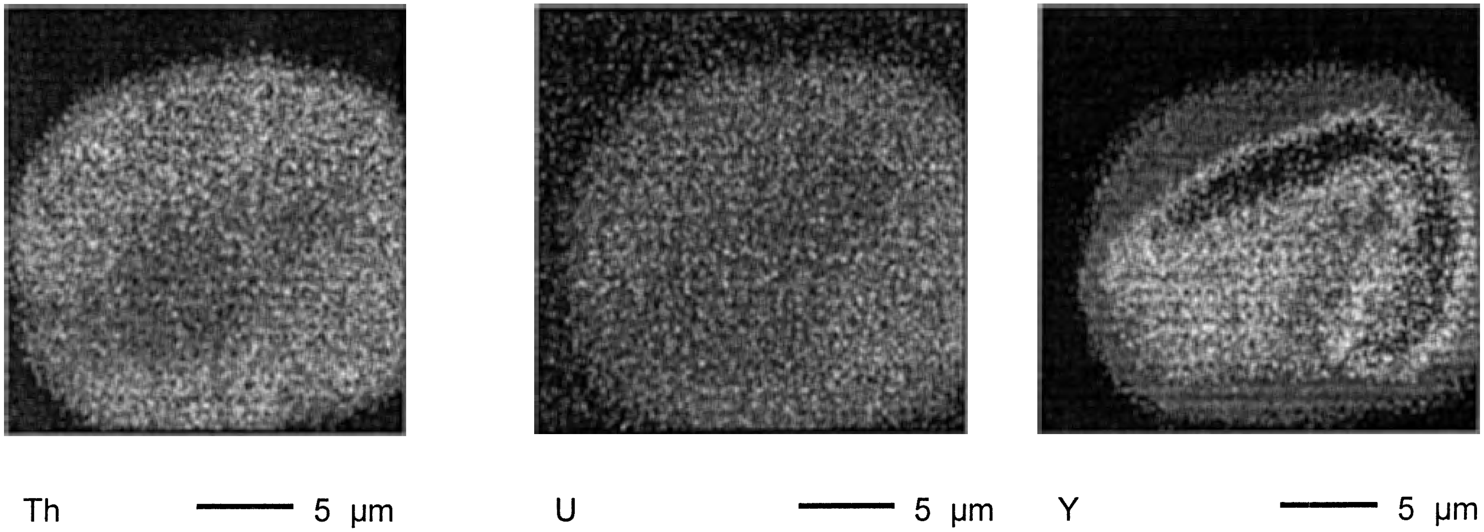

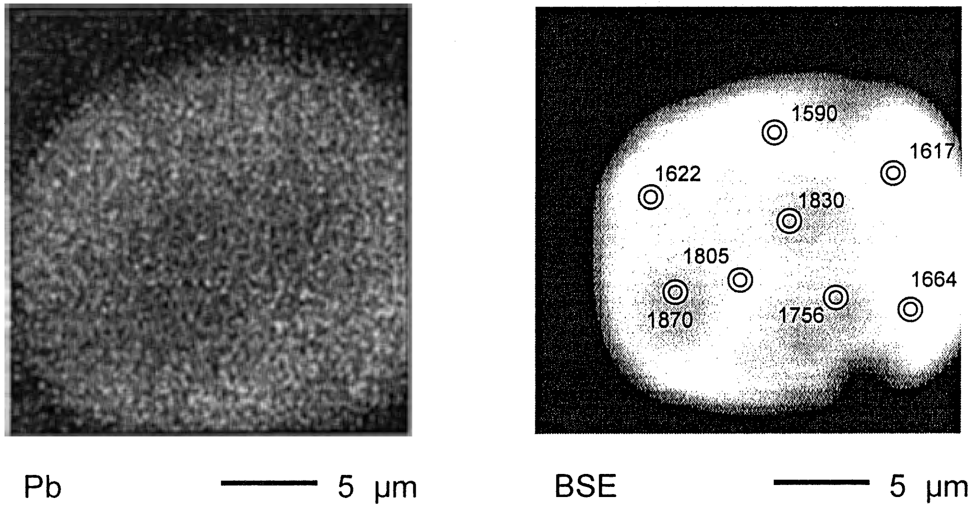

Figure 5.3. Compositional maps of Monaz 1B. A horseshoe shaped Y anomaly curves from the upper right to the left, and down. BSE image shows dated points with ages; note the difference between the age of the core and the age of the rim, corresponding to the Y anomaly seen in the Y X-ray map. Figure 5.2 shows the location of the grain in the host garnet crystal.

Table 5.2. Chemical dating results from Monaz 1A. Ages calculated using the iterative equations of Montel et al (1996); Appendix C contains a sample calculation. Pb (cor) represents a correction in the measured amount of Pb; because of peak interference, some Pb is in reality Y. The Y correction is calculated by subtracting 0.18% of the measured Y from the measured Pb. Pb(calc) is the calculated amount of Pb based on the age; age is determined by matching Pb(calc) to Pb(cor).

Decay Constants		**Analytical parameters:**	
Th^{232}	4.95E-11	acquisition time:	**600 sec.**
U^{238}	1.55E-10	bias (sp3):	**1955 V**
U^{235}	9.85E-10	other:	**Y on TAP sp1**

Point	**Grain/zone**	**Y**	**Th**	**U**	**Pb**	**Pb (cor)**	**Pb(calc)**	**Age (Ma)**
Monaz 1A								
1		0	41211	1487	3069	3069	3069	**1436**
2		2000	35066	6826	3989	3985	3985	**1460**
3		6694	35547	8222	4325	4313	4314	**1449**
4		0	39858	1608	3146	3146	3147	**1499**
5		0	37497	1594	2997	2997	2997	**1507**
6		8762	31853	5747	3703	3687	3686	**1526**
7		3984	34021	7941	4237	4230	4228	**1475**
8		4145	34754	8177	4224	4217	4218	**1439**

Average age= 1474 Ma ± 34

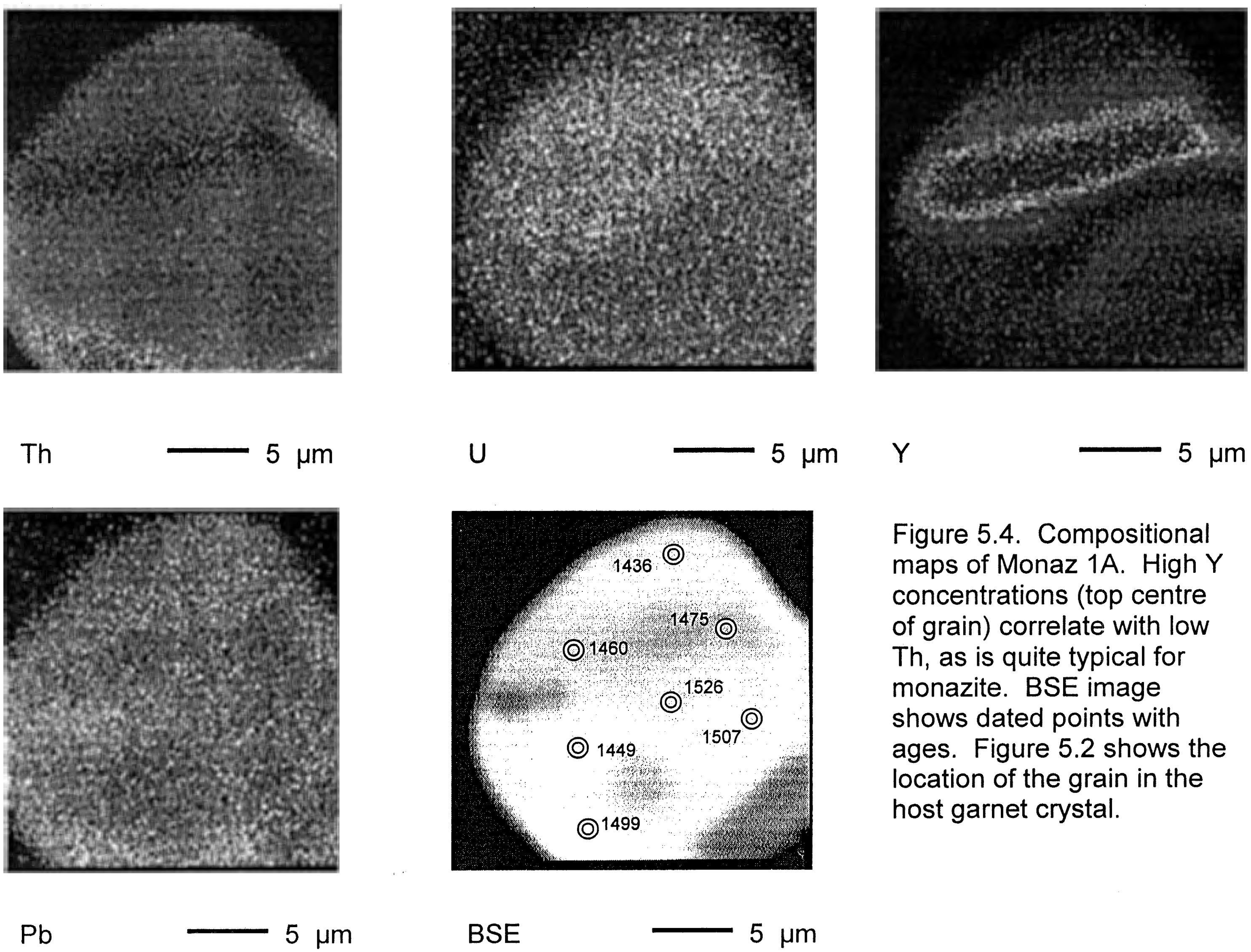

Figure 5.4. Compositional maps of Monaz 1A. High Y concentrations (top centre of grain) correlate with low Th, as is quite typical for monazite. BSE image shows dated points with ages. Figure 5.2 shows the location of the grain in the host garnet crystal.

5.4 Discussion

Figure 5.1 shows the compilation histogram of CGB ages (Fig. 5.1) with the ages from Monaz 1B-1, Monaz 1B-2, and Monaz 1A.

Ages from Monaz 1B may be inherited or detrital. Age estimates from the Britt and Algonquin domains (Slagstad, 2003, and references therein) conform within errors to the ages of Monaz 1B-1 (Algonquin domain, Hunstville subdomain, and Britt domain) and Monaz 1B-2 (Britt domain; Fig. 1.1). Whether Monaz 1B-1 and Monaz 1B-2 represent an igneous core inherited by a later plutonic event, a detrital grain with a metamorphic overgrowth, or two separate metamorphic episodes, is unknown.

Garnets in the polycyclic Birkendale assemblage must have grown during or after the growth of the Ca. 1474 Ma monazite (Monaz 1A). Garnet could have grown during the ca. 1450 Ma or ca. 1080 Ma high-grade metamorphism in the Algonquin and surrounding domains. Secondary fluid inclusions in garnet must post-date garnet formation; this constrains fluid inclusion entrapment to sometime after ca. 1474 Ma.

6.0 Discussion

Two questions are apparent in the fluid inclusion and geochronological data collected in this study: 1) when were fluid inclusions entrapped in garnet, and 2) do inclusions represent one or two fluid events?

6.1 Fluid inclusion entrapment

Fluid inclusion planes in garnet do not correlate with any chemical zoning within the garnet. Fluid inclusion planes cut across both Mg-zoning in biotite-adjacent grains and Ca-zoning on garnet rims. Garnet anneals at temperatures ca. 600 °C.

The P-T path suggested by Timmermann (1998) is one of high-T decompression. Garnet may have fractured during decompression; the high temperatures could anneal garnet, trapping the co-existing fluid. Secondary fluid inclusions in garnet may represent fluids present at temperatures at or above those at which garnet can anneal, i.e., 600 °C +. This suggests fluid inclusions were entrapped at high-T (near peak) metamorphic conditions.

6.2 Time of entrapment

Both GSI-a and GSI-b fluid inclusions are secondary fluid inclusions, meaning the fluid was entrapped sometime after garnet formation. Garnet grew during or after the growth of monazite *ca.* 1474 Ma. Are fluid inclusions in garnet representative of a *ca.* 1450 Ma metamorphic fluid or a *ca.* 1080 Ma metamorphic fluid?

For fluid inclusions to be pre-Grenvillian, *ca.* 1450 Ma, the inclusions must have survived the later, high-grade, Grenvillian metamorphic event (800-850 °C, 10-12 kbar; Timmermann, 1998). Roedder (1984) and Touret (2001) cite metamorphism as a primary reason for the relative scarcity of fluid inclusions in higher-grade metamorphic rocks; recrystallization and metamorphic reactions tend to destroy or obscure fluid inclusions (Roedder, 1984). This suggests that fluid inclusions are likely Grenvillian (*ca.* 1080 Ma), as opposed to pre-Grenvillian (*ca.* 1450 Ma)

6.3 Fluid evolution

Textural features, such as the secondary nature of the inclusions and the presence of the solid phases, suggest a single fluid event (section 4.7). Compositional evidence suggests that at least two different fluids have been entrapped.

An evolving fluid, trapped at various stages during its evolution, could satisfy both sets of evidence. An evolving fluid, trapped during a single event, would have variable composition with similar textural features. Garnet fracturing and annealing in the presence of an evolving fluid would trap the fluid at various states in its evolution.

6.3.1 Fluid evolution model

Slagstad (2003) proposed a low a_{H_2O} fluid-present melting model for migmatite formation in the nearby Muskoka domain. Granulites associated with fluid-derived features, such as pegmatites and veins, also suggest the presence of a low a_{H_2O} fluid during peak metamorphism (Timmermann, 2003).

Figure 6.1 shows a possible evolution path for the fluids in the Algonquin domain, and is discussed in the following paragraphs.

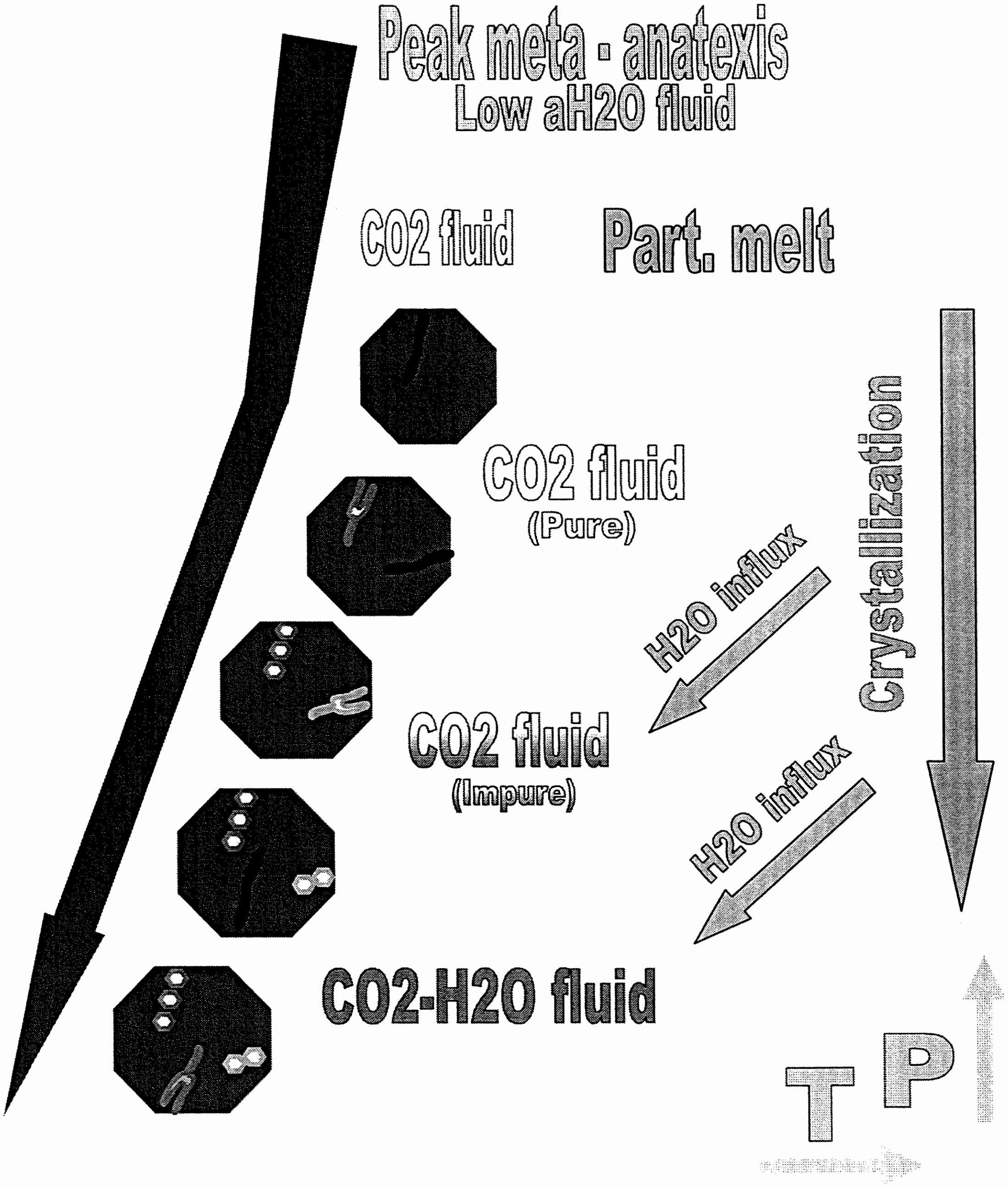

Figure 6.1. Fluid evolution model, including pressure and temperature, and migmatite formation. Anatexis at peak metamorphic conditions partitions water from a low a_{H_2O} fluid, leaving a CO_2 residuum. Migmatite crystallization fluxes water into the fluid. Fracturing and annealing of garnet at high-T traps the fluid before, during and after H_2O influx.

The stability of hydrous phases such as biotite in migmatitic rocks suggests that the original fluid at the time of anatexis was hydrous (Slagstad, 2003). As melt formed, water in the fluid was partitioned into the melt. CO_2 was not soluble in the melt, and formed the residual fluid (Slagstad, 2003).

After peak metamorphism, the rocks began to decompress, fracturing garnet in the presence of the CO_2-fluid. High temperatures annealed garnet, trapping the CO_2 in fractures formed during decompression. Garnet continued to fracture and anneal as the rocks decompressed at high temperatures.

Cooling led to crystallization of the leucosome. Water was expelled from the crystallizing melt, and fluxed into the fluid. H_2O influx changed the composition of the fluid. Decompression and relatively high temperatures continued to fracture and anneal garnet during water influx, trapping first a near-pure CO_2 fluid with a minor H_2O impurity at an early stage of H_2O influx, then trapping the CO_2 - H_2O composite fluid at a later stage.

Fluid inclusion entrapment ended when temperatures became too low to anneal fractures in garnet (*ca*. 600 °C).

7.0 Conclusions

Fluid inclusions in the polycyclic migmatitic gneiss of the Algonquin domain have been documented and described in the text. Two distinct types of fluid inclusions are recognized: monophase, negative crystal-shaped, pure or near-pure CO_2 inclusions (GSI-a); and two-phase, necking, H_2O-CO_2, inclusions (GSI-b).

The fluid inclusions represent the evolution of fluid in the Algonquin domain trapped at various stages during high-T decompression, *ca.* 1080 Ma. Anatexis results in a CO_2-rich fluid. Leucosome crystallization

7.1 Suggestions for future work

In-depth study of GSI-b type fluid inclusions could provide important information with regards to exact fluid composition and density at time of entrapment.

More intensive study of monazite and other geochronometer minerals included in garnet may provide better constraints on the age of garnet, and therefore, the age of fluid inclusions.

Isotopic analysis of CO_2 in GSI-a and GSI-b inclusions may provide insight into the source of the CO_2.

Appendix A:
Microprobe analyses of selected garnets and inclusions

Appendix A. Electron microprobe analyses of compositionally mapped garnets, and inclusions therein.

Table A1. X-ray mapped garnets with identified points (see appendix D for point maps).
Analyses recalculated for 12 oxygens.

Sample and point	1A-0.5 pt 1	1A-0.5 pt 2	1A-0.5 pt 3	1A-0.5 pt 4	1A-0.5 pt 5	1A-0.5 pt 7	1A-0.5 pt 8
Location	Rim	Rim	Core	Core	Core	Core	Core
Remarks							
SiO2	35.82	36.50	36.50	36.75	36.96	37.12	37.29
TiO2	0.02	0.00	0.00	0.01	0.00	0.00	0.00
Al2O3	22.03	22.46	22.44	22.44	22.42	22.40	22.35
FeO	34.52	31.54	31.42	31.29	31.28	31.39	31.30
MnO	0.81	0.75	0.74	0.73	0.74	0.74	0.74
MgO	5.25	6.86	7.05	7.20	7.20	7.08	6.97
CaO	1.78	2.97	2.81	2.70	2.67	2.66	2.80
Na2O	0.02	0.01	0.01	0.01	0.01	0.01	0.01
K2O	0.00	0.00	0.00	0.00	0.00	0.00	0.00
P2O5	0.02	0.04	0.03	0.01	0.01	0.01	0.04
Total	100.27	101.13	101.01	101.14	101.28	101.41	1.50
Si	0.239	0.238	0.238	0.239	0.240	0.241	0.242
Ti	0.000	0.00	0.00	0.000	0.00	0.00	0.00
Al	0.173	0.173	0.173	0.172	0.172	0.171	0.171
Fe	0.193	0.172	0.172	0.170	0.170	0.170	0.170
Mn	0.005	0.004	0.004	0.004	0.004	0.004	0.004
Mg	0.052	0.067	0.069	0.070	0.070	0.068	0.067
Ca	0.013	0.021	0.020	0.019	0.019	0.019	0.019
Na	0.000	0.000	0.000	0.000	0.000	0.000	0.000
K	0.00	0.00	0.00	0.00	0.00	0.00	0.00
P	0.000	0.000	0.000	0.000	0.00	0.00	0.000
Total	0.675	0.675	0.675	0.675	0.674	0.674	0.673
Si	2.866	2.858	2.860	2.870	2.881	2.890	2.898
Ti	-	-	-	0.001	-	-	-
Al	2.078	2.072	2.072	2.065	2.060	2.056	2.047
Fe	2.310	2.066	2.058	2.045	2.039	2.044	2.035
Mn	0.055	0.049	0.049	0.048	0.049	0.049	0.049
Mg	0.626	0.800	0.823	0.839	0.836	0.821	0.808
Ca	0.152	0.250	0.236	0.226	0.223	0.222	0.233
Na	0.002	0.002	0.001	0.002	0.002	0.001	0.002
K	-	-	-	-	-	-	-
P	0.001	0.002	0.002	0.001	-	-	0.002
Total	8.094	8.101	8.102	8.098	8.092	8.083	8.076
% Almand	0.735	0.653	0.650	0.648	0.648	0.652	0.651
% Spess	0.018	0.016	0.016	0.015	0.016	0.016	0.016
% Pyrope	0.199	0.253	0.260	0.266	0.266	0.262	0.258
% Gross	0.048	0.079	0.075	0.071	0.071	0.071	0.075

Appendix A. Electron microprobe analyses of compositionally mapped garnets, and inclusions therein.

Table A1. X-ray mapped garnets with identified points (see appendix D for point maps).
Analyses recalculated for 12 oxygens.

Sample and point	1A-0.5 pt 9	1A-0.5 pt 10	1A-0.3 pt 1	1A-0.3 pt 2	1A-0.3 pt 3	1A-0.3 pt 4	1A-0.3 pt 5
Location	Rim	Rim	Rim	Core	Core	Core	Core
Remarks							
SiO2	37.58	37.60	37.46	38.03	38.00	38.17	38.05
TiO2	0.00	0.00	0.01	0.01	0.00	0.01	0.00
Al2O3	22.38	22.36	22.10	22.20	22.17	22.30	22.30
FeO	31.59	31.89	33.84	32.25	32.02	31.92	31.60
MnO	0.75	0.76	0.92	0.85	0.83	0.83	0.83
MgO	7.04	7.30	5.59	6.23	6.46	6.49	6.50
CaO	2.59	1.89	1.99	3.04	2.77	3.07	3.07
Na2O	0.01	0.02	0.01	0.01	0.02	0.01	0.01
K2O	0.00	0.00	0.00	0.00	0.00	0.00	0.00
P2O5	0.02	0.02	0.02	0.02	0.03	0.03	0.00
Total	101.96	101.85	1.93	102.63	102.30	102.82	102.37
Si	0.242	0.243	0.244	0.244	0.245	0.244	0.245
Ti	0.00	0.00	0.00	0.00	0.00	0.00	0.00
Al	0.170	0.170	0.170	0.168	0.168	0.168	0.169
Fe	0.170	0.172	0.184	0.173	0.172	0.171	0.170
Mn	0.004	0.004	0.005	0.005	0.005	0.005	0.005
Mg	0.068	0.070	0.054	0.060	0.062	0.062	0.062
Ca	0.018	0.013	0.014	0.021	0.019	0.021	0.021
Na	0.000	0.000	0.000	0.000	0.000	0.000	0.000
K	0.00	0.00	0.00	0.00	0.00	0.00	0.00
P	0.000	0.000	0.000	0.000	0.000	0.000	0.00
Total	0.673	0.673	0.671	0.671	0.671	0.671	0.671
Si	2.908	2.911	2.927	2.933	2.935	2.932	2.934
Ti	-	-	-	-	-	-	-
Al	2.041	2.040	2.035	2.017	2.018	2.018	2.027
Fe	2.044	2.064	2.212	2.080	2.069	2.051	2.038
Mn	0.049	0.050	0.061	0.055	0.054	0.054	0.054
Mg	0.811	0.841	0.650	0.716	0.744	0.744	0.746
Ca	0.215	0.157	0.167	0.252	0.229	0.252	0.253
Na	0.002	0.004	0.002	0.001	0.002	0.001	0.001
K	-	-	-	-	-	-	-
P	0.001	0.001	0.001	0.001	0.002	0.002	-
Total	8.072	8.070	8.057	8.057	8.054	8.054	8.053
% Almand	0.655	0.663	0.716	0.670	0.668	0.661	0.659
% Spess	0.016	0.016	0.020	0.018	0.017	0.017	0.017
% Pyrope	0.260	0.270	0.210	0.231	0.240	0.240	0.241
% Gross	0.069	0.051	0.054	0.081	0.074	0.081	0.082

Appendix A. Electron microprobe analyses of compositionally mapped garnets, and inclusions therein.

Table A1. X-ray mapped garnets with identified points (see appendix D for point maps).
Analyses recalculated for 12 oxygens.

Sample and point	1A-0.3 pt 6	1A-0.3 pt 7	1A-0.3 pt 8	1A-0.3 pt 9	1A-0.3 pt 10	1A-0.2 pt 1	1A-0.2 pt 2
Location	Core	Core	Core	Rim	Rim	Rim	Rim
Remarks							
SiO2	38.04	38.02	37.99	38.03	38.14	33.81	33.63
TiO2	0.01	0.01	0.01	0.01	0.01	0.00	0.05
Al2O3	22.37	22.24	22.22	22.26	22.21	22.29	22.35
FeO	31.87	31.64	31.84	32.25	32.89	30.16	30.70
MnO	0.85	0.84	0.83	0.86	0.88	0.67	0.68
MgO	6.44	6.30	6.25	6.21	6.45	7.85	8.19
CaO	3.15	3.20	3.18	3.06	1.97	2.81	1.89
Na2O	0.01	0.01	0.02	0.02	0.01	0.02	0.02
K2O	0.00	0.00	0.00	0.00	0.00	0.00	0.00
P2O5	0.03	0.01	0.05	0.05	0.03	0.02	0.02
Total	102.77	102.27	102.39	2.75	102.58	97.62	97.52
Si	0.244	0.245	0.244	0.244	0.245	0.229	0.228
Ti	0.00	0.00	0.00	0.000	0.00	0.00	0.000
Al	0.169	0.169	0.169	0.168	0.168	0.178	0.179
Fe	0.171	0.170	0.171	0.173	0.177	0.171	0.174
Mn	0.005	0.005	0.005	0.005	0.005	0.004	0.004
Mg	0.062	0.061	0.060	0.060	0.062	0.079	0.083
Ca	0.022	0.022	0.022	0.021	0.014	0.020	0.014
Na	0.000	0.000	0.000	0.000	0.000	0.000	0.000
K	0.00	0.00	0.00	0.00	0.00	0.00	0.00
P	0.000	0.00	0.000	0.000	0.000	0.000	0.000
Total	0.672	0.671	0.671	0.672	0.671	0.682	0.682
Si	2.924	2.936	2.933	2.929	2.941	2.749	2.738
Ti	-	-	-	0.001	-	-	0.004
Al	2.028	2.024	2.022	2.021	2.020	2.136	2.144
Fe	2.050	2.044	2.056	2.077	2.122	2.051	2.090
Mn	0.055	0.055	0.054	0.056	0.058	0.046	0.047
Mg	0.738	0.726	0.719	0.714	0.742	0.952	0.994
Ca	0.259	0.264	0.263	0.252	0.163	0.245	0.164
Na	0.002	0.002	0.002	0.002	0.002	0.002	0.002
K	-	-	-	-	-	-	-
P	0.002	-	0.004	0.004	0.001	0.001	0.001
Total	8.059	8.053	8.052	8.058	8.050	8.182	8.186
% Almand	0.661	0.662	0.665	0.670	0.688	0.623	0.634
% Spess	0.018	0.018	0.017	0.018	0.019	0.014	0.014
% Pyrope	0.238	0.235	0.233	0.230	0.240	0.289	0.302
% Gross	0.084	0.085	0.085	0.081	0.053	0.074	0.050

Appendix A. Electron microprobe analyses of compositionally mapped garnets, and inclusions therein.

Table A1. X-ray mapped garnets with identified points (see appendix D for point maps). Analyses recalculated for 12 oxygens.

Sample and point	1A-0.2 pt 3	1A-0.2 pt 4	1A-0.2 pt 5	1A-0.2 pt 7	1A-0.2 pt 8	1A-0.2 pt 9	1A-0.2 pt 10
Location	Core	Core	Core	Core	Core	Rim	Rim
Remarks							
SiO2	33.77	33.59	33.38	33.67	33.21	33.67	32.91
TiO2	0.00	0.00	0.00	0.01	0.00	0.01	0.05
Al2O3	22.27	22.38	22.40	22.25	22.15	22.16	21.87
FeO	30.70	30.78	30.87	31.35	31.37	31.29	33.18
MnO	0.68	0.70	0.70	0.75	0.77	0.77	0.82
MgO	7.94	7.92	7.87	7.66	7.57	7.01	5.87
CaO	2.34	2.24	2.18	2.12	1.89	2.83	2.45
Na2O	0.03	0.03	0.03	0.02	0.02	0.02	0.02
K2O	0.00	0.00	0.00	0.00	0.00	0.00	0.00
P2O5	0.02	0.04	0.02	0.04	0.03	0.03	0.01
Total	97.74	97.67	97.45	97.85	97.01	97.79	97.20
Si	0.229	0.228	0.227	0.229	0.228	0.229	0.228
Ti	0.00	0.00	0.00	0.00	0.00	0.00	0.000
Al	0.178	0.179	0.180	0.178	0.179	0.178	0.179
Fe	0.174	0.175	0.176	0.178	0.180	0.178	0.192
Mn	0.004	0.004	0.004	0.004	0.004	0.004	0.005
Mg	0.080	0.080	0.080	0.078	0.077	0.071	0.061
Ca	0.017	0.016	0.016	0.015	0.014	0.021	0.018
Na	0.000	0.000	0.000	0.000	0.000	0.000	0.000
K	0.00	0.00	0.00	0.00	0.00	0.00	0.00
P	0.000	0.000	0.000	0.000	0.000	0.000	0.000
Total	0.682	0.683	0.683	0.682	0.683	0.682	0.683
Si	2.746	2.735	2.726	2.742	2.732	2.750	2.734
Ti	-	-	-	-	-	-	0.004
Al	2.135	2.148	2.156	2.136	2.148	2.134	2.142
Fe	2.088	2.096	2.108	2.135	2.158	2.137	2.305
Mn	0.047	0.048	0.048	0.052	0.053	0.053	0.058
Mg	0.962	0.961	0.959	0.930	0.929	0.854	0.727
Ca	0.204	0.196	0.191	0.185	0.167	0.247	0.218
Na	0.005	0.004	0.005	0.004	0.004	0.002	0.004
K	-	-	-	-	-	-	-
P	0.001	0.002	0.001	0.002	0.002	0.002	0.001
Total	8.189	8.191	8.196	8.185	8.192	8.180	8.192
% Almand	0.632	0.635	0.638	0.647	0.653	0.649	0.697
% Spess	0.014	0.015	0.015	0.016	0.016	0.016	0.017
% Pyrope	0.292	0.291	0.290	0.282	0.281	0.260	0.220
% Gross	0.062	0.059	0.058	0.056	0.050	0.075	0.066

Appendix A. Electron microprobe analyses of compositionally mapped garnets, and inclusions therein.

Table A1. X-ray mapped garnets with identified points (see appendix D for point maps).
Analyses recalculated for 12 oxygens.

Sample and point	1A-1.3 pt 1	1A-1.3 pt 2	1A-1.3 pt 3	1A-1.3 pt 4	1A-1.3 pt 5	1A-1.3 pt 6	1A-1.3 pt 7
Location	Rim	Rim	Core	Core	Core	Core	Core
Remarks							
SiO2	38.37	38.67	38.69	38.82	38.82	38.72	38.76
TiO2	0.00	0.00	0.01	0.01	0.00	0.00	0.00
Al2O3	21.15	21.43	21.46	21.49	21.41	21.61	21.54
FeO	32.91	30.84	30.79	30.76	31.03	30.89	31.02
MnO	0.85	0.74	0.72	0.72	0.70	0.69	0.68
MgO	5.77	7.44	7.85	8.01	8.05	8.13	8.04
CaO	1.96	2.23	1.66	1.41	1.25	1.26	1.28
Na2O	0.03	0.04	0.04	0.02	0.03	0.01	0.01
K2O	0.06	0.09	0.04	0.08	0.08	0.09	0.07
P2O5	0.03	0.06	0.05	0.03	0.00	0.01	0.04
Total	101.12	101.53	101.30	101.34	101.38	101.42	101.43
Si	0.251	0.249	0.249	0.250	0.250	0.249	0.249
Ti	0.000	0.000	0.000	0.000	0.000	0.000	0.000
Al	0.163	0.163	0.163	0.163	0.162	0.164	0.163
Fe	0.180	0.166	0.166	0.165	0.167	0.166	0.167
Mn	0.005	0.004	0.004	0.004	0.004	0.004	0.004
Mg	0.056	0.071	0.075	0.077	0.077	0.078	0.077
Ca	0.014	0.015	0.011	0.010	0.009	0.009	0.009
Na	0.000	0.001	0.001	0.000	0.000	0.000	0.000
K	0.001	0.001	0.000	0.001	0.001	0.001	0.001
P	0.000	0.000	0.000	0.000	0.000	0.000	0.000
Total	0.669	0.670	0.670	0.669	0.670	0.670	0.669
Si	3.006	2.987	2.988	2.994	2.996	2.986	2.989
Ti	-	-	-	-	-	-	-
Al	1.952	1.951	1.955	1.954	1.948	1.964	1.957
Fe	2.156	1.992	1.990	1.984	2.003	1.992	2.000
Mn	0.056	0.048	0.047	0.047	0.046	0.046	0.044
Mg	0.674	0.857	0.905	0.922	0.926	0.935	0.924
Ca	0.164	0.185	0.137	0.116	0.103	0.104	0.106
Na	0.004	0.006	0.006	0.004	0.005	0.001	0.001
K	0.006	0.008	0.005	0.007	0.008	0.008	0.007
P	0.002	0.004	0.004	0.002	-	0.001	0.002
Total	8.023	8.038	8.036	8.029	8.035	8.038	8.033
% Almand	0.707	0.646	0.646	0.646	0.651	0.647	0.651
% Spess	0.018	0.016	0.015	0.015	0.015	0.015	0.014
% Pyrope	0.221	0.278	0.294	0.300	0.301	0.304	0.301
% Gross	0.054	0.060	0.044	0.038	0.034	0.034	0.034

Appendix A. Electron microprobe analyses of compositionally mapped garnets, and inclusions therein.

Table A1. X-ray mapped garnets with identified points (see appendix D for point maps).
Analyses recalculated for 12 oxygens.

Sample and point	1A-1.3 pt 8	1A-1.3 pt 9	1A-1.3 pt 10	2A-0.4 pt 1	2A-0.4 pt 2	2A-0.4 pt 3	2A-0.4 pt 4
Location	Core	Rim	Rim	Rim	Rim	Rim	Core
Remarks							
SiO2	38.80	38.70	38.55	38.26	37.85	38.00	38.71
TiO2	0.00	0.02	0.00	0.05	0.04	0.03	0.02
Al2O3	21.51	21.53	21.48	21.53	21.33	21.44	21.45
FeO	31.00	30.68	31.84	30.39	31.05	30.28	30.27
MnO	0.68	0.74	0.80	0.65	0.66	0.61	0.56
MgO	7.89	7.42	6.83	7.45	6.87	7.56	7.98
CaO	1.50	2.06	1.93	1.70	1.63	1.56	1.54
Na2O	0.02	0.01	0.02	0.00	0.00	0.00	0.00
K2O	0.07	0.08	0.08	0.10	0.08	0.08	0.10
P2O5	0.04	0.02	0.01	0.00	0.02	0.00	0.02
Total	101.51	101.26	101.53	100.13	99.53	99.55	100.65
Si	0.249	0.250	0.249	0.249	0.249	0.249	0.250
Ti	0.000	0.000	0.000	0.000	0.000	0.000	0.000
Al	0.163	0.164	0.164	0.165	0.165	0.165	0.163
Fe	0.167	0.165	0.172	0.166	0.171	0.166	0.164
Mn	0.004	0.004	0.004	0.004	0.004	0.003	0.003
Mg	0.076	0.071	0.066	0.072	0.067	0.074	0.077
Ca	0.010	0.014	0.013	0.012	0.012	0.011	0.011
Na	0.000	0.000	0.000	0.000	0.000	0.000	0.000
K	0.001	0.001	0.001	0.001	0.001	0.001	0.001
P	0.000	0.000	0.000	0.000	0.000	0.000	0.000
Total	0.669	0.669	0.669	0.669	0.669	0.669	0.668
Si	2.992	2.994	2.990	2.989	2.987	2.984	3.000
Ti	-	0.001	-	-	-	-	-
Al	1.955	1.963	1.963	1.982	1.984	1.985	1.960
Fe	1.999	1.985	2.065	1.986	2.050	1.988	1.962
Mn	0.044	0.048	0.053	0.043	0.044	0.041	0.036
Mg	0.906	0.856	0.790	0.868	0.808	0.886	0.922
Ca	0.124	0.170	0.160	0.143	0.138	0.131	0.127
Na	0.002	0.001	0.002	0.000	0.000	0.000	0.000
K	0.007	0.007	0.007	0.011	0.008	0.008	0.010
P	0.002	0.001	-	0.000	0.001	0.000	0.001
Total	8.032	8.028	8.032	8.024	8.022	8.024	8.018
% Almand	0.651	0.649	0.673	0.653	0.674	0.654	0.645
% Spess	0.014	0.016	0.017	0.014	0.015	0.013	0.012
% Pyrope	0.295	0.280	0.257	0.285	0.266	0.291	0.303
% Gross	0.040	0.056	0.052	0.047	0.045	0.043	0.042

Appendix A. Electron microprobe analyses of compositionally mapped garnets, and inclusions therein.

Table A1. X-ray mapped garnets with identified points (see appendix D for point maps).
Analyses recalculated for 12 oxygens.

Sample and point	2A-0.4 pt 5	2A-0.4 pt 6	2A-0.4 pt 7	2A-0.4 pt 8	2A-0.4 pt 9	2A-0.4 pt 10	1B-0.3 pt 1
Location	Core	Core	Core	Core	Core	Rim	Rim
Remarks							
SiO2	38.31	38.61	38.45	38.29	38.88	38.51	38.61
TiO2	0.04	0.03	0.05	0.06	0.06	0.04	0.00
Al2O3	21.75	21.62	21.69	21.73	21.61	21.73	21.62
FeO	29.46	29.35	29.42	29.18	29.34	29.32	29.80
MnO	0.57	0.57	0.55	0.57	0.57	0.53	0.64
MgO	8.15	8.23	8.33	8.28	8.46	8.57	7.90
CaO	1.57	1.67	1.70	1.62	1.65	1.53	1.64
Na2O	0.00	0.00	0.00	0.00	0.00	0.00	0.01
K2O	0.08	0.09	0.08	0.07	0.07	0.12	0.05
P2O5	0.02	0.02	0.05	0.07	0.06	0.08	0.03
Total	99.94	100.19	100.33	99.86	100.69	100.44	100.30
Si	0.249	0.250	0.248	0.248	0.250	0.248	0.250
Ti	0.000	0.000	0.000	0.000	0.000	0.000	0.000
Al	0.166	0.165	0.165	0.166	0.164	0.165	0.165
Fe	0.160	0.159	0.159	0.158	0.158	0.158	0.161
Mn	0.003	0.003	0.003	0.003	0.003	0.003	0.004
Mg	0.079	0.079	0.080	0.080	0.081	0.082	0.076
Ca	0.011	0.012	0.012	0.011	0.011	0.011	0.011
Na	0.000	0.000	0.000	0.000	0.000	0.000	0.000
K	0.001	0.001	0.001	0.001	0.001	0.001	0.000
P	0.000	0.000	0.000	0.000	0.000	0.000	0.000
Total	0.668	0.668	0.669	0.668	0.668	0.669	0.668
Si	2.982	2.995	2.981	2.980	2.998	2.978	2.998
Ti	-	-	-	-	-	-	-
Al	1.996	1.976	1.982	1.992	1.963	1.981	1.979
Fe	1.918	1.904	1.908	1.898	1.892	1.896	1.936
Mn	0.037	0.037	0.036	0.037	0.037	0.035	0.042
Mg	0.946	0.952	0.962	0.960	0.973	0.988	0.914
Ca	0.131	0.139	0.142	0.136	0.137	0.127	0.136
Na	0.000	0.000	0.000	0.000	0.000	0.000	0.001
K	0.007	0.010	0.008	0.007	0.007	0.012	0.005
P	0.001	0.001	0.004	0.005	0.004	0.005	0.002
Total	8.020	8.017	8.027	8.018	8.015	8.024	8.014
% Almand	0.631	0.627	0.628	0.625	0.623	0.624	0.639
% Spess	0.012	0.012	0.012	0.012	0.012	0.011	0.014
% Pyrope	0.311	0.313	0.317	0.316	0.320	0.325	0.302
% Gross	0.043	0.046	0.047	0.045	0.045	0.042	0.045

Appendix A. Electron microprobe analyses of compositionally mapped garnets, and inclusions therein.

Table A1. X-ray mapped garnets with identified points (see appendix D for point maps).
Analyses recalculated for 12 oxygens.

Sample and point	1B-0.3 pt 2	1B-0.3 pt 3	1B-0.3 pt 4	1B-0.3 pt 5	1B-0.3 pt 6	1B-0.3 pt 7	1B-0.3 pt 8
Location	Rim	Core	Core	Core	Core	Core	Core
Remarks							
SiO2	38.55	38.63	38.74	38.55	38.40	38.41	38.57
TiO2	0.00	0.00	0.01	0.01	0.03	0.02	0.03
Al2O3	21.44	21.48	21.46	21.71	21.62	21.59	21.60
FeO	29.41	29.54	29.41	29.34	29.39	29.14	29.32
MnO	0.64	0.62	0.61	0.60	0.62	0.65	0.63
MgO	7.58	7.69	7.74	7.72	7.75	7.74	7.70
CaO	2.46	2.67	2.60	2.52	2.51	2.66	2.75
Na2O	0.01	0.00	0.01	0.02	0.01	0.00	0.00
K2O	0.06	0.07	0.05	0.10	0.09	0.09	0.07
P2O5	0.06	0.09	0.06	0.02	0.04	0.02	0.03
Total	100.21	100.78	100.69	100.61	100.46	100.33	100.70
Si	0.250	0.249	0.250	0.249	0.248	0.249	0.249
Ti	0.000	0.000	0.000	0.000	0.000	0.000	0.000
Al	0.164	0.163	0.163	0.165	0.165	0.165	0.164
Fe	0.159	0.159	0.159	0.158	0.159	0.158	0.158
Mn	0.004	0.003	0.003	0.003	0.003	0.004	0.004
Mg	0.073	0.074	0.074	0.074	0.075	0.075	0.074
Ca	0.017	0.018	0.018	0.018	0.017	0.019	0.019
Na	0.000	0.000	0.000	0.000	0.000	0.000	0.000
K	0.001	0.001	0.000	0.001	0.001	0.001	0.001
P	0.000	0.001	0.000	0.000	0.000	0.000	0.000
Total	0.668	0.669	0.668	0.669	0.669	0.669	0.669
Si	2.999	2.990	2.999	2.987	2.981	2.984	2.987
Ti	-	-	-	0.001	0.001	0.001	0.001
Al	1.966	1.961	1.958	1.982	1.979	1.978	1.972
Fe	1.913	1.913	1.903	1.901	1.908	1.894	1.900
Mn	0.042	0.041	0.041	0.040	0.041	0.043	0.042
Mg	0.878	0.888	0.893	0.892	0.896	0.896	0.889
Ca	0.205	0.221	0.215	0.210	0.209	0.222	0.228
Na	0.001	-	0.001	0.002	0.001	-	-
K	0.006	0.007	0.005	0.011	0.008	0.008	0.007
P	0.004	0.006	0.004	0.001	0.002	0.001	0.001
Total	8.014	8.028	8.020	8.027	8.028	8.029	8.027
% Almand	0.630	0.625	0.624	0.625	0.625	0.620	0.621
% Spess	0.014	0.013	0.013	0.013	0.013	0.014	0.014
% Pyrope	0.289	0.290	0.293	0.293	0.294	0.293	0.291
% Gross	0.068	0.072	0.070	0.069	0.068	0.073	0.075

Appendix A. Electron microprobe analyses of compositionally mapped garnets, and inclusions therein.

Table A1. X-ray mapped garnets with identified points (see appendix D for point maps).
Analyses recalculated for 12 oxygens.

Sample and point	1B-0.3 pt 9	1B-0.3 pt 10	1B-0.4 pt 1	1B-0.4 pt 2	1B-0.4 pt 3	1B-0.4 pt 4	1B-0.4 pt 5
Location	Rim	Rim	Rim	Rim	Core	Core	Core
Remarks							
SiO2	38.54	38.59	38.60	38.64	38.73	38.52	38.43
TiO2	0.00	0.00	0.01	0.02	0.01	0.01	0.03
Al2O3	21.52	21.63	21.71	21.47	21.50	21.77	21.52
FeO	29.56	29.83	29.01	29.10	29.08	29.28	29.23
MnO	0.63	0.64	0.61	0.61	0.62	0.59	0.61
MgO	7.69	7.97	8.33	8.14	8.06	8.12	8.10
CaO	2.32	1.77	1.84	2.37	2.43	2.27	2.09
Na2O	0.00	0.01	0.01	0.01	0.00	0.01	0.01
K2O	0.07	0.05	0.09	0.05	0.07	0.03	0.07
P2O5	0.06	0.02	0.06	0.03	0.07	0.07	0.09
Total	100.40	100.52	100.27	100.45	100.57	100.68	100.19
Si	0.249	0.249	0.249	0.249	0.250	0.248	0.249
Ti	0.000	0.000	0.000	0.000	0.000	0.000	0.000
Al	0.164	0.165	0.165	0.163	0.163	0.165	0.164
Fe	0.160	0.161	0.157	0.157	0.157	0.158	0.158
Mn	0.003	0.004	0.003	0.003	0.003	0.003	0.003
Mg	0.074	0.077	0.080	0.078	0.077	0.078	0.078
Ca	0.016	0.012	0.013	0.016	0.017	0.016	0.015
Na	0.000	0.000	0.000	0.000	0.000	0.000	0.000
K	0.001	0.000	0.001	0.000	0.001	0.000	0.001
P	0.000	0.000	0.000	0.000	0.000	0.000	0.001
Total	0.668	0.669	0.668	0.669	0.668	0.669	0.669
Si	2.993	2.992	2.989	2.993	2.995	2.977	2.986
Ti	-	-	0.001	0.001	0.001	0.001	0.001
Al	1.970	1.976	1.981	1.961	1.960	1.982	1.970
Fe	1.920	1.934	1.879	1.885	1.882	1.892	1.900
Mn	0.041	0.042	0.040	0.041	0.041	0.038	0.040
Mg	0.890	0.920	0.961	0.940	0.929	0.935	0.938
Ca	0.193	0.148	0.152	0.197	0.202	0.188	0.174
Na	-	0.002	0.001	0.001	-	0.002	0.002
K	0.007	0.005	0.008	0.005	0.006	0.002	0.007
P	0.004	0.001	0.005	0.002	0.005	0.005	0.006
Total	8.018	8.022	8.020	8.027	8.021	8.024	8.024
% Almand	0.631	0.635	0.620	0.616	0.616	0.620	0.622
% Spess	0.013	0.014	0.013	0.013	0.013	0.013	0.013
% Pyrope	0.292	0.302	0.317	0.307	0.304	0.306	0.308
% Gross	0.063	0.048	0.050	0.064	0.066	0.062	0.057

Appendix A. Electron microprobe analyses of compositionally mapped garnets, and inclusions therein.

Table A1. X-ray mapped garnets with identified points (see appendix D for point maps).
Analyses recalculated for 12 oxygens.

Sample and point	1B-0.4 pt 6	1B-0.4 pt 7	1B-0.4 pt 8	1B-0.4 pt 9	1B-0.4 pt 10	1B-0.5 pt 1	1B-0.5 pt 2
Location	Core	Core	Core	Rim	Rim	Rim	Rim
Remarks							
SiO2	38.46	38.48	38.41	38.15	37.91	37.83	37.93
TiO2	0.00	0.04	0.02	0.00	0.02	0.05	0.00
Al2O3	21.54	21.40	21.54	21.60	21.05	21.18	21.43
FeO	29.58	29.70	30.07	30.69	32.89	32.66	30.63
MnO	0.59	0.61	0.62	0.68	0.82	0.77	0.67
MgO	8.05	7.91	7.55	7.04	5.23	5.78	7.13
CaO	2.06	2.15	2.26	2.46	2.26	1.80	2.37
Na2O	0.02	0.01	0.01	0.01	0.02	0.00	0.00
K2O	0.05	0.08	0.03	0.02	0.12	0.10	0.05
P2O5	0.06	0.06	0.08	0.11	0.08	0.07	0.05
Total	100.41	100.42	100.59	100.77	100.40	100.24	100.26
Si	0.249	0.249	0.249	0.248	0.250	0.249	0.248
Ti	0.000	0.000	0.000	0.000	0.000	0.000	0.000
Al	0.164	0.163	0.164	0.165	0.164	0.164	0.165
Fe	0.160	0.161	0.163	0.167	0.181	0.180	0.167
Mn	0.003	0.003	0.003	0.004	0.005	0.004	0.004
Mg	0.078	0.076	0.073	0.068	0.051	0.057	0.069
Ca	0.014	0.015	0.016	0.017	0.016	0.013	0.017
Na	0.000	0.000	0.000	0.000	0.000	0.000	0.000
K	0.000	0.001	0.000	0.000	0.001	0.001	0.000
P	0.000	0.000	0.000	0.001	0.000	0.000	0.000
Total	0.669	0.669	0.669	0.669	0.668	0.668	0.670
Si	2.984	2.989	2.983	2.970	2.998	2.989	2.970
Ti	-	0.002	0.001	-	0.001	0.002	-
Al	1.970	1.960	1.973	1.982	1.962	1.972	1.978
Fe	1.920	1.930	1.954	1.998	2.176	2.158	2.006
Mn	0.038	0.040	0.041	0.044	0.055	0.052	0.044
Mg	0.931	0.916	0.874	0.817	0.617	0.680	0.833
Ca	0.172	0.179	0.188	0.205	0.192	0.152	0.199
Na	0.002	0.001	0.002	0.002	0.004	-	-
K	0.005	0.007	0.004	0.002	0.012	0.010	0.005
P	0.004	0.004	0.005	0.007	0.005	0.005	0.004
Total	8.027	8.028	8.024	8.029	8.021	8.021	8.040
% Almand	0.627	0.630	0.639	0.652	0.716	0.709	0.651
% Spess	0.013	0.013	0.013	0.014	0.018	0.017	0.014
% Pyrope	0.304	0.299	0.286	0.267	0.203	0.224	0.270
% Gross	0.056	0.058	0.062	0.067	0.063	0.050	0.065

Appendix A. Electron microprobe analyses of compositionally mapped garnets, and inclusions therein.

Table A1. X-ray mapped garnets with identified points (see appendix D for point maps).
Analyses recalculated for 12 oxygens.

Sample and point	1B-0.5 pt 3	1B-0.5 pt 4	1B-0.5 pt 5	1B-0.5 pt 6	1B-0.5 pt 7	1B-0.5 pt 8	1B-0.5 pt 9
Location	Core	Core	Core	Core	Core	Core	Rim
Remarks							
SiO2	38.22	38.35	38.07	38.43	38.68	38.39	38.56
TiO2	0.01	0.04	0.02	0.02	0.00	0.02	0.01
Al2O3	21.43	21.54	21.47	21.50	21.48	21.44	21.41
FeO	30.15	30.08	30.32	30.27	30.20	29.70	29.94
MnO	0.68	0.69	0.61	0.64	0.65	0.65	0.63
MgO	7.43	7.68	7.70	7.70	7.79	7.60	7.50
CaO	2.15	1.93	1.92	1.95	2.06	2.39	2.39
Na2O	0.00	0.01	0.00	0.00	0.00	0.02	0.00
K2O	0.07	0.07	0.06	0.07	0.08	0.09	0.08
P2O5	0.06	0.08	0.05	0.03	0.02	0.03	0.06
Total	100.21	100.46	100.23	100.61	100.97	100.32	100.58
Si	0.249	0.249	0.248	0.249	0.249	0.249	0.250
Ti	0.000	0.000	0.000	0.000	0.000	0.000	0.000
Al	0.164	0.165	0.165	0.164	0.163	0.164	0.163
Fe	0.164	0.163	0.165	0.164	0.163	0.161	0.162
Mn	0.004	0.004	0.003	0.004	0.004	0.004	0.004
Mg	0.072	0.074	0.075	0.074	0.075	0.074	0.072
Ca	0.015	0.013	0.013	0.014	0.014	0.017	0.017
Na	0.000	0.000	0.000	0.000	0.000	0.000	0.000
K	0.001	0.001	0.001	0.001	0.001	0.001	0.001
P	0.000	0.000	0.000	0.000	0.000	0.000	0.000
Total	0.669	0.669	0.670	0.669	0.669	0.669	0.669
Si	2.984	2.982	2.972	2.987	2.993	2.989	2.995
Ti	0.001	0.002	0.001	0.001	-	0.001	-
Al	1.973	1.974	1.976	1.969	1.960	1.967	1.961
Fe	1.968	1.956	1.980	1.967	1.955	1.934	1.945
Mn	0.044	0.046	0.041	0.042	0.043	0.043	0.042
Mg	0.865	0.890	0.896	0.892	0.899	0.882	0.869
Ca	0.180	0.161	0.161	0.163	0.172	0.199	0.199
Na	-	0.001	-	-	-	0.002	-
K	0.006	0.007	0.006	0.007	0.008	0.008	0.008
P	0.005	0.005	0.004	0.002	0.001	0.002	0.004
Total	8.028	8.024	8.039	8.030	8.032	8.029	8.024
% Almand	0.644	0.641	0.643	0.642	0.637	0.632	0.637
% Spess	0.015	0.015	0.013	0.014	0.014	0.014	0.014
% Pyrope	0.283	0.292	0.291	0.291	0.293	0.288	0.284
% Gross	0.059	0.053	0.052	0.053	0.056	0.065	0.065

Appendix A. Electron microprobe analyses of compositionally mapped garnets, and inclusions therein.

Table A1. X-ray mapped garnets with identified points (see appendix D for point maps).
Analyses recalculated for 12 oxygens.

Sample and point	1B-0.5 pt 10	2A-0.5 pt 1	2A-0.5 pt 2	2A-0.5 pt 3	2A-0.5 pt 4	2A-0.5 pt 5	2A-0.5 pt 6
Location	Rim	Rim	Rim	Core	Core	Rim	Core
Remarks							
SiO2	38.56	38.24	38.26	38.69	38.45	38.77	38.61
TiO2	0.01	0.02	0.00	0.00	0.00	0.02	0.03
Al2O3	21.53	21.72	21.59	21.67	21.80	21.67	21.79
FeO	30.15	31.31	30.73	30.86	30.82	30.79	30.88
MnO	0.70	0.64	0.64	0.60	0.62	0.62	0.58
MgO	7.84	7.17	7.40	7.57	7.64	7.76	7.66
CaO	1.74	1.58	1.63	1.50	1.54	1.51	1.52
Na2O	0.01	0.03	0.08	0.02	0.03	0.04	0.03
K2O	0.09	0.09	0.08	0.06	0.05	0.04	0.05
P2O5	0.02	0.05	0.05	0.05	0.06	0.05	0.05
Total	100.65	100.83	100.47	101.01	101.01	101.28	101.20
Si	0.249	0.248	0.249	0.250	0.248	0.249	0.249
Ti	0.000	0.000	0.000	0.000	0.000	0.000	0.000
Al	0.164	0.166	0.165	0.165	0.166	0.164	0.165
Fe	0.163	0.170	0.167	0.167	0.166	0.166	0.166
Mn	0.004	0.004	0.004	0.003	0.003	0.003	0.003
Mg	0.076	0.069	0.072	0.073	0.074	0.074	0.074
Ca	0.012	0.011	0.011	0.010	0.011	0.010	0.011
Na	0.000	0.000	0.001	0.000	0.000	0.001	0.000
K	0.001	0.001	0.001	0.001	0.000	0.000	0.000
P	0.000	0.000	0.000	0.000	0.000	0.000	0.000
Total	0.669	0.669	0.669	0.668	0.669	0.669	0.669
Si	2.992	2.976	2.982	2.994	2.977	2.992	2.983
Ti	-	0.001	-	-	-	0.001	0.002
Al	1.969	1.993	1.984	1.976	1.990	1.970	1.984
Fe	1.956	2.038	2.003	1.998	1.996	1.987	1.996
Mn	0.046	0.042	0.042	0.040	0.041	0.041	0.038
Mg	0.907	0.832	0.860	0.874	0.882	0.893	0.882
Ca	0.144	0.132	0.136	0.124	0.127	0.125	0.126
Na	0.001	0.005	0.013	0.004	0.004	0.006	0.005
K	0.008	0.008	0.008	0.006	0.005	0.004	0.005
P	0.001	0.002	0.004	0.004	0.004	0.004	0.004
Total	8.026	8.029	8.032	8.020	8.024	8.023	8.024
% Almand	0.641	0.670	0.659	0.658	0.655	0.652	0.656
% Spess	0.015	0.014	0.014	0.013	0.013	0.013	0.013
% Pyrope	0.297	0.273	0.283	0.288	0.290	0.293	0.290
% Gross	0.047	0.043	0.045	0.041	0.042	0.041	0.041

Appendix A. Electron microprobe analyses of compositionally mapped garnets, and inclusions therein.

Table A1. X-ray mapped garnets with identified points (see appendix D for point maps).
Analyses recalculated for 12 oxygens.

Sample and point	2A-0.5 pt 7	2A-0.5 pt 8	2A-0.5 pt 9	2A-0.5 pt 10	2A-0.6a pt 1	2A-0.6a pt 2	2A-0.6a pt 3
Location	Core	Core	Core	Rim	Rim	Rim	Core
Remarks							
SiO2	38.52	38.40	38.49	38.36	38.78	39.03	39.00
TiO2	0.01	0.00	0.03	0.04	0.02	0.00	0.00
Al2O3	21.73	21.58	21.77	21.67	21.82	21.77	21.92
FeO	30.47	30.52	31.59	32.67	29.87	29.88	30.07
MnO	0.60	0.62	0.62	0.66	0.56	0.57	0.57
MgO	7.69	7.49	7.33	6.48	8.23	8.32	8.27
CaO	1.47	1.57	1.51	1.49	1.54	1.67	1.50
Na2O	0.19	0.27	0.04	0.04	0.05	0.04	0.03
K2O	0.17	0.20	0.10	0.09	0.06	0.05	0.12
P2O5	0.09	0.07	0.04	0.04	0.05	0.03	0.04
Total	100.95	100.72	101.52	101.54	100.97	101.35	101.51
Si	0.249	0.249	0.248	0.248	0.249	0.250	0.249
Ti	0.000	0.000	0.000	0.000	0.000	0.000	0.000
Al	0.165	0.165	0.165	0.166	0.165	0.164	0.165
Fe	0.164	0.165	0.170	0.177	0.160	0.160	0.161
Mn	0.003	0.003	0.003	0.004	0.003	0.003	0.003
Mg	0.074	0.072	0.070	0.063	0.079	0.079	0.079
Ca	0.010	0.011	0.010	0.010	0.011	0.011	0.010
Na	0.002	0.003	0.001	0.001	0.001	0.001	0.000
K	0.001	0.002	0.001	0.001	0.001	0.000	0.001
P	0.001	0.000	0.000	0.000	0.000	0.000	0.000
Total	0.670	0.671	0.670	0.669	0.669	0.668	0.669
Si	2.982	2.984	2.976	2.981	2.989	2.996	2.990
Ti	-	-	0.002	0.002	0.001	-	-
Al	1.984	1.978	1.984	1.986	1.982	1.969	1.981
Fe	1.973	1.984	2.042	2.124	1.925	1.918	1.928
Mn	0.040	0.041	0.041	0.043	0.037	0.037	0.037
Mg	0.887	0.869	0.845	0.750	0.944	0.952	0.944
Ca	0.122	0.131	0.125	0.124	0.127	0.137	0.124
Na	0.029	0.041	0.006	0.006	0.007	0.006	0.005
K	0.017	0.020	0.010	0.008	0.006	0.005	0.011
P	0.006	0.005	0.002	0.002	0.002	0.001	0.002
Total	8.040	8.053	8.034	8.027	8.022	8.021	8.023
% Almand	0.653	0.656	0.669	0.699	0.634	0.630	0.636
% Spess	0.013	0.013	0.013	0.014	0.012	0.012	0.012
% Pyrope	0.293	0.287	0.277	0.247	0.311	0.313	0.311
% Gross	0.041	0.043	0.041	0.041	0.042	0.045	0.041

Appendix A. Electron microprobe analyses of compositionally mapped garnets, and inclusions therein.

Table A1. X-ray mapped garnets with identified points (see appendix D for point maps).
Analyses recalculated for 12 oxygens.

Sample and point	2A-0.6a pt 4	2A-0.6a pt 5	2A-0.6a pt 6	2A-0.6a pt 7	2A-0.6a pt 8	2A-0.6a pt 9
Location	Core	Rim	Rim	Rim	Core	Core
Remarks						
SiO2	39.15	38.82	39.00	38.39	38.35	38.59
TiO2	0.03	0.01	0.00	0.01	0.03	0.04
Al2O3	21.92	21.81	21.72	21.64	21.44	21.70
FeO	30.19	30.35	30.93	31.39	31.20	31.65
MnO	0.56	0.58	0.60	0.61	0.61	0.62
MgO	8.13	8.06	7.66	7.05	7.02	7.25
CaO	1.57	1.55	1.64	1.49	1.44	1.49
Na2O	0.02	0.03	0.02	0.02	0.19	0.03
K2O	0.07	0.09	0.09	0.09	0.13	0.06
P2O5	0.03	0.02	0.06	0.08	0.05	0.04
Total	101.67	101.33	101.72	100.76	100.46	101.47
Si	0.250	0.249	0.250	0.249	0.250	0.249
Ti	0.000	0.000	0.000	0.000	0.000	0.000
Al	0.165	0.165	0.164	0.165	0.165	0.165
Fe	0.161	0.163	0.166	0.170	0.170	0.171
Mn	0.003	0.003	0.003	0.003	0.003	0.003
Mg	0.077	0.077	0.073	0.068	0.068	0.070
Ca	0.011	0.011	0.011	0.010	0.010	0.010
Na	0.000	0.000	0.000	0.000	0.002	0.000
K	0.001	0.001	0.001	0.001	0.001	0.001
P	0.000	0.000	0.000	0.000	0.000	0.000
Total	0.668	0.669	0.668	0.668	0.669	0.669
Si	2.996	2.988	2.998	2.988	2.995	2.984
Ti	0.002	0.001	-	-	0.001	0.002
Al	1.978	1.979	1.967	1.985	1.974	1.979
Fe	1.933	1.954	1.987	2.044	2.038	2.047
Mn	0.036	0.038	0.038	0.040	0.040	0.041
Mg	0.928	0.924	0.877	0.818	0.817	0.835
Ca	0.128	0.128	0.136	0.125	0.121	0.124
Na	0.004	0.005	0.004	0.004	0.029	0.005
K	0.007	0.008	0.010	0.008	0.013	0.006
P	0.002	0.001	0.004	0.005	0.002	0.002
Total	8.015	8.028	8.020	8.016	8.030	8.027
% Almand	0.639	0.642	0.654	0.675	0.676	0.672
% Spess	0.012	0.013	0.013	0.013	0.013	0.013
% Pyrope	0.307	0.304	0.289	0.270	0.271	0.274
% Gross	0.042	0.042	0.045	0.041	0.040	0.041

Appendix A. Electron microprobe analyses of compositionally mapped garnets, and inclusions therein.

Table A1. X-ray mapped garnets with identified points (see appendix D for point maps).
Analyses recalculated for 12 oxygens.

Sample and point	2A-0.6a pt 10	2A-0.6b pt 1	2A-0.6b pt 2	2A-0.6b pt 3	2A-0.6b pt 4	2A-0.6b pt 5
Location	Rim	Rim	Core	Core	Core	Core
Remarks						
SiO2	36.62	40.91	38.41	38.39	38.49	38.42
TiO2	0.00	0.09	0.08	0.09	0.08	0.09
Al2O3	20.48	23.36	21.79	21.88	21.88	21.88
FeO	30.40	34.20	30.30	30.33	30.03	30.23
MnO	0.65	0.80	0.65	0.60	0.61	0.61
MgO	5.86	3.75	7.75	8.12	8.20	8.18
CaO	1.57	2.34	1.59	1.55	1.61	1.59
Na2O	1.35	0.80	0.11	0.07	0.06	0.01
K2O	0.70	0.33	0.12	0.13	0.12	0.15
P2O5	0.09	0.04	0.04	0.02	0.06	0.06
Total	97.72	106.62	100.84	101.17	101.15	101.23
Si	0.248	0.253	0.248	0.247	0.247	0.247
Ti	0.000	0.000	0.000	0.001	0.000	0.001
Al	0.163	0.170	0.166	0.166	0.166	0.166
Fe	0.172	0.177	0.164	0.163	0.161	0.163
Mn	0.004	0.004	0.004	0.003	0.003	0.003
Mg	0.059	0.035	0.075	0.078	0.079	0.078
Ca	0.011	0.016	0.011	0.011	0.011	0.011
Na	0.018	0.010	0.001	0.001	0.001	0.000
K	0.006	0.003	0.001	0.001	0.001	0.001
P	0.001	0.000	0.000	0.000	0.000	0.000
Total	0.682	0.667	0.670	0.671	0.670	0.670
Si	2.974	3.036	2.976	2.964	2.968	2.963
Ti	-	0.005	0.005	0.006	0.005	0.006
Al	1.960	2.044	1.990	1.991	1.988	1.990
Fe	2.064	2.123	1.963	1.958	1.937	1.950
Mn	0.044	0.050	0.043	0.040	0.040	0.040
Mg	0.709	0.414	0.895	0.934	0.942	0.940
Ca	0.137	0.186	0.132	0.128	0.133	0.132
Na	0.212	0.115	0.017	0.010	0.008	0.002
K	0.072	0.031	0.012	0.013	0.012	0.014
P	0.006	0.002	0.002	0.001	0.004	0.004
Total	8.178	8.006	8.035	8.046	8.036	8.041
% Almand	0.699	0.765	0.647	0.640	0.635	0.637
% Spess	0.015	0.018	0.014	0.013	0.013	0.013
% Pyrope	0.240	0.149	0.295	0.305	0.309	0.307
% Gross	0.046	0.067	0.044	0.042	0.044	0.043

Appendix A. Electron microprobe analyses of compositionally mapped garnets, and inclusions therein.

Table A1. X-ray mapped garnets with identified points (see appendix D for point maps). Analyses recalculated for 12 oxygens.

Sample and point	2A-0.6b pt 6	2A-0.6b pt 7	2A-0.6b pt 8	2A-0.6b pt 9	2A-0.6b pt 10
Location	Core	Core	Core	Rim	Core
Remarks					
SiO2	34.32	38.21	38.29	38.79	38.77
TiO2	0.34	0.07	0.10	0.09	0.09
Al2O3	24.28	21.74	21.75	22.02	21.98
FeO	16.07	29.98	29.65	29.82	29.43
MnO	0.11	0.59	0.60	0.60	0.57
MgO	9.06	8.07	8.35	8.46	8.32
CaO	0.34	1.57	1.57	1.51	1.79
Na2O	0.07	0.15	0.17	0.05	0.03
K2O	0.78	0.23	0.18	0.09	0.10
P2O5	0.03	0.06	0.05	0.01	0.03
Total	85.40	100.67	100.71	101.45	101.12
Si	0.245	0.247	0.247	0.248	0.248
Ti	0.002	0.000	0.001	0.001	0.000
Al	0.204	0.166	0.165	0.166	0.166
Fe	0.096	0.162	0.160	0.159	0.158
Mn	0.001	0.003	0.003	0.003	0.003
Mg	0.096	0.078	0.080	0.081	0.080
Ca	0.003	0.011	0.011	0.010	0.012
Na	0.001	0.002	0.002	0.001	0.000
K	0.007	0.002	0.002	0.001	0.001
P	0.000	0.000	0.000	0.000	0.000
Total	0.655	0.671	0.671	0.669	0.669
Si	2.940	2.965	2.964	2.975	2.980
Ti	0.022	0.005	0.006	0.006	0.005
Al	2.450	1.988	1.985	1.991	1.991
Fe	1.151	1.945	1.920	1.913	1.891
Mn	0.008	0.038	0.040	0.038	0.037
Mg	1.157	0.934	0.964	0.967	0.954
Ca	0.031	0.131	0.130	0.124	0.148
Na	0.012	0.023	0.026	0.007	0.005
K	0.085	0.023	0.018	0.010	0.010
P	0.002	0.004	0.004	-	0.002
Total	7.860	8.057	8.057	8.032	8.023
% Almand	0.490	0.638	0.629	0.629	0.624
% Spess	0.004	0.013	0.013	0.013	0.012
% Pyrope	0.493	0.306	0.316	0.318	0.315
% Gross	0.013	0.043	0.042	0.041	0.049

Appendix A. Electron microprobe analyses of compositionally mapped garnets, and inclusions therein.

Table A2. Inclusions from compositionally mapped garnets (see appendix D for point maps, inclusions locations).
Mineral identification included. Garnet analyses are possibly missed points, or non-inclusions.

Sample and point	1A-0.5 pt 6	1A-0.5 pt 11	1A-0.5 pt 12	1A-0.5 pt 13	1A-0.5 pt 14	1A-0.5 pt 15	1A-0.5 pt 16	1A-0.5 pt 17	1A-0.5 pt 18	1A-0.5 pt 19
Remark										
Mineral	Qtz	Qtz	Kspar	Qtz	Plag	Plag	Plag	Kspar	Qtz	??
SiO2	94.30	96.25	64.32	95.84	59.91	58.81	59.37	63.01	96.28	8.33
TiO2	0.02	0.00	0.00	0.00	0.00	0.00	0.00	0.06	0.00	0.00
Al2O3	0.00	0.00	19.73	0.00	25.66	25.41	25.22	19.54	0.00	2.78
FeO	0.23	0.28	0.62	0.39	0.67	0.52	0.40	0.82	0.29	0.53
MnO	0.00	0.00	0.03	0.01	0.03	0.01	0.02	0.03	0.00	0.60
MgO	0.00	0.00	0.00	0.00	0.00	0.01	0.00	0.00	0.00	0.48
CaO	0.00	0.01	0.09	0.01	6.89	7.13	6.71	0.12	0.01	61.53
Na2O	0.02	0.00	0.97	0.00	3.42	5.98	5.03	0.73	0.00	0.10
K2O	0.00	0.00	10.19	0.01	0.15	0.18	0.15	11.55	0.00	0.04
P2O5	0.00	0.00	0.03	0.00	0.01	0.00	0.02	0.02	0.00	0.01
Total	94.57	96.54	95.98	96.24	96.74	98.04	96.90	95.88	96.58	74.40
Si	0.499	0.499	0.375	0.499	0.339	0.333	0.338	0.372	0.499	0.093
Ti	0.000	0.000	0.000	0.000	0.000	0.000	0.000	0.000	0.000	0.000
Al	0.000	0.000	0.136	0.000	0.171	0.170	0.169	0.136	0.000	0.037
Fe	0.001	0.001	0.003	0.002	0.003	0.003	0.002	0.004	0.001	0.005
Mn	0.000	0.000	0.000	0.000	0.000	0.000	0.000	0.000	0.000	0.006
Mg	0.000	0.000	0.000	0.000	0.000	0.000	0.000	0.000	0.000	0.008
Ca	0.000	0.000	0.001	0.000	0.042	0.043	0.041	0.001	0.000	0.738
Na	0.000	0.000	0.011	0.000	0.038	0.066	0.056	0.008	0.000	0.002
K	0.000	0.000	0.076	0.000	0.001	0.001	0.001	0.087	0.000	0.001
P	0.000	0.000	0.000	0.000	0.000	0.000	0.000	0.000	0.000	0.000
Total	0.501	0.501	0.601	0.501	0.595	0.616	0.606	0.608	0.501	0.890

Appendix A. Electron microprobe analyses of compositionally mapped garnets, and inclusions therein.

Table A2. Inclusions from compositionally mapped garnets (see appendix D for point maps, inclusions locations). Mineral identification included. Garnet analyses are possibly missed points, or non-inclusions.

Sample and point	1A-0.5 pt 22?	1A-0.5 pt ?	1A-0.5 pt ?	1A-0.5 pt ?	1A-0.2 pt 6	1A-0.3 pt 11	1A-0.3 pt 12	1A-0.3 pt 13	1A-0.3 pt 14	1A-0.3 pt 15	1A-0.3 pt 16
Remark											
Mineral	Zircon	Garn	Garn	Garn	Plag	Rutile	Zircon	Monazite	Rutile	Biot	Qtz
SiO2	22.53	32.30	36.82	36.60	48.43	0.04	33.95	0.40	0.04	35.75	97.71
TiO2	11.11	0.00	0.00	0.00	0.00	97.40	0.22	0.57	97.98	6.46	0.00
Al2O3	2.33	20.24	22.41	22.45	19.58	0.04	0.11	0.08	0.02	15.91	0.02
FeO	5.51	22.38	30.96	31.05	0.06	1.41	0.76	0.98	1.21	12.38	0.47
MnO	0.18	0.62	0.82	0.80	0.00	0.04	0.13	0.35	0.03	0.00	0.00
MgO	1.27	5.90	7.10	7.11	0.04	0.00	0.07	0.07	0.01	13.59	0.01
CaO	0.26	1.86	2.74	2.72	13.55	0.07	0.05	1.35	0.08	0.00	0.00
Na2O	0.09	0.00	0.00	0.00	3.18	0.00	0.06	0.05	0.00	0.34	0.02
K2O	0.10	0.02	0.04	0.04	0.00	0.00	0.03	0.09	0.00	10.22	0.00
P2O5	0.19	0.00	0.00	0.00	0.02	0.00	0.31	25.60	0.00	0.00	0.00
Total	43.55	83.31	100.89	100.76	84.85	99.00	35.68	29.54	99.37	94.64	98.22
Si	0.307	0.248	0.240	0.239	0.325	0.000	0.485	0.007	0.000	0.244	0.499
Ti	0.114	0.000	0.000	0.000	0.000	0.495	0.002	0.007	0.496	0.033	0.000
Al	0.037	0.183	0.172	0.173	0.155	0.000	0.002	0.002	0.000	0.128	0.000
Fe	0.063	0.144	0.169	0.170	0.000	0.008	0.009	0.014	0.007	0.071	0.002
Mn	0.002	0.004	0.005	0.004	0.000	0.000	0.002	0.005	0.000	0.000	0.000
Mg	0.026	0.067	0.069	0.069	0.000	0.000	0.001	0.002	0.000	0.138	0.000
Ca	0.004	0.015	0.019	0.019	0.097	0.001	0.001	0.025	0.001	0.000	0.000
Na	0.002	0.000	0.000	0.000	0.041	0.000	0.002	0.002	0.000	0.004	0.000
K	0.002	0.000	0.000	0.000	0.000	0.000	0.001	0.002	0.000	0.089	0.000
P	0.002	0.000	0.000	0.000	0.000	0.000	0.004	0.369	0.000	0.000	0.000
Total	0.559	0.661	0.674	0.675	0.619	0.504	0.508	0.434	0.504	0.706	0.501

Appendix A. Electron microprobe analyses of compositionally mapped garnets, and inclusions therein.

Table A2. Inclusions from compositionally mapped garnets (see appendix D for point maps, inclusions locations).
Mineral identification included. Garnet analyses are possibly missed points, or non-inclusions.

Sample and point	1A-0.3 pt 17	1A-0.2 pt 11	1A-0.2 pt 12	1A-0.2 pt 13	1A-0.2 pt 14	1A-0.2 pt 15	1A-0.2 pt 16	1A-0.2 pt ??	1A-0.2 pt 18	1A-0.2 pt 19
Remark										
Mineral	Qtz	Zircon	Kspar	Plag	Plag	Kspar	Rutile	Biot	Zircon	Qtz
SiO2	96.12	31.13	62.11	59.53	59.58	62.78	0.00	35.95	33.28	96.22
TiO2	0.00	0.00	0.00	0.00	0.00	0.00	99.72	0.00	0.05	0.00
Al2O3	0.02	0.24	17.66	24.52	23.63	17.71	0.00	24.80	0.00	0.00
FeO	0.37	1.43	0.33	0.33	0.00	0.00	0.10	14.69	1.41	0.00
MnO	0.00	0.09	0.00	0.00	0.00	0.00	0.00	0.00	0.01	0.00
MgO	0.00	0.07	0.00	0.03	0.00	0.00	0.00	8.85	0.01	0.00
CaO	0.00	0.75	0.00	2.45	6.25	0.00	0.00	0.13	0.02	0.00
Na2O	0.02	0.09	0.92	5.14	8.45	0.88	0.00	0.10	0.02	0.00
K2O	0.00	0.00	16.69	0.08	0.13	17.16	0.00	1.33	0.01	0.00
P2O5	0.00	1.53	0.00	0.00	0.00	0.00	0.00	0.00	0.04	0.00
Total	96.54	35.35	97.70	92.09	98.03	98.53	99.82	85.83	34.85	96.22
Si	0.499	0.456	0.371	0.349	0.339	0.372	0.000	0.253	0.490	0.500
Ti	0.000	0.000	0.000	0.000	0.000	0.000	0.500	0.000	0.001	0.000
Al	0.000	0.004	0.124	0.170	0.158	0.124	0.000	0.205	0.000	0.000
Fe	0.002	0.018	0.002	0.002	0.000	0.000	0.001	0.086	0.017	0.000
Mn	0.000	0.001	0.000	0.000	0.000	0.000	0.000	0.000	0.000	0.000
Mg	0.000	0.002	0.000	0.000	0.000	0.000	0.000	0.093	0.000	0.000
Ca	0.000	0.012	0.000	0.015	0.038	0.000	0.000	0.001	0.000	0.000
Na	0.000	0.003	0.011	0.059	0.093	0.010	0.000	0.001	0.000	0.000
K	0.000	0.000	0.127	0.001	0.001	0.130	0.000	0.012	0.000	0.000
P	0.000	0.019	0.000	0.000	0.000	0.000	0.000	0.000	0.001	0.000
Total	0.501	0.514	0.636	0.595	0.629	0.636	0.500	0.651	0.509	0.500

Appendix A. Electron microprobe analyses of compositionally mapped garnets, and inclusions therein.

Table A2. Inclusions from compositionally mapped garnets (see appendix D for point maps, inclusions locations).
Mineral identification included. Garnet analyses are possibly missed points, or non-inclusions.

Sample and point	1A-0.2 pt 20	1A-0.2 pt ??	1A-1.3 pt 11	1A-1.3 pt 12	1A-1.3 pt 13	1A-1.3 pt 14	1A-1.3 pt 15	1A-1.3 pt 16	1A-1.3 pt 17	1A-1.3 pt 18
Remark										
Mineral	Qtz	Qtz	Zircon	Monazite	Zircon	Garn	Biot	Qtz	Kspar	Garn
SiO2	96.44	94.07	34.84	0.11	31.97	32.66	37.38	100.13	64.99	38.45
TiO2	0.00	0.00	0.13	0.39	0.10	0.00	0.00	0.00	0.00	0.14
Al2O3	0.00	0.00	0.08	0.07	0.11	17.80	20.48	0.00	18.75	16.41
FeO	0.29	0.22	1.18	0.90	1.00	16.52	26.03	0.51	0.66	17.78
MnO	0.00	0.00	0.17	0.37	0.12	0.32	0.60	0.00	0.00	0.42
MgO	0.00	0.00	0.07	0.06	0.07	6.59	7.11	0.00	0.01	4.37
CaO	0.00	0.00	0.08	1.21	0.07	1.22	2.23	0.00	0.01	1.64
Na2O	0.00	0.00	0.06	0.07	0.10	1.10	1.15	0.01	1.64	1.17
K2O	0.00	0.00	0.17	0.36	0.18	0.01	0.09	0.01	13.32	0.39
P2O5	0.00	0.00	0.23	26.44	0.50	0.05	0.01	0.00	0.19	0.01
Total	96.73	94.29	37.01	29.97	34.21	76.26	95.07	100.65	99.58	80.77
Si	0.499	0.500	0.484	0.002	0.480	0.265	0.254	0.499	0.373	0.294
Ti	0.000	0.000	0.001	0.005	0.001	0.000	0.000	0.000	0.000	0.001
Al	0.000	0.000	0.001	0.001	0.002	0.170	0.164	0.000	0.127	0.148
Fe	0.001	0.001	0.014	0.013	0.013	0.112	0.148	0.002	0.003	0.114
Mn	0.000	0.000	0.002	0.005	0.002	0.002	0.003	0.000	0.000	0.003
Mg	0.000	0.000	0.001	0.002	0.002	0.080	0.072	0.000	0.000	0.050
Ca	0.000	0.000	0.001	0.022	0.001	0.011	0.016	0.000	0.000	0.013
Na	0.000	0.000	0.002	0.002	0.003	0.017	0.015	0.000	0.018	0.017
K	0.000	0.000	0.003	0.008	0.003	0.000	0.001	0.000	0.098	0.004
P	0.000	0.000	0.003	0.375	0.006	0.000	0.000	0.000	0.001	0.000
Total	0.501	0.501	0.512	0.435	0.512	0.658	0.673	0.501	0.620	0.643

Appendix A. Electron microprobe analyses of compositionally mapped garnets, and inclusions therein.

Table A2. Inclusions from compositionally mapped garnets (see appendix D for point maps, inclusions locations).
Mineral identification included. Garnet analyses are possibly missed points, or non-inclusions.

Sample and point	1A-0.3 pt 18	1A-0.3 pt 19	1A-0.3 pt ?	1A-1.3 pt ?	1A-1.3 pt ?	2A-0.4 pt 11	2A-0.4 pt 12	2A-0.4 pt 13	2A-0.4 pt 14	2A-0.4 pt 15	2A-0.4 pt 16
Remark											
Mineral	Garn	Garn	Garn	Qtz	Qtz	Rutile	Rutile	Plag	Biot	Qtz	Qtz
SiO2	38.72	31.76	33.26	98.75	97.27	0.00	0.00	58.26	35.98	97.09	97.75
TiO2	0.00	0.00	0.00	0.00	0.00	98.68	98.90	0.00	6.35	0.00	0.00
Al2O3	20.48	17.41	17.90	0.01	0.03	0.00	0.00	24.60	16.56	0.00	0.04
FeO	31.09	16.91	19.29	0.66	0.64	0.24	0.64	0.26	10.69	0.59	0.75
MnO	0.82	0.48	0.49	0.00	0.00	0.05	0.05	0.01	0.02	0.00	0.00
MgO	6.25	5.56	5.83	0.00	0.03	0.00	0.00	0.00	14.81	0.00	0.00
CaO	3.04	1.39	1.48	0.00	0.00	0.07	0.04	7.24	0.01	0.00	0.01
Na2O	0.06	0.01	0.02	0.04	0.02	0.00	0.00	7.84	0.12	0.00	0.00
K2O	0.00	0.00	0.00	0.02	0.02	0.11	0.12	0.35	8.03	0.04	0.03
P2O5	0.00	0.00	0.00	0.00	0.01	0.02	0.01	0.04	0.01	0.00	0.00
Total	100.45	73.51	78.26	99.47	98.01	99.17	99.75	98.59	92.58	97.72	98.58
Si	0.253	0.268	0.266	0.499	0.498	0.000	0.000	0.331	0.245	0.499	0.498
Ti	0.000	0.000	0.000	0.000	0.000	0.499	0.498	0.000	0.033	0.000	0.000
Al	0.158	0.173	0.169	0.000	0.000	0.000	0.000	0.165	0.133	0.000	0.000
Fe	0.170	0.119	0.129	0.003	0.003	0.001	0.004	0.001	0.061	0.003	0.003
Mn	0.005	0.003	0.003	0.000	0.000	0.000	0.000	0.000	0.000	0.000	0.000
Mg	0.061	0.070	0.070	0.000	0.000	0.000	0.000	0.000	0.150	0.000	0.000
Ca	0.021	0.013	0.013	0.000	0.000	0.001	0.000	0.044	0.000	0.000	0.000
Na	0.001	0.000	0.000	0.000	0.000	0.000	0.000	0.086	0.002	0.000	0.000
K	0.000	0.000	0.000	0.000	0.000	0.001	0.001	0.003	0.070	0.000	0.000
P	0.000	0.000	0.000	0.000	0.000	0.000	0.000	0.000	0.000	0.000	0.000
Total	0.668	0.646	0.650	0.502	0.502	0.502	0.503	0.631	0.692	0.502	0.502

Appendix A. Electron microprobe analyses of compositionally mapped garnets, and inclusions therein.

Table A2. Inclusions from compositionally mapped garnets (see appendix D for point maps, inclusions locations).
Mineral identification included. Garnet analyses are possibly missed points, or non-inclusions.

Sample and point	2A-0.4 pt 17	2A-0.4 pt 18	2A-0.4 pt 19	1B-0.3 pt 11	1B-0.3 pt 12	1B-0.3 pt 13	1B-0.3 pt 14	1B-0.3 pt 15	1B-0.3 pt 16	1B-0.3 pt 17	1B-0.3 pt ?
Remark											
Mineral	Kspar	Qtz	Kspar?	Zircon	Zircon	Monazite	Kspar	Biot?	Qtz	Qtz	Kspar
SiO2	62.50	97.20	59.24	33.95	31.77	0.39	61.16	40.03	98.72	98.79	60.55
TiO2	0.01	0.00	0.00	0.16	0.18	0.41	0.02	0.00	0.00	0.00	0.00
Al2O3	18.00	0.01	23.42	0.06	0.06	0.15	17.03	21.25	0.00	0.00	19.08
FeO	0.62	0.68	1.08	1.62	1.60	3.14	0.55	14.59	0.39	0.75	2.89
MnO	0.01	0.00	0.00	0.17	0.16	0.42	0.00	0.06	0.00	0.00	0.00
MgO	0.02	0.00	0.11	0.06	0.05	0.09	0.00	10.30	0.00	0.00	1.06
CaO	0.03	0.00	1.98	0.06	0.06	0.91	0.08	0.35	0.00	0.00	0.22
Na2O	0.44	0.00	5.51	0.05	0.05	0.06	0.92	0.87	0.00	0.00	1.34
K2O	13.87	0.03	1.91	0.19	0.17	0.36	12.28	0.76	0.00	0.02	7.78
P2O5	0.07	0.00	0.02	0.28	0.51	24.76	0.09	0.05	0.01	0.00	0.01
Total	95.56	97.92	93.27	36.60	34.61	30.69	92.14	88.26	99.12	99.56	92.93
Si	0.375	0.498	0.349	0.481	0.476	0.007	0.378	0.272	0.499	0.498	0.366
Ti	0.000	0.000	0.000	0.002	0.002	0.005	0.000	0.000	0.000	0.000	0.000
Al	0.127	0.000	0.163	0.001	0.001	0.003	0.124	0.170	0.000	0.000	0.136
Fe	0.003	0.003	0.005	0.019	0.020	0.045	0.003	0.083	0.002	0.003	0.015
Mn	0.000	0.000	0.000	0.002	0.002	0.006	0.000	0.000	0.000	0.000	0.000
Mg	0.000	0.000	0.001	0.001	0.001	0.002	0.000	0.104	0.000	0.000	0.010
Ca	0.000	0.000	0.013	0.001	0.001	0.017	0.001	0.003	0.000	0.000	0.001
Na	0.005	0.000	0.063	0.001	0.002	0.002	0.011	0.012	0.000	0.000	0.016
K	0.106	0.000	0.014	0.003	0.003	0.008	0.097	0.007	0.000	0.000	0.060
P	0.000	0.000	0.000	0.003	0.007	0.359	0.001	0.000	0.000	0.000	0.000
Total	0.617	0.502	0.608	0.515	0.514	0.453	0.614	0.651	0.501	0.502	0.604

Appendix A. Electron microprobe analyses of compositionally mapped garnets, and inclusions therein.

Table A2. Inclusions from compositionally mapped garnets (see appendix D for point maps, inclusions locations). Mineral identification included. Garnet analyses are possibly missed points, or non-inclusions.

Sample and point	1B-0.3 pt ?	1B-0.4 pt 11	1B-0.4 pt 12	1B-0.4 pt 13	1B-0.4 pt 14	1B-0.4 pt 15	1B-0.4 pt ?	1B-0.5 pt 11	1B-0.5 pt 12	1B-0.5 pt 13	1B-0.5 pt 14
Remark											
Mineral	Kspar	Pyrite	Monazite	Monazite	Monazite	Kspar	Kspar	Zircon	Zircon	Zircon	Biot
SiO2	63.39	0.05	0.14	0.28	0.10	63.09	63.03	34.02	34.54	33.99	37.17
TiO2	0.00	0.13	0.41	0.42	0.66	0.01	0.05	0.17	0.21	0.17	4.92
Al2O3	20.07	0.04	0.02	0.02	0.01	17.60	17.65	0.04	0.05	0.04	15.40
FeO	2.93	76.36	1.37	1.75	1.62	0.74	0.69	1.27	2.22	1.95	9.27
MnO	0.00	0.13	0.38	0.36	0.39	0.00	0.00	0.15	0.18	0.16	0.00
MgO	1.11	0.07	0.03	0.04	0.05	0.00	0.00	0.05	0.05	0.05	15.67
CaO	0.22	0.07	0.67	0.67	0.44	0.00	0.00	0.07	0.10	0.07	0.00
Na2O	0.88	0.06	0.08	0.07	0.06	0.87	0.90	0.05	0.06	0.06	0.38
K2O	5.69	0.18	0.35	0.38	0.42	10.93	10.70	0.17	0.18	0.18	6.50
P2O5	0.01	0.08	24.30	24.02	24.03	0.09	0.08	0.31	0.31	0.41	0.00
Total	94.31	77.17	27.76	28.01	27.76	93.32	93.09	36.31	37.91	37.09	89.33
Si	0.371	0.001	0.003	0.005	0.002	0.380	0.380	0.482	0.476	0.477	0.257
Ti	0.000	0.002	0.006	0.006	0.009	0.000	0.000	0.002	0.002	0.002	0.026
Al	0.138	0.001	0.001	0.000	0.000	0.125	0.126	0.001	0.001	0.001	0.126
Fe	0.014	0.985	0.021	0.027	0.025	0.004	0.004	0.015	0.026	0.023	0.054
Mn	0.000	0.002	0.006	0.006	0.006	0.000	0.000	0.002	0.002	0.002	0.000
Mg	0.010	0.002	0.001	0.001	0.001	0.000	0.000	0.001	0.001	0.001	0.162
Ca	0.001	0.001	0.013	0.013	0.009	0.000	0.000	0.001	0.001	0.001	0.000
Na	0.010	0.002	0.003	0.003	0.002	0.010	0.011	0.001	0.002	0.002	0.005
K	0.042	0.004	0.008	0.009	0.010	0.084	0.082	0.003	0.003	0.003	0.057
P	0.000	0.001	0.375	0.370	0.373	0.000	0.000	0.004	0.004	0.005	0.000
Total	0.587	0.999	0.435	0.439	0.436	0.604	0.603	0.512	0.518	0.516	0.686

Appendix A. Electron microprobe analyses of compositionally mapped garnets, and inclusions therein.

Table A2. Inclusions from compositionally mapped garnets (see appendix D for point maps, inclusions locations). Mineral identification included. Garnet analyses are possibly missed points, or non-inclusions.

Sample and point	1B-0.5 pt 15	1B-0.5 pt 16	1B-0.5 pt 17	1B-0.5 pt 18	1B-0.5 pt 19	1B-0.5 pt 20	1B-0.5 pt 21	1B-0.5 pt ?	2A-0.5 pt 11	2A-0.5 pt 12
Remark										
Mineral	Qtz	Zircon	Qtz	Qtz	Qtz	Biot	Qtz	Qtz	Garn	Qtz
SiO2	98.04	33.65	98.93	98.69	97.83	37.13	99.09	97.11	34.82	98.89
TiO2	0.00	0.16	0.00	0.00	0.00	1.78	0.00	0.00	0.00	0.00
Al2O3	0.00	0.05	0.01	0.00	0.00	18.18	0.00	0.02	20.20	0.00
FeO	0.36	1.90	0.90	0.69	0.62	10.14	0.34	0.37	35.63	0.69
MnO	0.00	0.16	0.00	0.00	0.00	0.00	0.00	0.00	0.58	0.00
MgO	0.00	0.06	0.00	0.00	0.00	16.28	0.00	0.01	6.02	0.00
CaO	0.00	0.09	0.00	0.00	0.00	0.00	0.00	0.00	1.41	0.00
Na2O	0.00	0.05	0.00	0.01	0.00	0.08	0.01	0.01	0.06	0.03
K2O	0.05	0.16	0.03	0.03	0.00	7.39	0.09	0.06	0.11	0.00
P2O5	0.00	0.24	0.00	0.00	0.00	0.04	0.00	0.04	0.03	0.00
Total	98.45	36.53	99.88	99.42	98.45	91.02	99.53	97.62	98.86	99.61
Si	0.499	0.479	0.498	0.499	0.499	0.253	0.499	0.499	0.238	0.499
Ti	0.000	0.002	0.000	0.000	0.000	0.009	0.000	0.000	0.000	0.000
Al	0.000	0.001	0.000	0.000	0.000	0.146	0.000	0.000	0.163	0.000
Fe	0.002	0.023	0.004	0.003	0.003	0.058	0.001	0.002	0.204	0.003
Mn	0.000	0.002	0.000	0.000	0.000	0.000	0.000	0.000	0.003	0.000
Mg	0.000	0.001	0.000	0.000	0.000	0.166	0.000	0.000	0.061	0.000
Ca	0.000	0.001	0.000	0.000	0.000	0.000	0.000	0.000	0.010	0.000
Na	0.000	0.002	0.000	0.000	0.000	0.001	0.000	0.000	0.001	0.000
K	0.000	0.003	0.000	0.000	0.000	0.064	0.001	0.000	0.001	0.000
P	0.000	0.003	0.000	0.000	0.000	0.000	0.000	0.000	0.000	0.000
Total	0.501	0.516	0.502	0.502	0.502	0.697	0.501	0.501	0.681	0.502

Appendix A. Electron microprobe analyses of compositionally mapped garnets, and inclusions therein.

Table A2. Inclusions from compositionally mapped garnets (see appendix D for point maps, inclusions locations).
Mineral identification included. Garnet analyses are possibly missed points, or non-inclusions.

Sample and point	2A-0.5 pt 12?	2A-0.5 pt 13	2A-0.5 pt 14	2A-0.5 pt 15	2A-0.5 pt 16	2A-0.5 pt 17	2A-0.5 pt 18	2A-0.5 pt 19	2A-0.5 pt 20	2A-0.5 pt 22
Remark										
Mineral	??	Plag	Kspar	Plag	Qtz	Biot	Qtz	??	Garn	Qtz
SiO2	21.15	59.12	62.13	58.48	99.24	45.97	98.90	34.56	39.21	97.62
TiO2	0.03	0.00	0.03	0.00	0.00	0.01	0.00	4.71	0.03	0.00
Al2O3	8.88	23.96	17.54	23.73	0.00	21.29	0.00	16.29	21.34	0.01
FeO	6.87	0.54	0.88	0.34	0.62	23.90	0.76	16.04	30.74	0.82
MnO	0.00	0.00	0.00	0.00	0.00	0.49	0.00	0.12	0.56	0.00
MgO	1.22	0.00	0.00	0.00	0.00	4.20	0.00	11.41	7.10	0.00
CaO	1.70	6.90	0.04	6.80	0.00	1.72	0.00	0.36	1.52	0.00
Na2O	1.84	8.21	1.19	8.00	0.03	0.53	0.04	0.09	0.15	0.14
K2O	0.36	0.24	10.99	0.35	0.01	2.41	0.06	5.96	0.21	0.01
P2O5	0.07	0.08	0.09	0.06	0.00	0.06	0.00	0.02	0.01	0.02
Total	42.12	99.05	92.90	97.75	99.89	100.59	99.76	89.56	100.87	98.62
Si	0.304	0.335	0.378	0.335	0.499	0.287	0.498	0.247	0.253	0.498
Ti	0.000	0.000	0.000	0.000	0.000	0.000	0.000	0.025	0.000	0.000
Al	0.151	0.160	0.126	0.160	0.000	0.157	0.000	0.137	0.162	0.000
Fe	0.083	0.003	0.005	0.002	0.003	0.125	0.003	0.096	0.166	0.004
Mn	0.000	0.000	0.000	0.000	0.000	0.003	0.000	0.001	0.003	0.000
Mg	0.026	0.000	0.000	0.000	0.000	0.039	0.000	0.122	0.068	0.000
Ca	0.026	0.042	0.000	0.042	0.000	0.012	0.000	0.003	0.011	0.000
Na	0.051	0.090	0.014	0.089	0.000	0.007	0.000	0.001	0.002	0.001
K	0.007	0.002	0.085	0.003	0.000	0.019	0.000	0.054	0.002	0.000
P	0.001	0.000	0.001	0.000	0.000	0.000	0.000	0.000	0.000	0.000
Total	0.648	0.631	0.608	0.630	0.502	0.647	0.502	0.687	0.667	0.503

Appendix A. Electron microprobe analyses of compositionally mapped garnets, and inclusions therein.

Table A2. Inclusions from compositionally mapped garnets (see appendix D for point maps, inclusions locations).
Mineral identification included. Garnet analyses are possibly missed points, or non-inclusions.

Sample and point	2A-0.5 pt 22	2A-0.5 pt 23	2A-0.5 pt 24	2A-0.5 pt 25	2A-0.5 pt 25?	2A-0.6a pt 11	2A-0.6a pt 12	2A-0.6a pt 13	2A-0.6a pt 14	2A-0.6a pt 15
Remark										
Mineral	Garn	Biot	??	Plag	Plag	Biot	Qtz	Qtz	Qtz	Qtz
SiO2	37.89	36.95	84.41	59.30	58.95	36.67	99.28	98.90	99.37	98.89
TiO2	0.00	4.46	1.27	0.00	0.00	3.40	0.00	0.00	0.00	0.00
Al2O3	21.41	16.68	4.69	24.09	24.22	17.03	0.10	0.00	0.00	0.00
FeO	32.35	13.72	4.24	0.31	0.29	12.49	0.75	0.70	0.47	0.71
MnO	0.63	0.00	0.00	0.00	0.00	0.00	0.00	0.00	0.00	0.00
MgO	6.48	13.45	3.77	0.00	0.00	14.79	0.01	0.00	0.00	0.00
CaO	1.66	0.00	0.00	7.05	7.14	0.00	0.00	0.00	0.00	0.00
Na2O	0.03	0.08	0.11	7.28	7.15	0.04	0.02	0.05	0.01	0.02
K2O	0.07	6.97	2.23	0.73	0.76	6.68	0.01	0.03	0.02	0.02
P2O5	0.00	0.02	0.00	0.05	0.05	0.00	0.00	0.01	0.00	0.00
Total	100.53	92.32	100.73	98.81	98.55	91.10	100.17	99.69	99.87	99.64
Si	0.248	0.253	0.445	0.336	0.335	0.252	0.498	0.498	0.499	0.498
Ti	0.000	0.023	0.005	0.000	0.000	0.018	0.000	0.000	0.000	0.000
Al	0.165	0.135	0.029	0.161	0.162	0.138	0.001	0.000	0.000	0.000
Fe	0.177	0.079	0.019	0.002	0.001	0.072	0.003	0.003	0.002	0.003
Mn	0.004	0.000	0.000	0.000	0.000	0.000	0.000	0.000	0.000	0.000
Mg	0.063	0.137	0.030	0.000	0.000	0.152	0.000	0.000	0.000	0.000
Ca	0.012	0.000	0.000	0.043	0.043	0.000	0.000	0.000	0.000	0.000
Na	0.000	0.001	0.001	0.080	0.079	0.001	0.000	0.001	0.000	0.000
K	0.001	0.061	0.015	0.005	0.006	0.059	0.000	0.000	0.000	0.000
P	0.000	0.000	0.000	0.000	0.000	0.000	0.000	0.000	0.000	0.000
Total	0.670	0.688	0.544	0.626	0.626	0.691	0.502	0.502	0.501	0.502

Appendix A. Electron microprobe analyses of compositionally mapped garnets, and inclusions therein.

Table A2. Inclusions from compositionally mapped garnets (see appendix D for point maps, inclusions locations). Mineral identification included. Garnet analyses are possibly missed points, or non-inclusions.

Sample and point	2A-0.6a pt 16	2A-0.6a pt 17	2A-0.6a pt 18	2A-0.6b pt 11	2A-0.6b pt 12	2A-0.6b pt 13	2A-0.6b pt 14	2A-0.6b pt 15	2A-0.6b pt 16
Remark									
Mineral	Qtz	Garn	Garn	Qtz	Garn	Plag	Plag	Qtz	Garn
SiO2	98.21	37.49	38.09	98.91	38.49	59.30	58.96	98.63	38.20
TiO2	0.01	0.04	0.08	0.00	0.08	0.01	0.00	0.02	0.12
Al2O3	0.04	21.54	21.50	0.00	21.75	24.08	24.05	0.00	21.63
FeO	0.81	28.31	29.50	0.76	29.89	0.47	0.70	0.70	30.71
MnO	0.03	0.57	0.60	0.03	0.60	0.01	0.01	0.02	0.61
MgO	0.00	7.84	7.85	0.00	8.25	0.02	0.00	0.00	7.66
CaO	0.01	1.48	1.55	0.02	1.64	6.91	7.18	0.01	1.47
Na2O	0.01	0.07	0.06	0.04	0.01	7.99	8.00	0.04	0.04
K2O	0.05	0.16	0.16	0.08	0.12	0.38	0.31	0.10	0.08
P2O5	0.00	0.07	0.05	0.00	0.02	0.04	0.07	0.01	0.03
Total	99.17	97.55	99.43	99.84	100.85	99.21	99.29	99.54	100.54
Si	0.498	0.249	0.249	0.498	0.248	0.335	0.333	0.498	0.248
Ti	0.000	0.000	0.000	0.000	0.000	0.000	0.000	0.000	0.001
Al	0.000	0.168	0.166	0.000	0.165	0.160	0.160	0.000	0.165
Fe	0.004	0.157	0.161	0.003	0.161	0.002	0.003	0.003	0.167
Mn	0.000	0.003	0.003	0.000	0.003	0.000	0.000	0.000	0.003
Mg	0.000	0.078	0.076	0.000	0.079	0.000	0.000	0.000	0.074
Ca	0.000	0.011	0.011	0.000	0.011	0.042	0.044	0.000	0.010
Na	0.000	0.001	0.001	0.000	0.000	0.088	0.088	0.000	0.001
K	0.000	0.001	0.001	0.001	0.001	0.003	0.002	0.001	0.001
P	0.000	0.000	0.000	0.000	0.000	0.000	0.000	0.000	0.000
Total	0.502	0.668	0.669	0.502	0.670	0.630	0.631	0.503	0.669

Appendix A. Electron microprobe analyses of compositionally mapped garnets, and inclusions therein.

Table A2. Inclusions from compositionally mapped garnets (see appendix D for point maps, inclusions locations). Mineral identification included. Garnet analyses are possibly missed points, or non-inclusions.

Sample and point	2A-0.6b pt 17	2A-0.6b pt 18	2A-0.6b pt 19	2A-0.6b pt 20	2A-0.6b pt 21	2A-0.6b pt 22
Remark						
Mineral	Garn	Qtz	Qtz	Garn	Garn	Garn
SiO2	38.46	98.30	98.43	38.04	38.45	38.59
TiO2	0.09	0.00	0.00	0.07	0.06	0.08
Al2O3	21.71	0.00	0.00	21.74	21.72	21.95
FeO	30.22	0.65	0.36	30.24	29.67	29.82
MnO	0.60	0.02	0.00	0.62	0.58	0.58
MgO	8.06	0.00	0.00	8.18	8.38	8.39
CaO	1.58	0.02	0.01	1.60	1.66	1.64
Na2O	0.06	0.07	0.03	0.04	0.04	0.04
K2O	0.09	0.05	0.06	0.11	0.08	0.10
P2O5	0.03	0.01	0.02	0.05	0.09	0.07
Total	100.90	99.11	98.91	100.70	100.74	101.25
Si	0.248	0.498	0.499	0.246	0.248	0.247
Ti	0.000	0.000	0.000	0.000	0.000	0.000
Al	0.165	0.000	0.000	0.166	0.165	0.166
Fe	0.163	0.003	0.002	0.164	0.160	0.160
Mn	0.003	0.000	0.000	0.003	0.003	0.003
Mg	0.077	0.000	0.000	0.079	0.081	0.080
Ca	0.011	0.000	0.000	0.011	0.011	0.011
Na	0.001	0.001	0.000	0.001	0.000	0.001
K	0.001	0.000	0.000	0.001	0.001	0.001
P	0.000	0.000	0.000	0.000	0.001	0.000
Total	0.670	0.502	0.501	0.671	0.669	0.670

Appendix B:
Microprobe analyses
for thermobarometry
(sample MZ-2B)

Appendix B. Electron microprobe analyses from sample MZ-2B; used for thermobarometry.
Table B1. Garnet analyses from sample MZ-2B. Compositions based on 12 O's.
Rb = rim adjacent to biotite; not used for P-T estimation. Mol X = mol. fraction X of garnet.
Points are shown in Appendix E.

Sample point	MZ-2B pt 1	MZ-2B pt 2	MZ-2B pt 3	MZ-2B pt 4	MZ-2B pt 5	MZ-2B pt 6	MZ-2B pt 7
Mineral	Garn	Garn	Garn	Garn	Garn	Garn	Garn
Remark					Rb		Rb
SiO2	38.73	38.75	38.47	38.99	38.38	39.05	38.12
TiO2	0.06	0.04	0.04	0.06	0.04	0.05	0.06
Al2O3	21.81	21.77	21.79	21.78	21.47	21.93	21.47
FeO	31.96	32.38	32.27	33.06	34.04	32.41	34.74
MnO	0.46	0.49	0.49	0.52	0.53	0.49	0.57
MgO	6.67	6.39	6.30	6.09	5.12	6.60	4.51
CaO	1.38	1.42	1.51	1.25	1.48	1.31	1.40
Na2O	0.02	0.02	0.00	0.03	0.01	0.00	-
K2O	0.12	0.14	0.10	0.13	0.15	0.10	0.11
P2O5	0.04	0.03	0.00	0.03	0.03	0.07	0.04
Total	101.27	101.43	100.97	101.94	101.25	102.02	101.02
Si	0.250	0.250	0.250	0.251	0.251	0.250	0.250
Ti	0.000	0.000	0.000	0.000	0.000	0.000	0.000
Al	0.166	0.166	0.167	0.165	0.165	0.166	0.166
Fe	0.173	0.175	0.175	0.178	0.186	0.174	0.191
Mn	0.003	0.003	0.003	0.003	0.003	0.003	0.003
Mg	0.064	0.062	0.061	0.059	0.050	0.063	0.044
Ca	0.010	0.010	0.011	0.009	0.010	0.009	0.010
Na	0.000	0.000	0.000	0.000	0.000	0.000	0.000
K	0.001	0.001	0.001	0.001	0.001	0.001	0.001
P	0.000	0.000	0.000	0.000	0.000	0.000	0.000
Total	0.667	0.667	0.667	0.666	0.667	0.666	0.666
Si	3.001	3.005	2.998	3.013	3.008	3.005	3.005
Ti	0.004	0.002	0.002	0.004	0.002	0.002	0.004
Al	1.992	1.990	2.000	1.985	1.984	1.990	1.996
Fe	2.071	2.100	2.102	2.137	2.232	2.086	2.291
Mn	0.030	0.032	0.032	0.034	0.035	0.032	0.038
Mg	0.770	0.739	0.731	0.702	0.599	0.757	0.530
Ca	0.115	0.118	0.126	0.103	0.124	0.108	0.119
Na	0.002	0.002	0.001	0.004	0.001	0.000	0.000
K	0.012	0.014	0.011	0.013	0.016	0.010	0.011
P	0.002	0.002	0.000	0.002	0.002	0.005	0.002
Total	8.000	8.005	8.004	7.997	8.003	7.994	7.996
Mol Alm	0.693	0.703	0.703	0.718	0.747	0.699	0.769
Mol Spess	0.010	0.011	0.011	0.011	0.012	0.011	0.013
Mol Pyrp	0.258	0.247	0.244	0.236	0.200	0.254	0.178
Mol Gros	0.039	0.039	0.042	0.035	0.041	0.036	0.040

Appendix B. Electron microprobe analyses from sample MZ-2B; used for thermobarometry.
Table B1. Garnet analyses from sample MZ-2B. Compositions based on 12 O's.
Rb = rim adjacent to biotite; not used for P-T estimation. Mol X = mol. fraction X of garnet.
Points are shown in Appendix E.

Sample point	MZ-2B pt 8	MZ-2B pt 9	MZ-2B pt 10	MZ-2B pt 11	MZ-2B pt 12	MZ-2B pt 13
Mineral	Garn	Garn	Garn	Garn	Garn	Garn
Remark			Rb			
SiO2	39.06	38.96	38.54	38.64	39.09	39.02
TiO2	0.05	0.04	0.06	0.06	0.06	0.04
Al2O3	21.85	21.95	21.57	21.74	21.82	21.86
FeO	31.97	32.64	34.52	32.39	32.63	32.59
MnO	0.48	0.50	0.53	0.49	0.50	0.48
MgO	6.55	6.42	4.78	6.28	6.42	6.42
CaO	1.38	1.27	1.38	1.49	1.39	1.43
Na2O	0.01	-	-	0.01	-	0.01
K2O	0.08	0.09	0.13	0.11	0.11	0.12
P2O5	0.04	0.05	0.04	0.03	0.05	0.00
Total	101.46	101.91	101.53	101.25	102.07	101.97
Si	0.251	0.250	0.251	0.250	0.251	0.251
Ti	0.000	0.000	0.000	0.000	0.000	0.000
Al	0.166	0.166	0.166	0.166	0.165	0.166
Fe	0.172	0.175	0.188	0.175	0.175	0.175
Mn	0.003	0.003	0.003	0.003	0.003	0.003
Mg	0.063	0.062	0.047	0.061	0.062	0.062
Ca	0.010	0.009	0.010	0.010	0.010	0.010
Na	0.000	0.000	0.000	0.000	0.000	0.000
K	0.001	0.001	0.001	0.001	0.001	0.001
P	0.000	0.000	0.000	0.000	0.000	0.000
Total	0.665	0.666	0.666	0.667	0.667	0.667
Si	3.017	3.005	3.016	3.002	3.011	3.008
Ti	0.002	0.002	0.004	0.004	0.004	0.002
Al	1.990	1.996	1.990	1.991	1.981	1.987
Fe	2.065	2.105	2.258	2.105	2.102	2.101
Mn	0.031	0.032	0.035	0.032	0.032	0.031
Mg	0.754	0.738	0.558	0.727	0.738	0.738
Ca	0.114	0.104	0.115	0.125	0.115	0.118
Na	0.001	0.000	0.000	0.001	0.000	0.001
K	0.007	0.008	0.012	0.011	0.011	0.012
P	0.002	0.004	0.002	0.001	0.004	0.000
Total	7.985	7.994	7.990	7.999	7.998	8.000
Mol Alm	0.697	0.706	0.761	0.704	0.704	0.703
Mol Spess	0.011	0.011	0.012	0.011	0.011	0.010
Mol Pyrp	0.254	0.248	0.188	0.243	0.247	0.247
Mol Gros	0.038	0.035	0.039	0.042	0.039	0.039

Appendix B. Electron microprobe analyses from sample MZ-2B; used for thermobarometry.
Table B1. Garnet analyses from sample MZ-2B. Compositions based on 12 O's.
Rb = rim adjacent to biotite; not used for P-T estimation. Mol X = mol. fraction X of garnet.
Points are shown in Appendix E.

Sample point	MZ-2B pt 14	MZ-2B pt 15	MZ-2B pt 16	MZ-2B pt 17
Mineral	Garn	Garn	Garn	Garn
Remark			Rb	Rb
SiO2	38.82	39.01	38.83	38.86
TiO2	0.08	0.03	0.03	0.05
Al2O3	21.93	21.89	21.71	21.59
FeO	32.11	32.28	33.05	33.62
MnO	0.46	0.48	0.51	0.52
MgO	6.69	6.75	5.91	5.62
CaO	1.29	1.37	1.28	1.35
Na2O	0.03	-	0.01	0.01
K2O	0.15	0.12	0.12	0.13
P2O5	0.08	0.04	0.05	0.04
Total	101.64	101.95	101.51	101.78
Si	0.250	0.250	0.251	0.252
Ti	0.000	0.000	0.000	0.000
Al	0.166	0.166	0.166	0.165
Fe	0.173	0.173	0.179	0.182
Mn	0.003	0.003	0.003	0.003
Mg	0.064	0.065	0.057	0.054
Ca	0.009	0.009	0.009	0.009
Na	0.000	0.000	0.000	0.000
K	0.001	0.001	0.001	0.001
P	0.000	0.000	0.000	0.000
Total	0.667	0.667	0.666	0.666
Si	2.998	3.004	3.014	3.018
Ti	0.005	0.001	0.002	0.002
Al	1.996	1.986	1.987	1.976
Fe	2.074	2.078	2.146	2.184
Mn	0.030	0.031	0.034	0.035
Mg	0.769	0.775	0.684	0.650
Ca	0.107	0.113	0.107	0.113
Na	0.005	0.000	0.002	0.001
K	0.014	0.012	0.012	0.013
P	0.005	0.002	0.004	0.002
Total	8.003	8.003	7.992	7.997
Mol Alm	0.696	0.693	0.722	0.732
Mol Spess	0.010	0.010	0.011	0.012
Mol Pyrp	0.258	0.259	0.230	0.218
Mol Gros	0.036	0.038	0.036	0.038

Appendix B. Electron microprobe analyses from sample MZ-2B (thermobarometry sample).

Table B2. Biotite analyses from sample MZ-2B.
Compositions based on 22 O's.
Points shown in Appendix E.

Sample point	MZ-2B pt 30	MZ-2B pt 31
Mineral	Biot	Biot
Remark		
SiO2	36.94	36.98
TiO2	4.35	4.36
Al2O3	17.35	17.37
FeO	14.80	14.68
MnO	0.01	0.02
MgO	12.78	12.53
CaO	0.03	0.00
Na2O	0.10	0.11
K2O	7.47	7.56
P2O5	0.04	0.01
Total	93.85	93.62
Si	0.250	0.251
Ti	0.022	0.022
Al	0.139	0.139
Fe	0.084	0.083
Mn	0.000	0.000
Mg	0.129	0.127
Ca	0.000	0.000
Na	0.001	0.002
K	0.065	0.066
P	0.000	0.000
Total	0.691	0.691
Si	5.51	5.53
Ti	0.49	0.49
Al	3.05	3.06
Fe	1.85	1.83
Mn	0.00	0.00
Mg	2.84	2.79
Ca	0.00	0.00
Na	0.03	0.03
K	1.42	1.44
P	0.00	0.00
Total	15.19	15.19
X_{Fe}	0.322	0.321
X_{Mg}	0.495	0.489

Appendix B. Electron microprobe analyses from sample MZ-2B (thermobarometry sample).

Table B3. Plagioclase analyses from sample MZ-2B. Compositions based on 8 O's.

Points shown in Appendix E.

Sample point	MZ-2B pt 34	MZ-2B pt 35	MZ-2B pt 36	MZ-2B pt 37	MZ-2B pt 38	MZ-2B pt 39	MZ-2B pt 40
Mineral	Plag	Plag	Plag	Plag	Plag	Plag	Plag
Remark							
SiO2	61.31	59.75	59.66	61.00	61.34	60.87	61.23
Al2O3	24.12	24.67	24.75	24.25	24.05	24.14	24.20
FeO	0.00	0.47	0.71	0.01	0.00	0.00	0.01
MgO	0.00	0.08	0.25	0.00	0.00	0.00	0.00
CaO	6.00	5.96	5.58	6.20	6.24	6.17	6.12
Na2O	8.85	8.07	7.96	8.81	8.68	8.73	8.78
K2O	0.12	0.13	0.18	0.12	0.19	0.16	0.15
P2O5	0.06	0.08	0.08	0.07	0.05	0.07	0.06
Total	100.46	99.22	99.16	100.45	100.55	100.13	100.55
Si	0.340	0.336	0.335	0.338	0.340	0.339	0.339
Al	0.158	0.163	0.164	0.159	0.157	0.158	0.158
Fe	0.000	0.002	0.003	0.000	0.000	0.000	0.000
Mg	0.000	0.001	0.002	0.000	0.000	0.000	0.000
Ca	0.036	0.036	0.034	0.037	0.037	0.037	0.036
Na	0.095	0.088	0.087	0.095	0.093	0.094	0.094
K	0.001	0.001	0.001	0.001	0.001	0.001	0.001
P	0.000	0.000	0.000	0.000	0.000	0.000	0.000
Total	0.629	0.627	0.627	0.630	0.629	0.629	0.629
Si	2.72	2.68	2.68	2.71	2.72	2.71	2.71
Al	1.26	1.31	1.31	1.27	1.26	1.27	1.26
Fe	0.00	0.02	0.03	0.00	0.00	0.00	0.00
Mg	0.00	0.01	0.02	0.00	0.00	0.00	0.00
Ca	0.28	0.29	0.27	0.30	0.30	0.29	0.29
Na	0.76	0.70	0.69	0.76	0.75	0.75	0.75
K	0.01	0.01	0.01	0.01	0.01	0.01	0.01
P	0.00	0.00	0.00	0.00	0.00	0.00	0.00
Total	5.03	5.01	5.01	5.04	5.03	5.03	5.03
X_{Ca}	0.273	0.290	0.279	0.280	0.285	0.281	0.278
X_{Na}	0.727	0.710	0.721	0.720	0.715	0.719	0.722

Appendix B. Electron microprobe analyses from sample MZ-2B (thermobarometry sample).

Table B4. Sillimanite and quartz analyses from sample MZ-2B.

Sillimanite compositions based on 5 O's, quartz based on 2 O's.

Points shown in Appendix E.

Sample point	MZ-2B pt 26	MZ-2B pt 27	MZ-2B pt 21	MZ-2B pt
Mineral	Sill	Qtz	Qtz	Qtz
Remark				
SiO2	41.67	100.49	100.53	100.24
Al2O3	46.67	0.01	0.02	0.03
FeO	2.87	0.16	0.72	0.04
MgO	0.85	0.00	0.00	0.00
CaO	0.03	0.00	0.00	0.00
Na2O	0.04	0.00	0.02	0.04
K2O	0.20	0.06	0.05	0.07
Total	92.33	100.72	101.34	100.42
Si	0.246	0.500	0.498	0.500
Ti	0.000	0.000	0.000	0.000
Al	0.324	0.000	0.000	0.000
Fe	0.014	0.001	0.003	0.000
Mn	0.000	0.000	0.000	0.000
Mg	0.008	0.000	0.000	0.000
Ca	0.000	0.000	0.000	0.000
Na	0.000	0.000	0.000	0.000
K	0.002	0.000	0.000	0.000
Total	0.593	0.501	0.502	0.501
Si	1.23	1.00	1.00	1.00
Al	1.62			
Fe	0.07			
Total	2.92	1.00	1.00	1.00

Appendix B. Electron microprobe analyses from sample MZ-2B (thermobarometry sample).

Table B5. Non-silicate analyses from sample MZ-2B. Not used in P-T estimation.

Rutile compositions based on 2 O's, pyrite based on 1 O (equivalent).

Points shown in Appendix E.

Sample point	MZ-2B pt 19	MZ-2B pt 33	MZ-2B pt 20	MZ-2B pt 23	MZ-2B pt 24	MZ-2B pt 25	MZ-2B pt 32
Mineral	Rutile	Rutile	Pyrite	Pyrite	Pyrite	Pyrite	Pyrite
Remark							
SiO2	-	-	-	-	-	-	-
TiO2	100.06	100.32	0.17	0.18	0.15	0.13	0.16
Al2O3	0.02	0.07	0.09	0.10	0.08	0.10	0.12
FeO	0.95	0.29	77.80	77.49	58.55	58.19	58.13
MnO	0.04	0.03	0.16	0.15	0.13	0.13	0.12
MgO	0.00	0.00	0.04	0.06	0.05	0.06	0.06
CaO	0.06	0.03	0.10	0.13	0.07	0.05	0.06
Na2O	0.00	0.00	0.04	0.01	0.14	0.13	0.36
K2O	0.14	0.09	0.21	0.21	0.23	0.23	0.25
P2O5	0.01	0.02	0.06	0.07	0.07	0.02	0.12
Total	101.28	100.84	78.67	78.40	59.48	59.03	59.37
Si	0.000	0.000	0.000	0.000	0.000	0.000	0.000
Ti	0.497	0.498	0.002	0.002	0.002	0.002	0.002
Al	0.000	0.001	0.002	0.002	0.002	0.002	0.003
Fe	0.005	0.002	0.985	0.983	0.979	0.981	0.971
Mn	0.000	0.000	0.002	0.002	0.002	0.002	0.002
Mg	0.000	0.000	0.001	0.001	0.001	0.002	0.002
Ca	0.000	0.000	0.002	0.002	0.002	0.001	0.001
Na	0.000	0.000	0.001	0.000	0.006	0.005	0.014
K	0.001	0.001	0.004	0.004	0.006	0.006	0.006
P	0.000	0.000	0.001	0.001	0.001	0.000	0.002
Total	0.504	0.502	0.999	0.998	1.001	1.002	1.003
Fe	0.01	0.00	0.98	0.98	0.98	0.98	0.97
Ti	0.99	1.00	0.00	0.00	0.00	0.00	0.00
Total	1.00	1.00	0.99	0.99	0.98	0.98	0.97

Appendix B. Electron microprobe analyses from sample MZ-2B (thermobarometry sample).

Table B6. Silicate analyses from sample MZ-2B. Not used in P-T estimate.

Plagioclase and K-feldspar compositions based on 8 O's, biotite based on 22 O's.

Points shown in Appendix E.

Sample point	MZ-2B pt 28	MZ-2B pt 29	MZ-2B pt 22	MZ-2B pt 18
Mineral	Plag	Kspar	Biot	Zircon
Remark			poor total	
SiO2	61.19	65.11	28.09	34.29
TiO2	-	-	0.01	0.19
Al2O3	24.15	18.30	15.36	0.11
FeO	0.03	-	20.94	1.89
MnO	-	-	0.31	0.15
MgO	-	0.00	4.16	0.06
CaO	6.16	0.01	1.27	0.09
Na2O	8.81	1.46	5.37	0.05
K2O	0.14	11.13	3.58	0.21
P2O5	0.06	0.10	0.16	0.82
Total	100.54	96.10	79.26	37.86
Si	0.339	0.380	0.241	0.471
Ti	0.000	0.000	0.000	0.002
Al	0.158	0.126	0.155	0.002
Fe	0.000	0.000	0.150	0.022
Mn	0.000	0.000	0.002	0.002
Mg	0.000	0.000	0.053	0.001
Ca	0.037	0.000	0.012	0.001
Na	0.095	0.017	0.089	0.001
K	0.001	0.083	0.039	0.004
P	0.000	0.001	0.001	0.010
Total	0.630	0.606	0.744	0.515
Si	2.71	3.04	5.30	
Ti	0.00	0.00	0.00	
Al	1.26	1.01	3.42	
Fe	0.00	0.00	3.31	
Mn	0.00	0.00	0.05	
Mg	0.00	0.00	1.17	
Ca	0.29	0.00	0.26	
Na	0.76	0.13	1.96	
K	0.01	0.66	0.86	
P	0.00	0.00	0.02	
Total	5.04	4.85	16.36	

Appendix C:
Compositional (X-ray) maps and BSE of selected garnets

Appendix C. Compositional maps of selected garnets.

Figure C1.

Garnet MZ-1A-0.2

Grains are identified in
BSE;

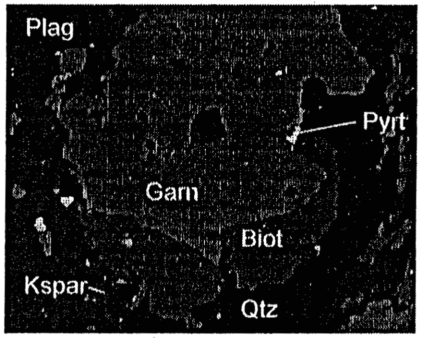

BSE 500 µm

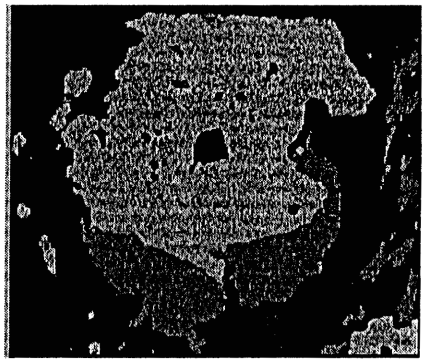

Fe 500 µm

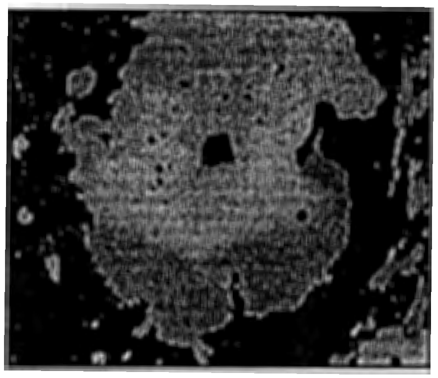

Mg 500 µm

Mn 500 µm

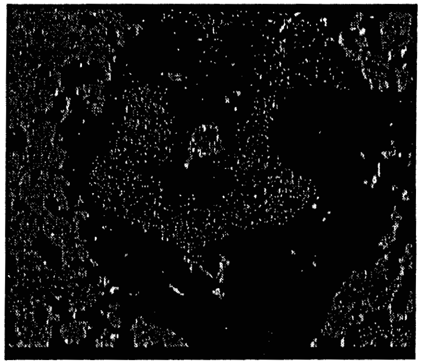

Ca 500 µm

Appendix C. Compositional maps of selected garnets.

Figure C3.

Garnet MZ-1A-0.5

Grains are identified in BSE.

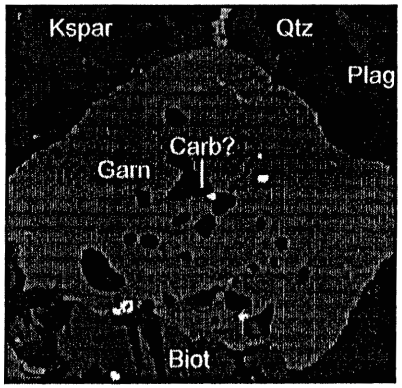

BSE — 200 µm

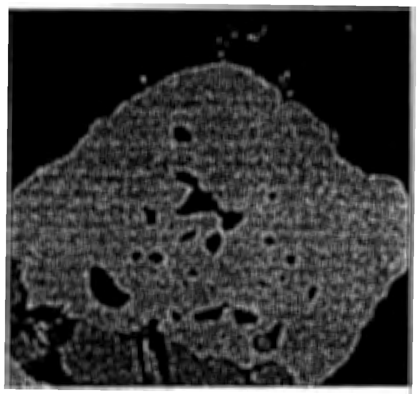

Fe — 200 µm

Mg — 200 µm

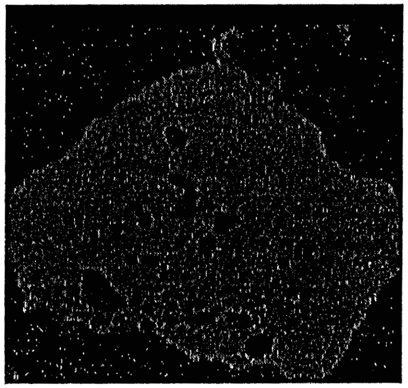

Mn — 200 µm

Ca — 200 µm

Appendix C. Compositional maps of selected garnets.

Figure C4.

Garnet MZ-1A-1.1a

Grains are identified in BSE.

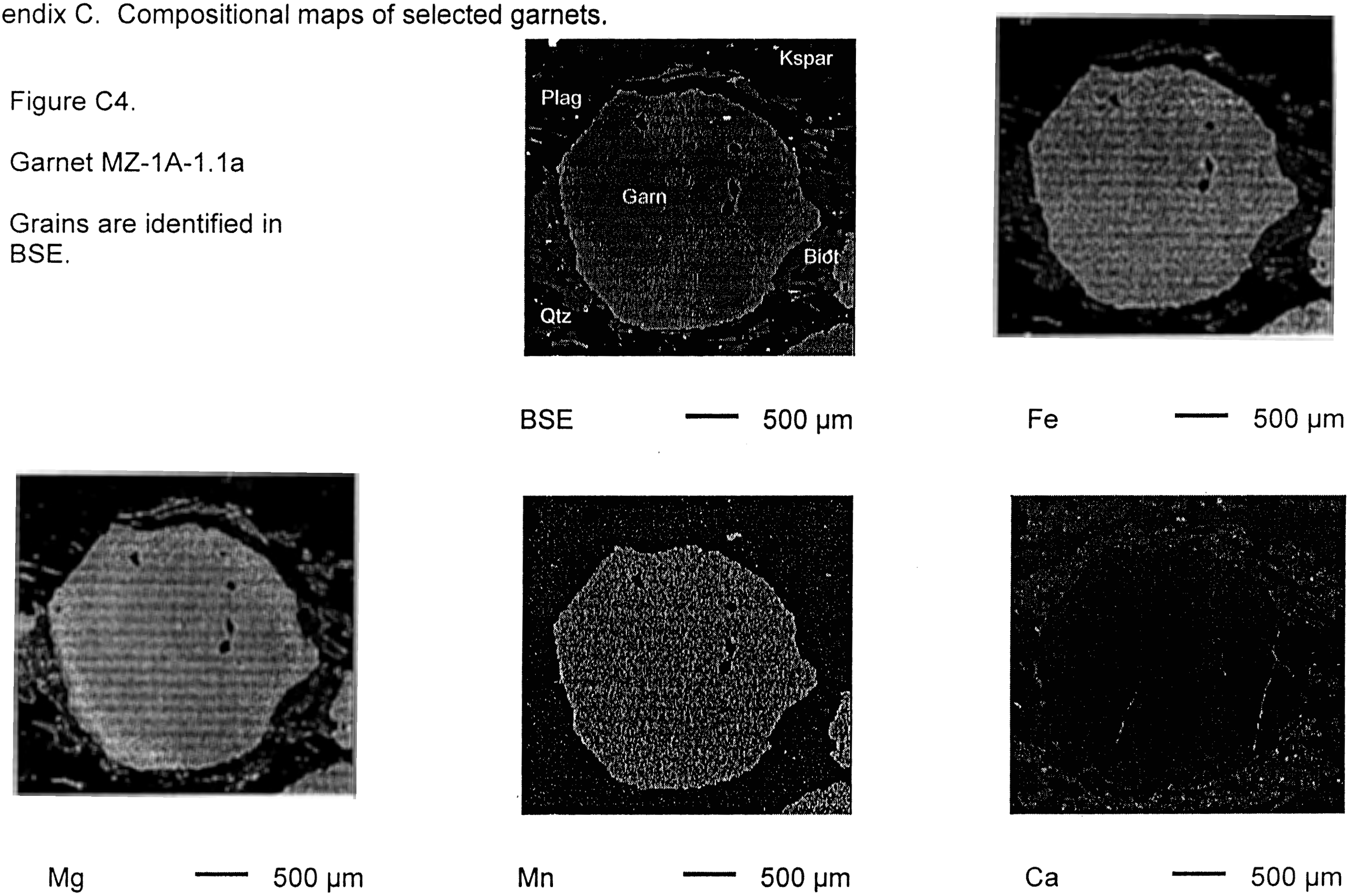

BSE

Fe

Mg

Mn

Ca

Appendix C. Compositional maps of selected garnets.

Figure C5.

Garnet MZ-1B-0.3

Grains are identified in BSE.

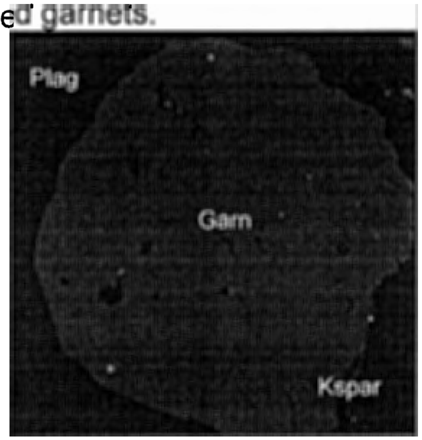

BSE — 500 µm

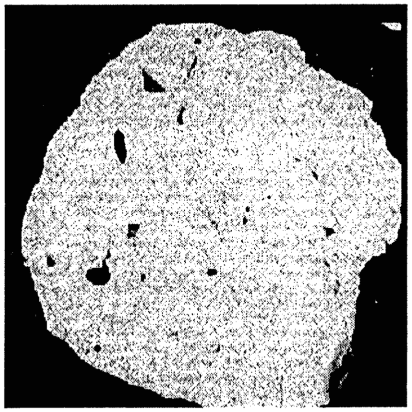

Fe — 500 µm

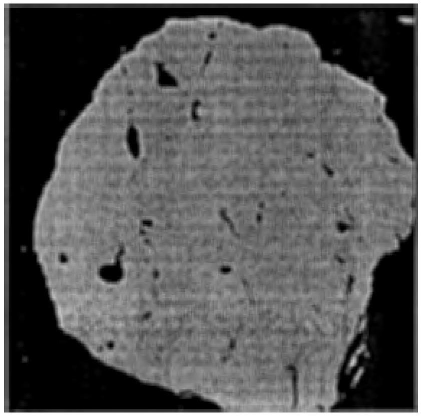

Mg — 500 µm

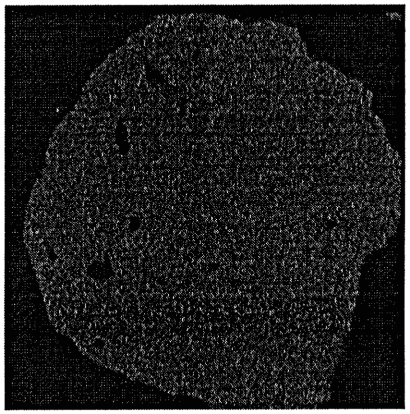

Mn — 500 µm

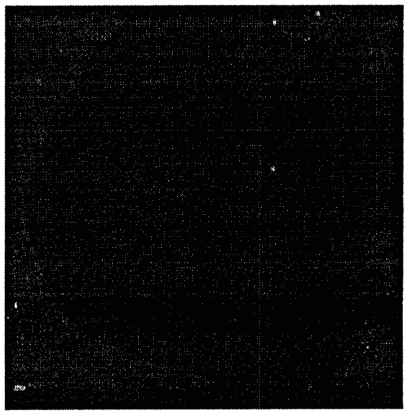

Ca — 500 µm

Appendix C. Compositional maps of selected garnets.

Figure C6.

Garnet MZ-1B-0.4

Grains are identified in BSE.

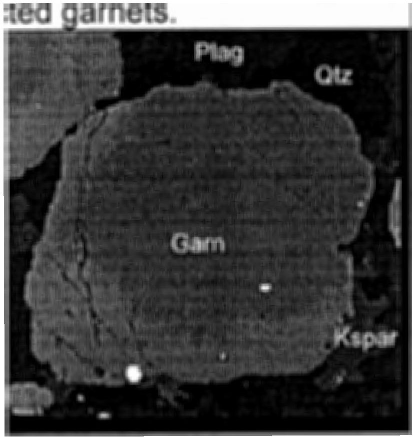

BSE — 200 µm

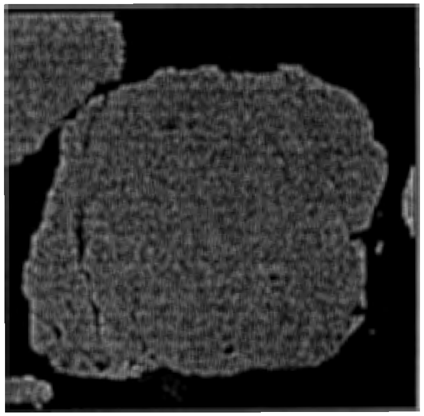

Fe — 200 µm

Mg — 200 µm

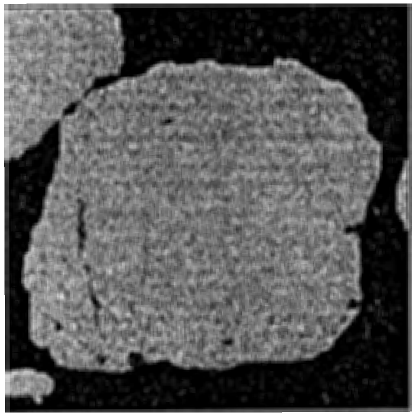

Mn — 200 µm

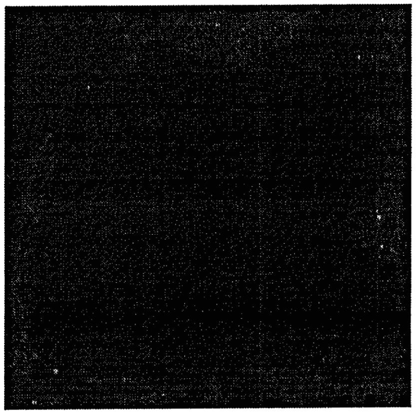

Ca — 200 µm

Appendix C. Compositional maps of selected garnets.

Figure C7.

Garnet MZ-1B-0.5

Grains are identified in BSE.

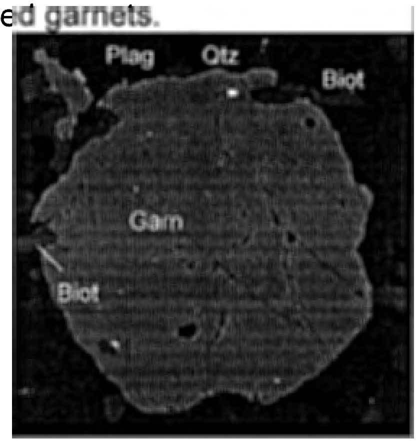

BSE — 200 µm

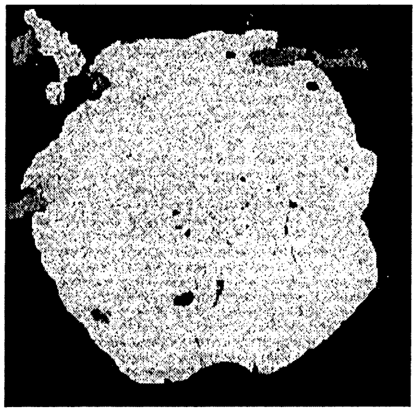

Fe — 200 µm

Mg — 200 µm

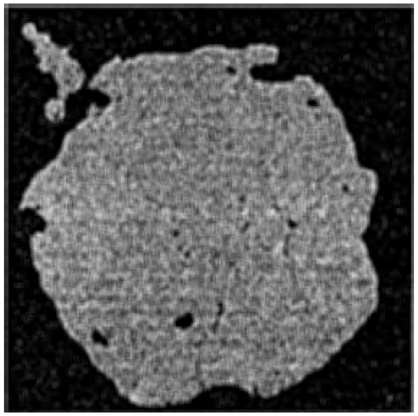

Mn — 200 µm

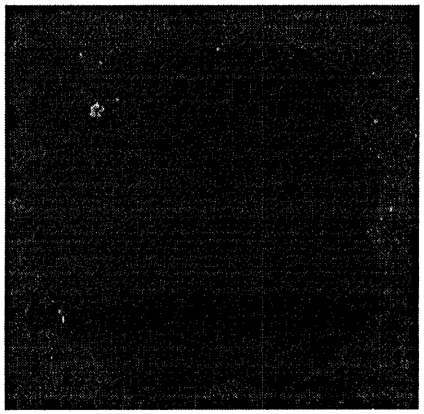

Ca — 200 µm

Appendix C. Compositional maps of selected garnets.

Figure C8.

Garnet MZ-2A-0.4

Grains are identified in BSE.

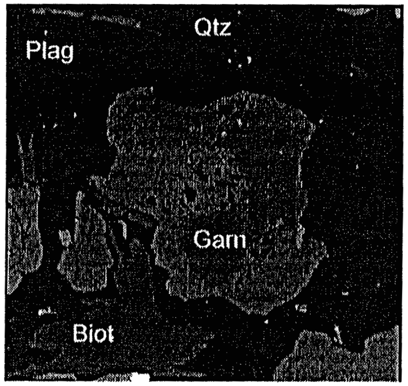

BSE 500 µm

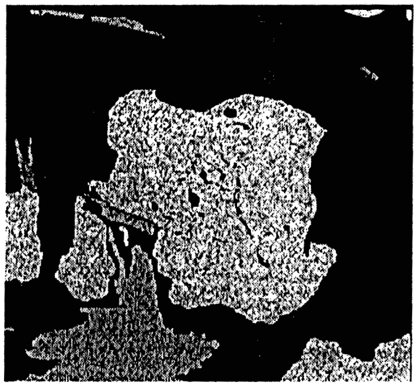

Fe 500 µm

Mg 500 µm

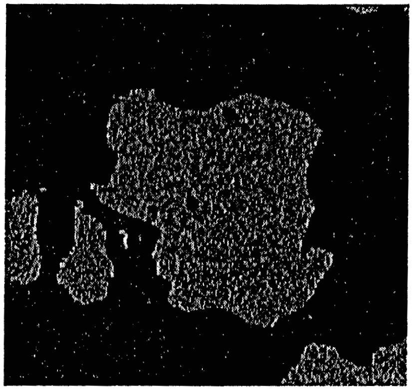

Mn 500 µm

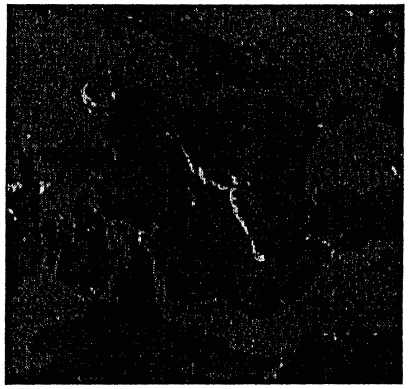

Ca 500 µm

Appendix D:
Point maps of selected garnets

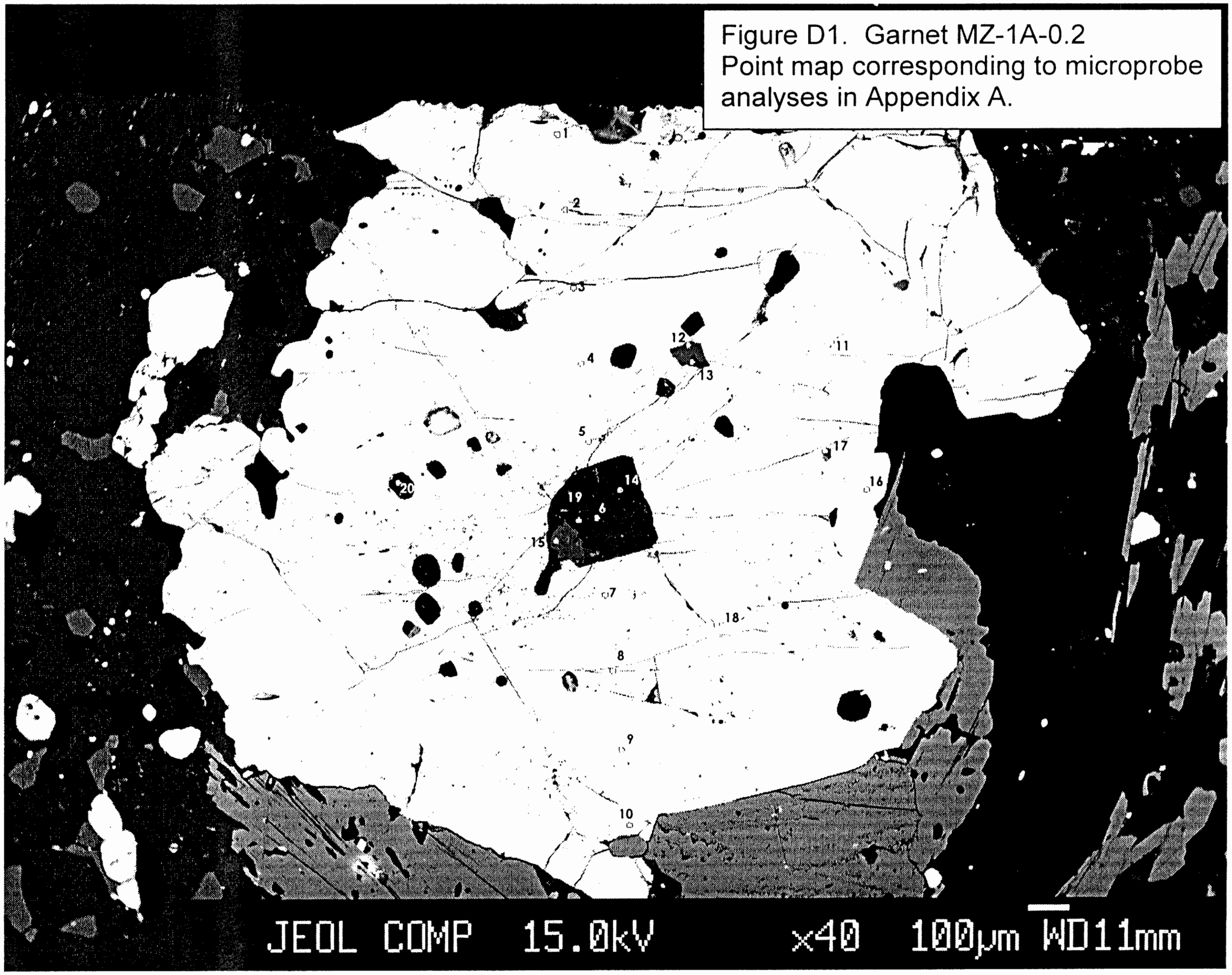

Figure D1. Garnet MZ-1A-0.2
Point map corresponding to microprobe analyses in Appendix A.

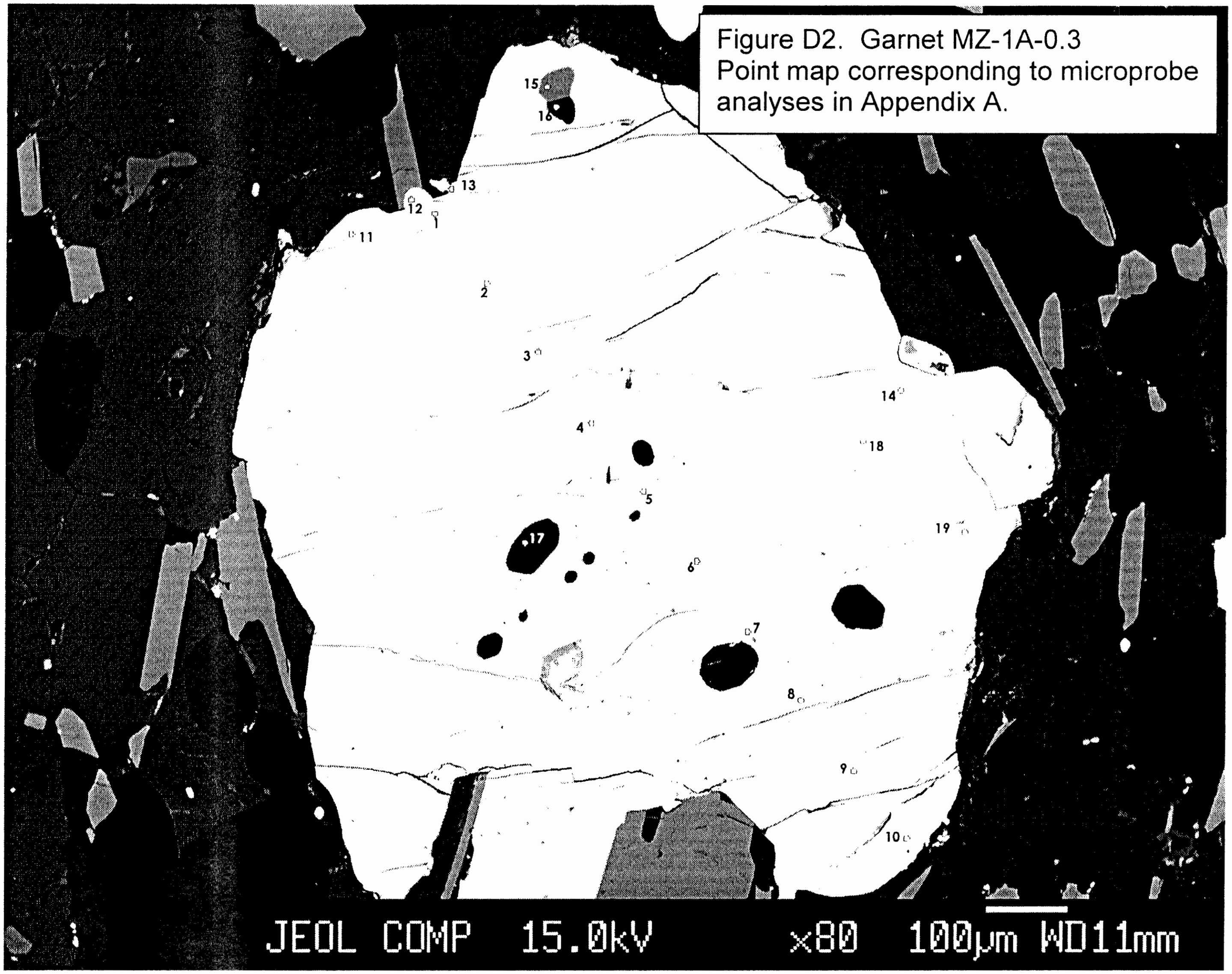

Figure D2. Garnet MZ-1A-0.3
Point map corresponding to microprobe analyses in Appendix A.

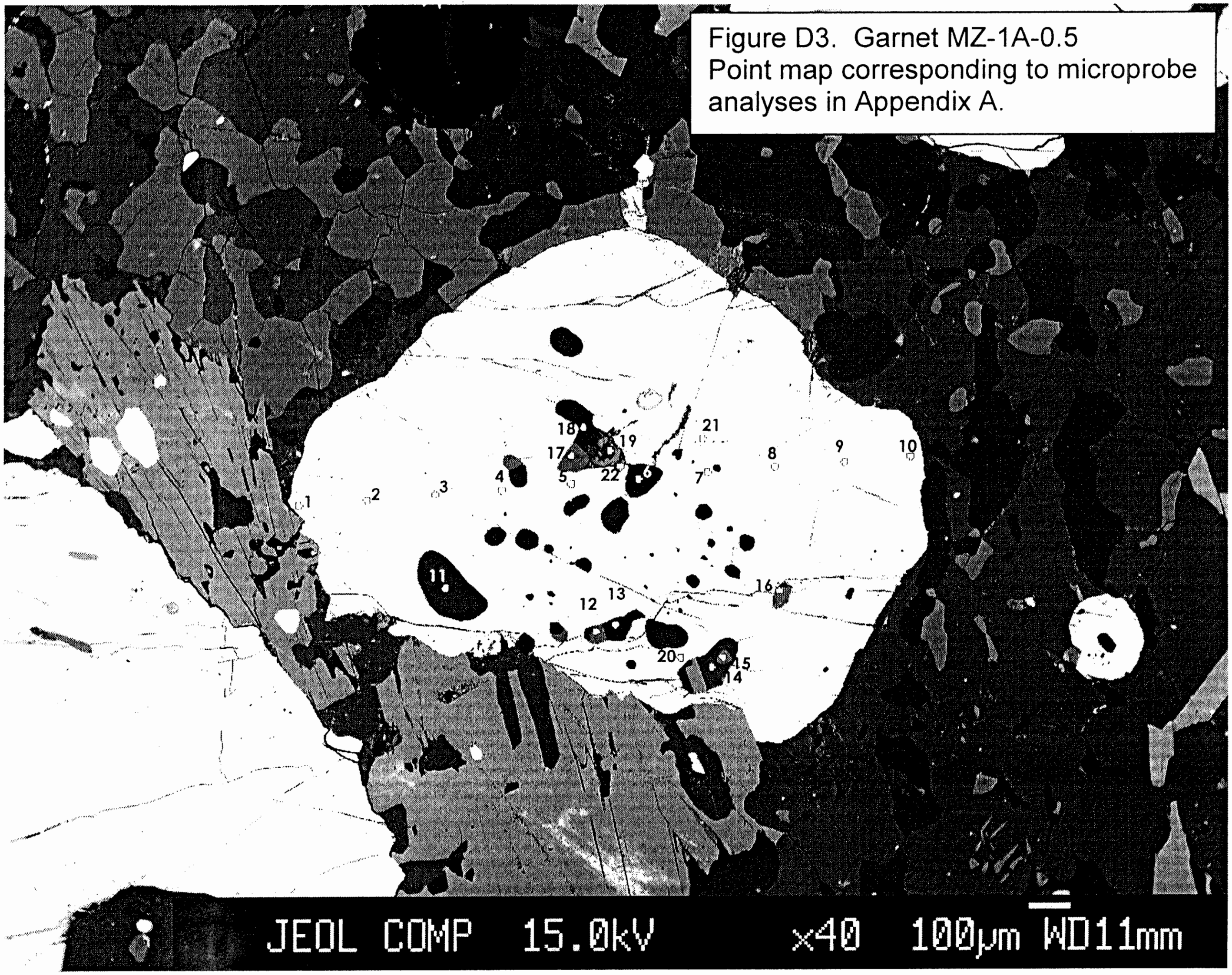

Figure D3. Garnet MZ-1A-0.5
Point map corresponding to microprobe analyses in Appendix A.

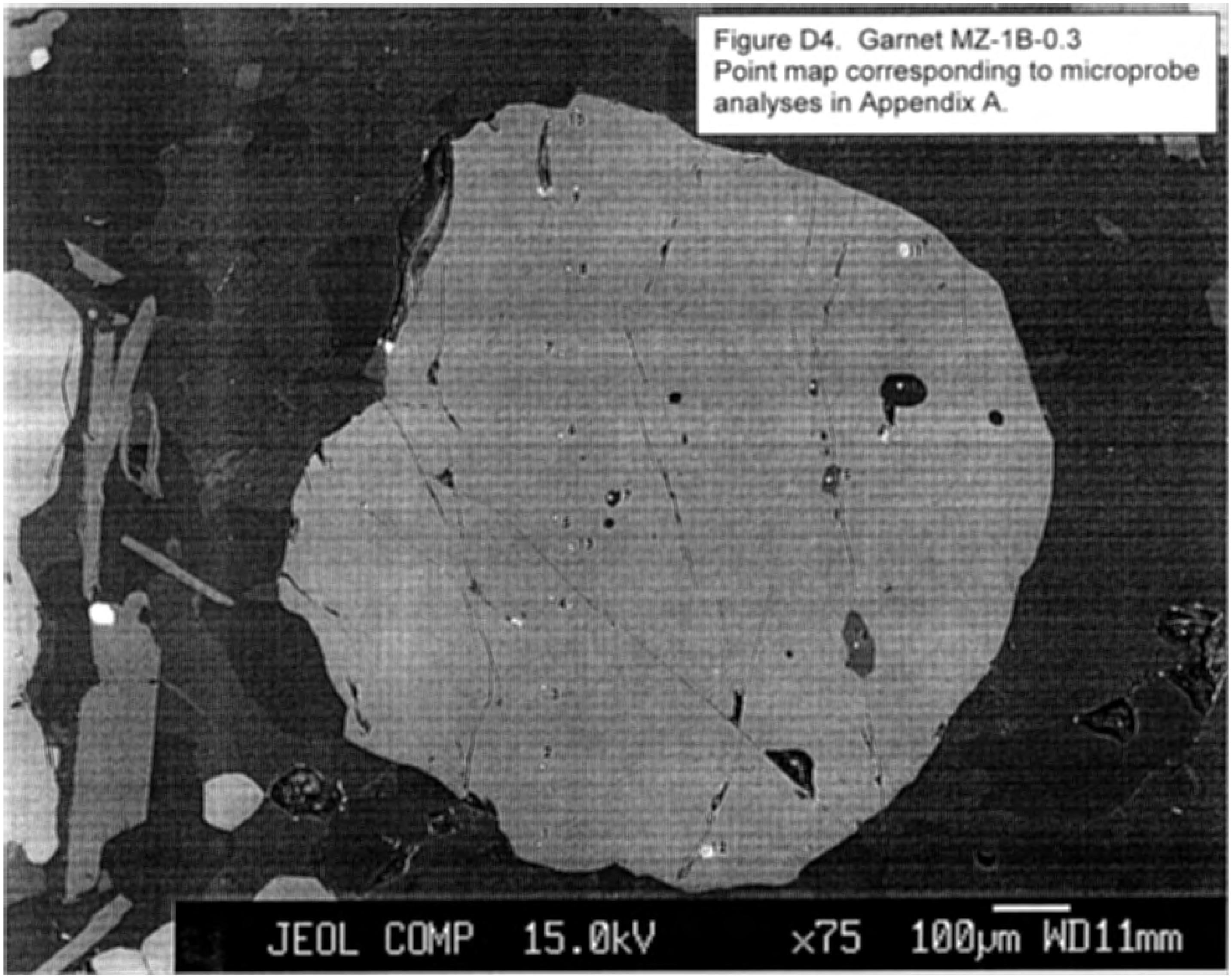

Figure D4. Garnet MZ-1B-0.3
Point map corresponding to microprobe analyses in Appendix A.

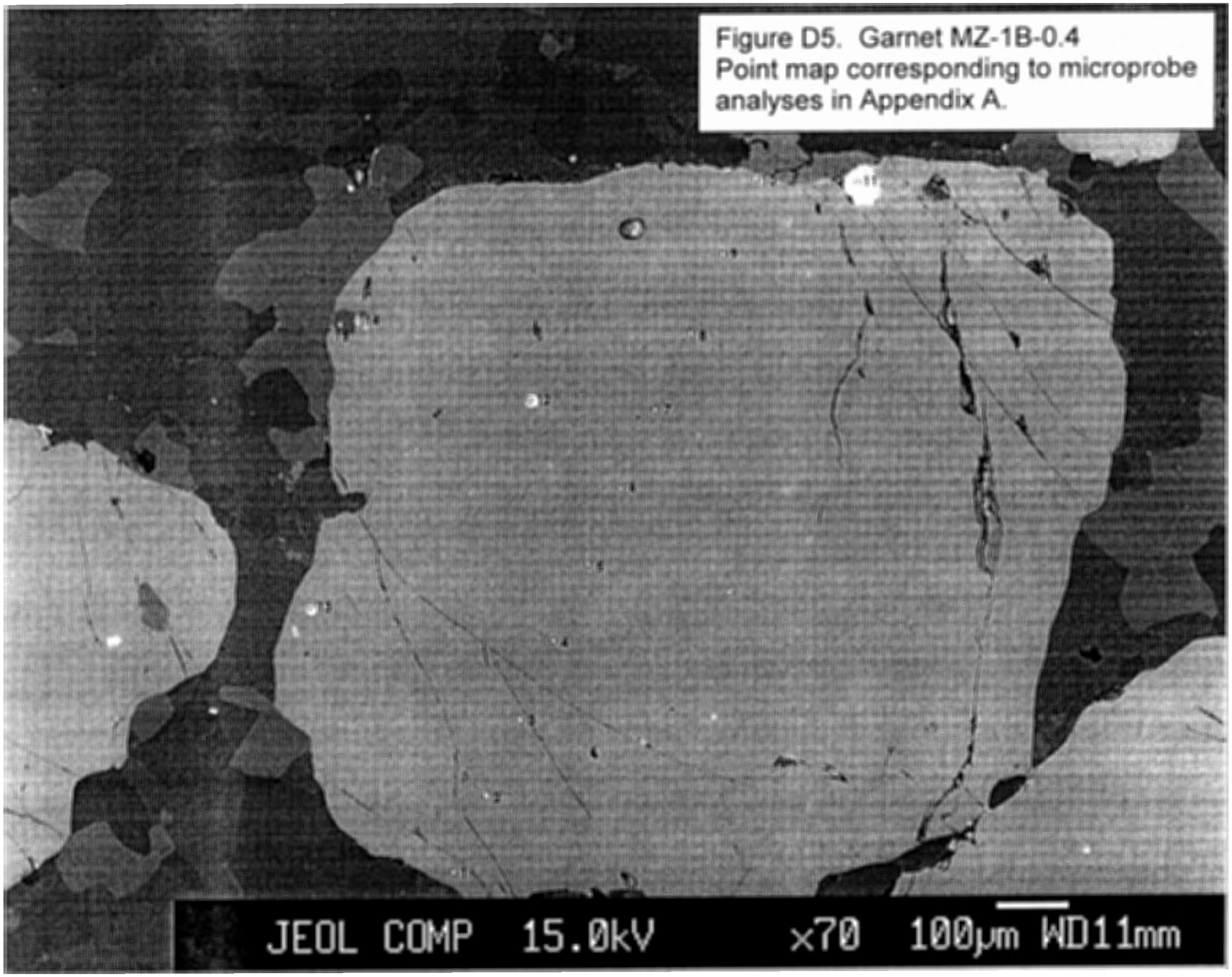

Figure D5. Garnet MZ-1B-0.4
Point map corresponding to microprobe analyses in Appendix A.

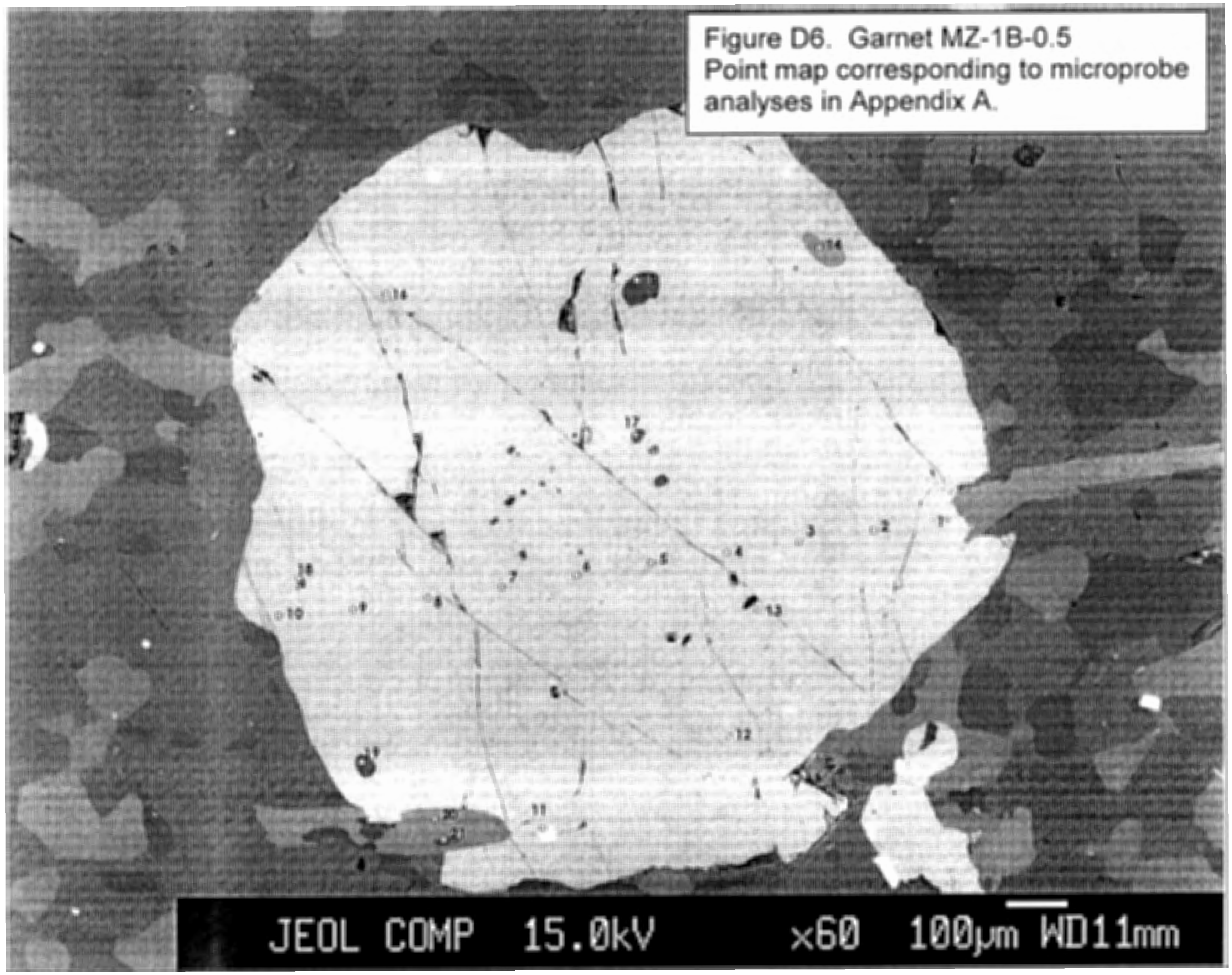

Figure D6. Garnet MZ-1B-0.5
Point map corresponding to microprobe analyses in Appendix A.

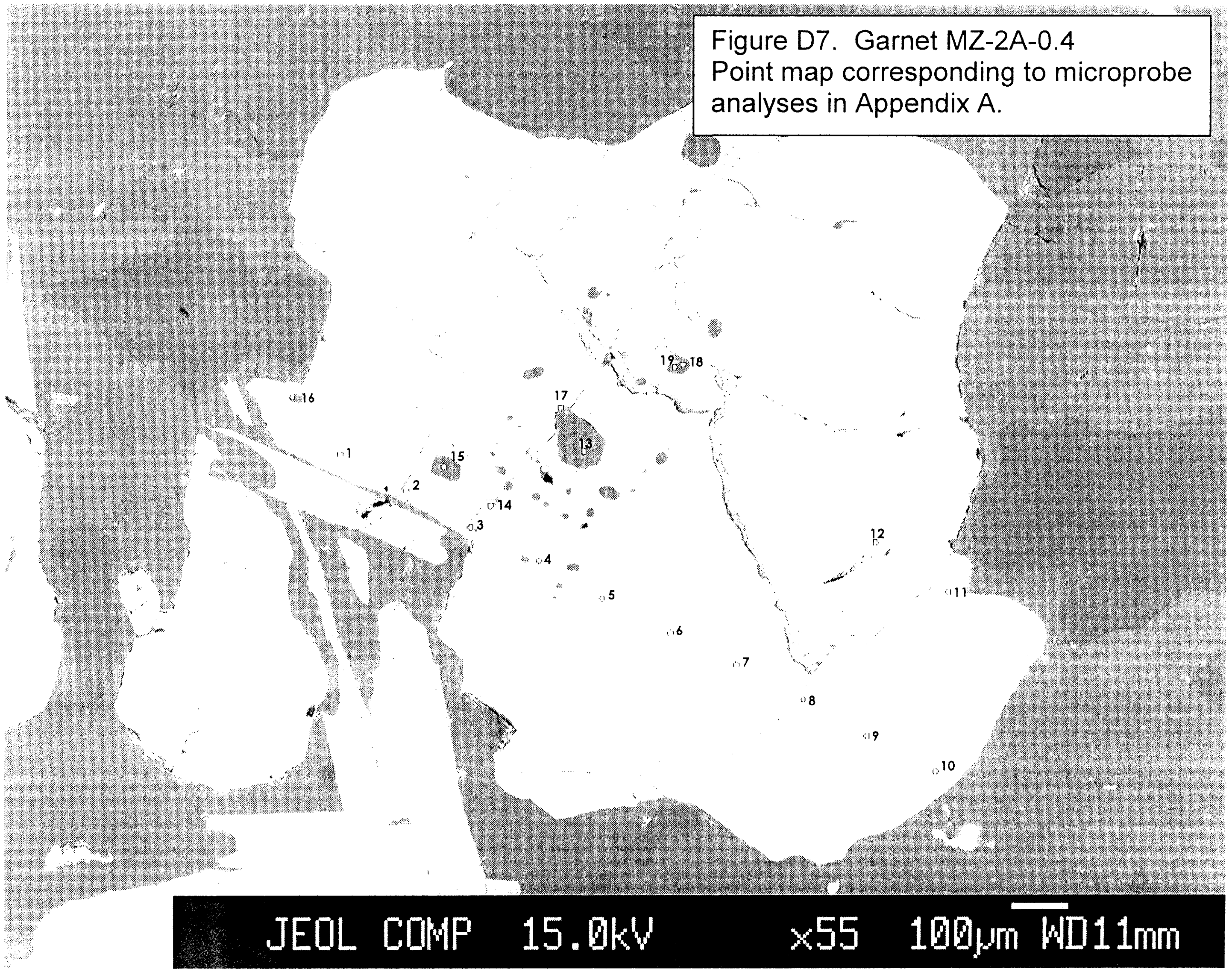

Figure D7. Garnet MZ-2A-0.4
Point map corresponding to microprobe analyses in Appendix A.

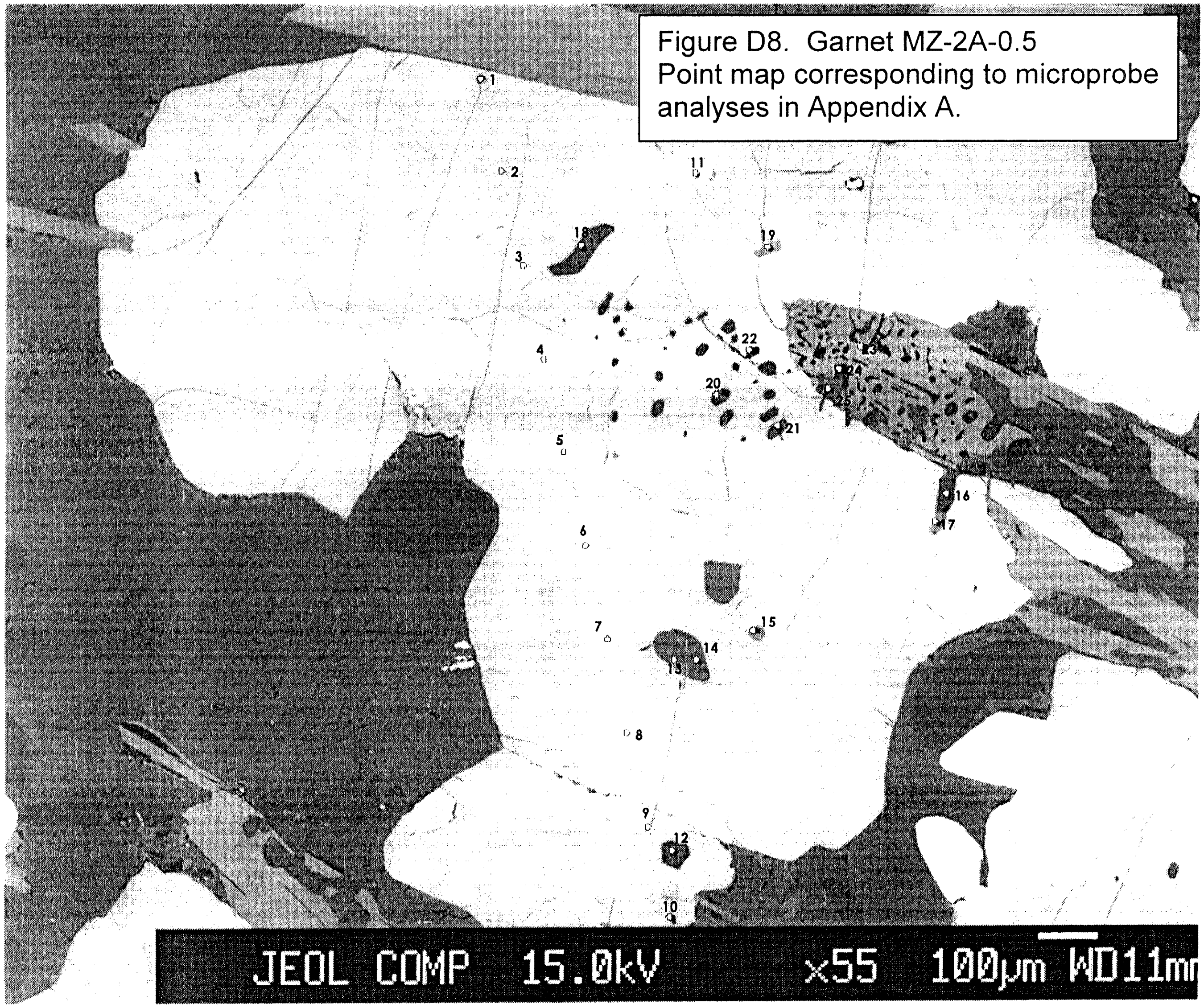

Figure D8. Garnet MZ-2A-0.5
Point map corresponding to microprobe analyses in Appendix A.

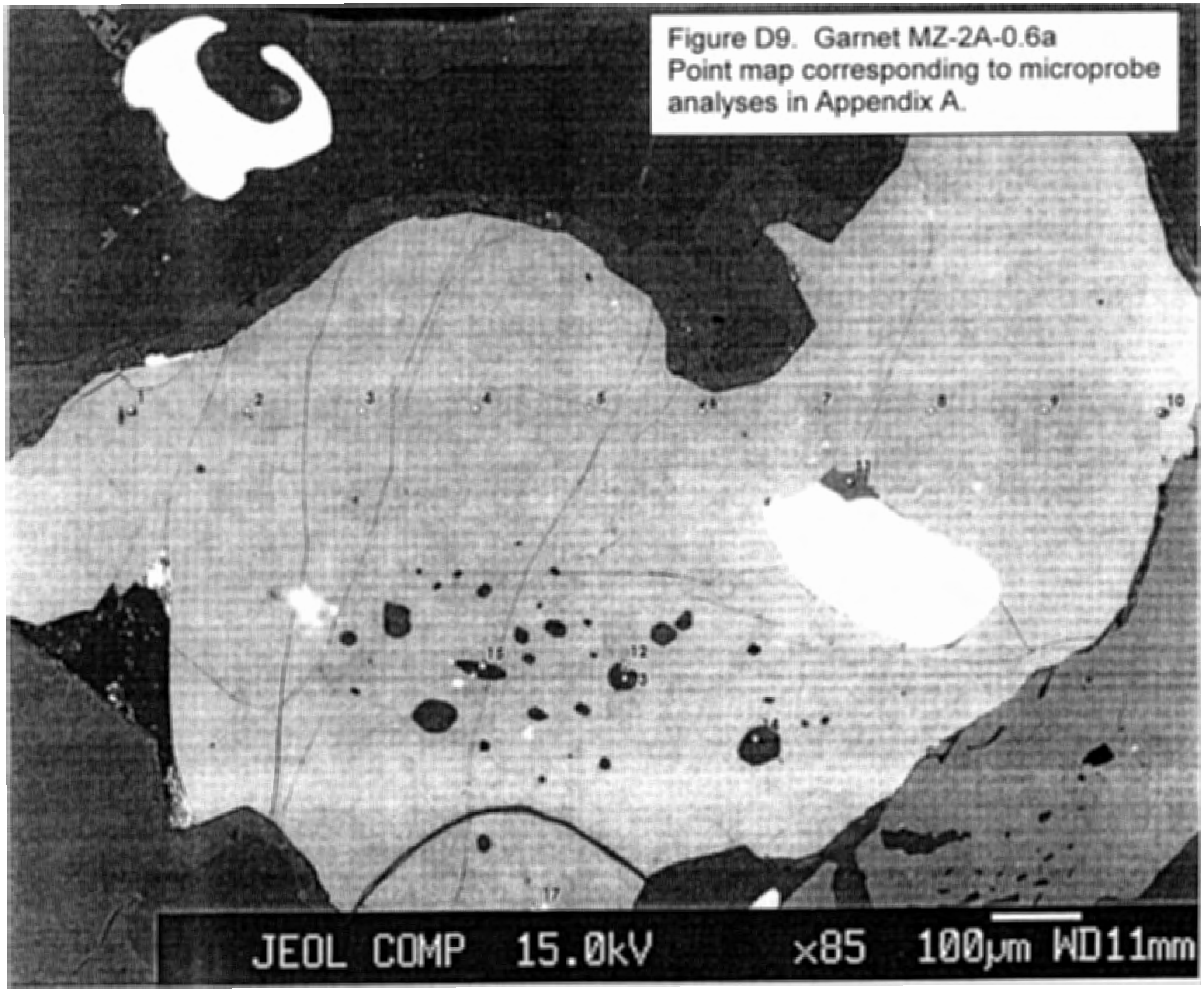

Figure D9. Garnet MZ-2A-0.6a
Point map corresponding to microprobe analyses in Appendix A.

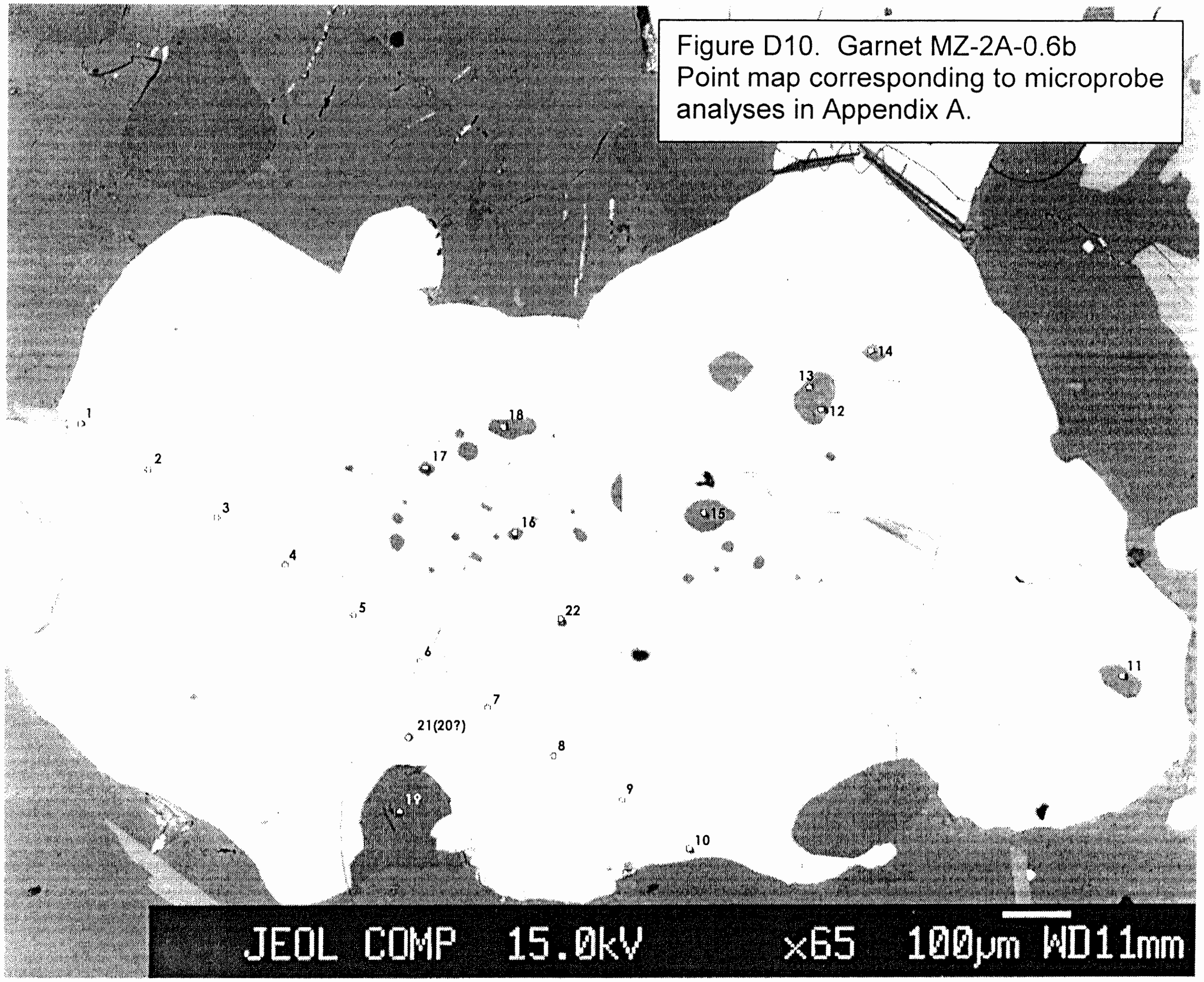

Figure D10. Garnet MZ-2A-0.6b Point map corresponding to microprobe analyses in Appendix A.

Appendix E:
Point maps for thermobarometry
(sample MZ-2B)

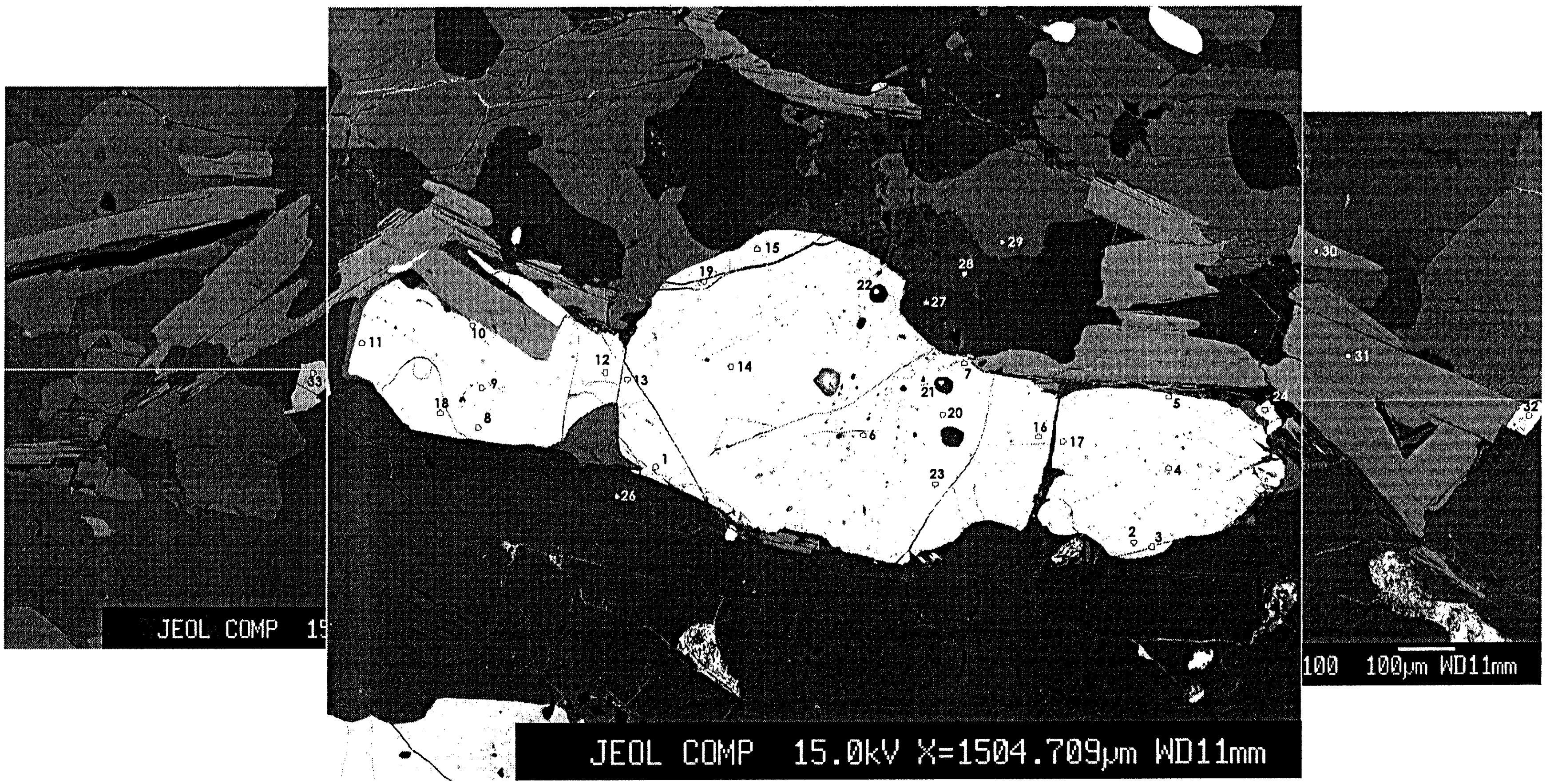

Figure E1. Garnet and surrounding points from MZ-2B, shown in a composite of three backscatter images. Points indicate microprobe analyses, given in Appendix B.

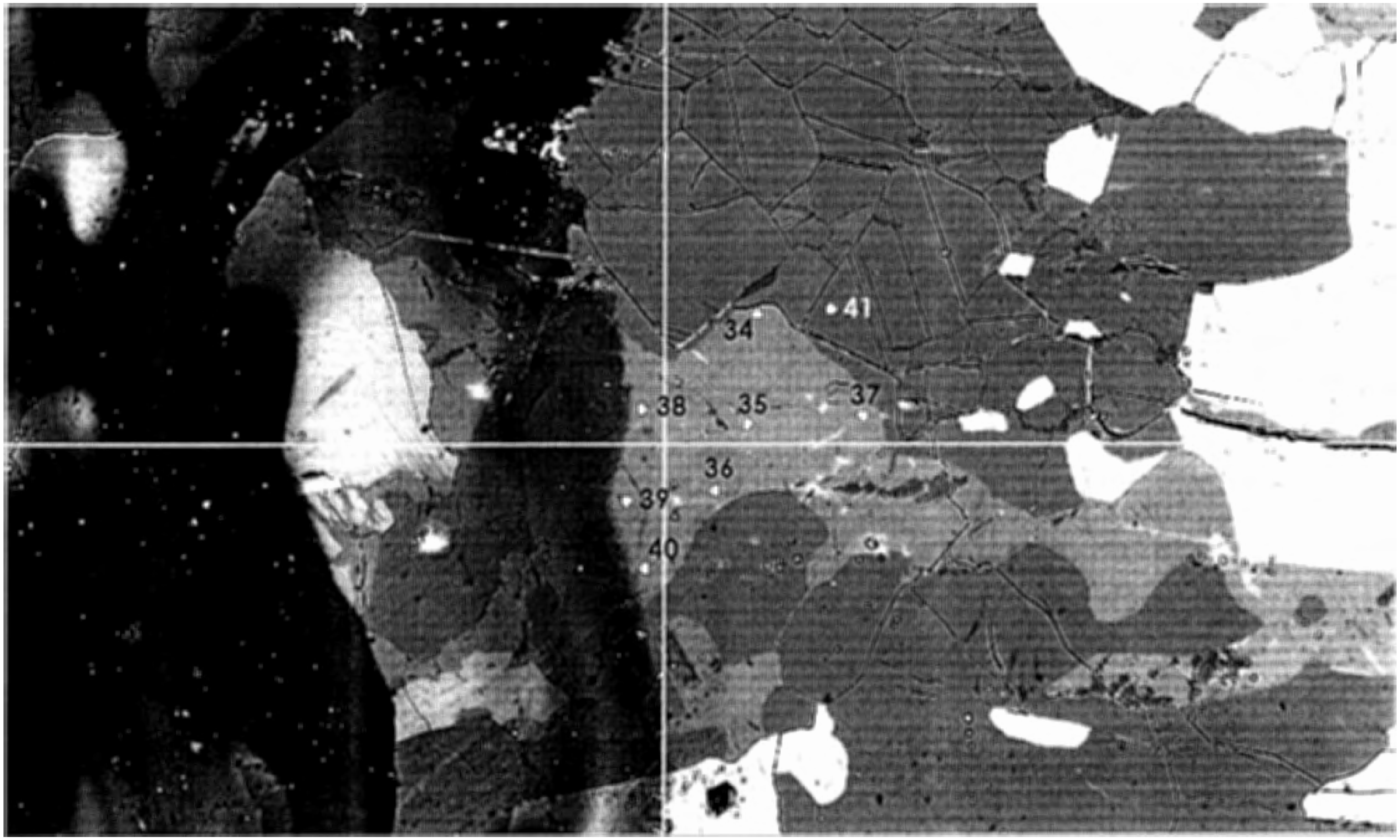

Figure E2. Plagioclase and surrounding points from MZ-2B. Points indicate microprobe analyses, given in Appendix B. The black discolouration on the left hand side is an ink mark used to relocate the plagioclase and garnet grains.

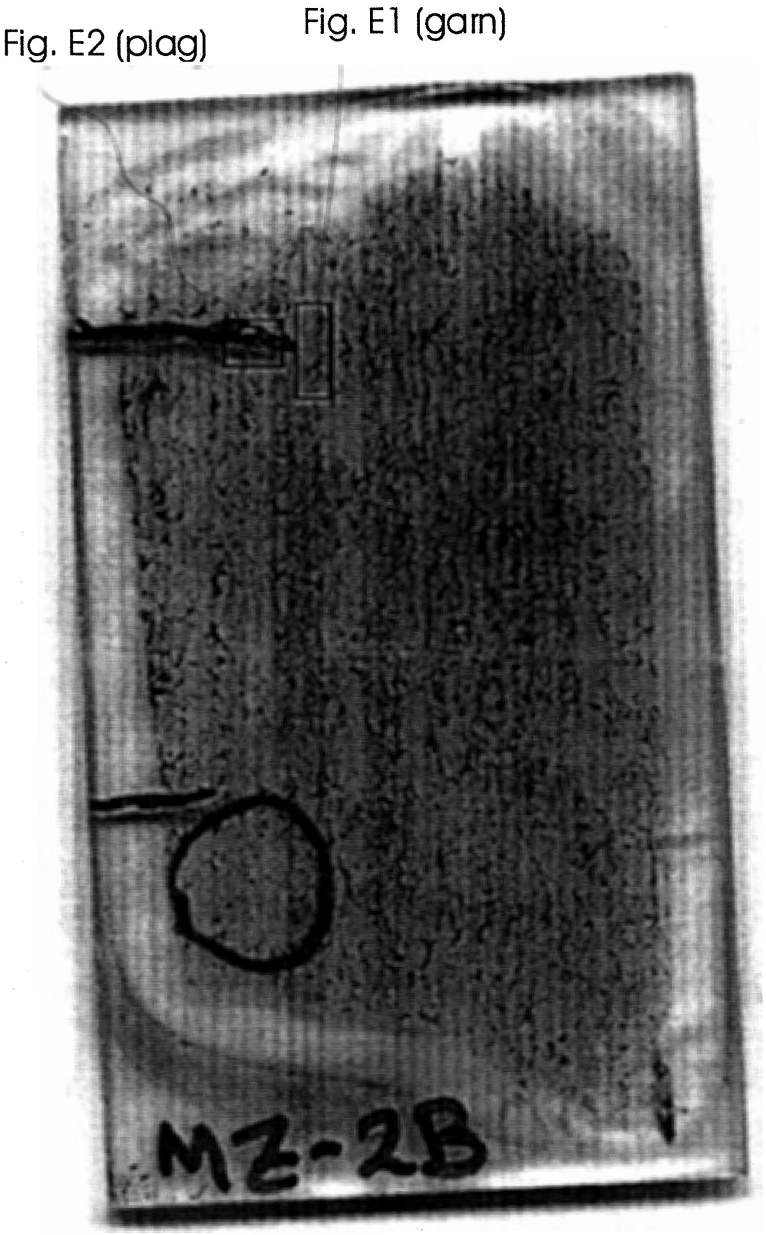

Figure E3. Photo of slide MZ-2B-1, showing the location of Figures E1 and E2.

Appendix F:
Microprobe analyses of monazite, for geochronology

Appendix F. Electron microprobe analyses of monazite.

Table F1. Monazite trace element analyses from monazite grain included in

Sample point	1B mon pt 1	1B mon pt 2	1B mon pt 3	1B mon pt 4	1B mon pt 5	1B mon pt 6	1B mon pt 7	1B mon pt 8
Remarks								
Y	0.8155	0.824	0.7256	0.7825	0.2378	0.2506	1.1473	1.0473
Th	2.237	1.7653	2.0838	1.8994	3.3587	3.3624	2.7346	3.1432
U	0.4432	0.2217	0.1873	0.24	0.541	0.555	0.664	0.658
Pb	0.3157	0.2265	0.2372	0.2346	0.3899	0.4026	0.3981	0.4141
P	13	13	13	13	13	13	13	13
La	11.37	11.37	11.37	11.37	11.37	11.37	11.37	11.37
Ce	26.58	26.58	26.58	26.58	26.58	26.58	26.58	26.58
Nd	11.48	11.48	11.48	11.48	11.48	11.48	11.48	11.48
Sm	1.85	1.85	1.85	1.85	1.85	1.85	1.85	1.85
O	26.91	26.91	26.91	26.91	26.91	26.91	26.91	26.91
Pr	3.02	3.02	3.02	3.02	3.02	3.02	3.02	3.02
Ca	0.41	0.41	0.41	0.41	0.41	0.41	0.41	0.41
Gd	1.21	1.21	1.21	1.21	1.21	1.21	1.21	1.21
Si	0.11	0.11	0.11	0.11	0.11	0.11	0.11	0.11
Dy	0.16	0.16	0.16	0.16	0.16	0.16	0.16	0.16
Total	99.9114	99.1376	99.3339	99.2566	100.6273	100.6705	101.0439	101.3625
Y	0.3623	0.3666	0.3228	0.3481	0.1057	0.1114	0.5083	0.4639
Th	0.3808	0.3009	0.3552	0.3237	0.572	0.5726	0.4642	0.5334
U	0.0736	0.0368	0.0311	0.0399	0.0898	0.0921	0.1099	0.1089
Pb	0.0602	0.0432	0.0453	0.0448	0.0744	0.0768	0.0757	0.0787
P	16.5813	16.6029	16.6018	16.6014	16.5872	16.5853	16.5343	16.5298
La	3.2333	3.2375	3.2373	3.2372	3.2344	3.2341	3.2241	3.2232
Ce	7.4933	7.503	7.5025	7.5024	7.4959	7.4951	7.472	7.47
Nd	3.1439	3.148	3.1478	3.1477	3.145	3.1447	3.135	3.1342
Sm	0.4861	0.4867	0.4867	0.4866	0.4862	0.4862	0.4847	0.4845
O	66.437	66.5237	66.5192	66.5177	66.4605	66.4532	66.2486	66.2306
Pr	0.8466	0.8477	0.8477	0.8476	0.8469	0.8468	0.8442	0.844
Ca	0.4041	0.4046	0.4046	0.4046	0.4042	0.4042	0.4029	0.4028
Gd	0.304	0.3044	0.3043	0.3043	0.3041	0.304	0.3031	0.303
Si	0.1547	0.1549	0.1549	0.1549	0.1547	0.1547	0.1542	0.1542
Dy	0.0389	0.0389	0.0389	0.0389	0.0389	0.0389	0.0388	0.0388
Total	100	99.9999	100.0001	99.9999	100	100.0001	100	100
Y(ppm)	8155	8240	7256	7825	2378	2506	11473	10473
Th(ppm)	22370	17653	20838	18994	33587	33624	27346	31432
U(ppm)	4432	2217	1873	2400	5410	5550	6640	6580
Pb(ppm)	3157	2265	2372	2346	3899	4026	3981	4141

Appendix F. Electron microprobe analyses of monazite.

Table F2. Monazite trace element analyses from monazite grain included in garnet MZ-1A-0.3

Sample point	1A mon pt 1	1A mon pt 2	1A mon pt 3	1A mon pt 4	1A mon pt 5	1A mon pt 6	1A mon pt 7
Remarks							
Y	0	0.2	0.6694	0	0	0.8762	0.3984
Th	4.1211	3.5066	3.5547	3.9858	3.7497	3.1853	3.4021
U	0.1487	0.6826	0.8222	0.1608	0.1594	0.5747	0.7941
Pb	0.3069	0.3989	0.4325	0.3146	0.2997	0.3703	0.4237
P	13	13	13	13	13	13	13
La	11.37	11.37	11.37	11.37	11.37	11.37	11.37
Ce	26.58	26.58	26.58	26.58	26.58	26.58	26.58
Nd	11.48	11.48	11.48	11.48	11.48	11.48	11.48
Sm	1.85	1.85	1.85	1.85	1.85	1.85	1.85
O	26.91	26.91	26.91	26.91	26.91	26.91	26.91
Pr	3.02	3.02	3.02	3.02	3.02	3.02	3.02
Ca	0.41	0.41	0.41	0.41	0.41	0.41	0.41
Gd	1.21	1.21	1.21	1.21	1.21	1.21	1.21
Si	0.11	0.11	0.11	0.11	0.11	0.11	0.11
Dy	0.16	0.16	0.16	0.16	0.16	0.16	0.16
Total	100.6766	100.888	101.5787	100.5611	100.3087	101.1064	101.1182
Y	0	0.0889	0.2967	0	0	0.3884	0.1769
Th	0.7022	0.597	0.6037	0.6793	0.6393	0.5411	0.5786
U	0.0247	0.1133	0.1361	0.0267	0.0265	0.0952	0.1317
Pb	0.0586	0.0761	0.0823	0.06	0.0572	0.0704	0.0807
P	16.5966	16.5816	16.5409	16.5998	16.607	16.5448	16.5661
La	3.2363	3.2333	3.2254	3.2369	3.2383	3.2262	3.2303
Ce	7.5002	7.4934	7.475	7.5016	7.5049	7.4768	7.4864
Nd	3.1468	3.144	3.1363	3.1474	3.1488	3.137	3.141
Sm	0.4865	0.4861	0.4849	0.4866	0.4868	0.485	0.4856
O	66.4983	66.4382	66.275	66.5113	66.5402	66.2908	66.3761
Pr	0.8474	0.8466	0.8445	0.8476	0.8479	0.8447	0.8458
Ca	0.4045	0.4041	0.4031	0.4045	0.4047	0.4032	0.4037
Gd	0.3042	0.304	0.3032	0.3043	0.3044	0.3033	0.3037
Si	0.1548	0.1547	0.1543	0.1549	0.1549	0.1543	0.1545
Dy	0.0389	0.0389	0.0388	0.0389	0.039	0.0388	0.0389
Total	100	100.0002	100.0001	99.9999	100	100	100
Y(ppm)	0	2000	6694	0	0	8762	3984
Th(ppm)	41211	35066	35547	39858	37497	31853	34021
U(ppm)	1487	6826	8222	1608	1594	5747	7941
Pb(ppm)	3069	3989	4325	3146	2997	3703	4237

Appendix G:
Sample calculation, monazite geochronology

Appendix G:

Sample monazite calculation, using data from Monaz 1B, point 1
(equation from Montel et al, 1996).

Eqn

$$\mathrm{Pb} = \frac{\mathrm{Th}}{232}\left[e^{(\lambda 232 * t)}-1\right]\ 208 + \frac{\mathrm{U}*0.9928}{238.04}\left[e^{(\lambda 238 * t)}-1\right]\ 206 + \frac{\mathrm{U}*0.0072}{235}\left[e^{(\lambda 235 * t)}-1\right]\ 207$$

$\lambda^{232} =$ 4.95E-11
$\lambda^{238} =$ 1.55E-10
$\lambda^{235} =$ 9.85E-10

Pb(ppm)	U (ppm)	Th (ppm)	^{238}U (ppm)	^{235}U (ppm)
3157	4432	22370	4400	32

208*(Th/232)	206*(^{238}U/238)	207*(^{235}U/235)
20056	3808	28.11

t (Ma)	Th term	^{238}U term	^{235}U term	Pb(ppm)	Pb(calc) ↓ Total	Notes
1000	1018	639	47	3157	1703	too low
2000	2087	1384	173		3645	too high
1500	1546	997	95		2638	too low
1750	1815	1187	129		3131	too low
1800	1869	1226	137		3232	too high
1775	1842	1206	133		3181	too high
1760	1826	1194	131		3151	too low
1765	1831	1198	132		3161	too high
1762	1828	1196	131		3155	too low
1763	1829	1197	131	3157	3157	Age

Measured quantities are given in grey shaded boxes. Age is determined iteratively, by inputting ages, and using trial and error to close in on the proper age, making **Total** [=**Pb(calc)**] equal to **Pb(ppm)** (the measured amount of Pb in sample).

Appendix H:

Fluid inclusion photomicrographs

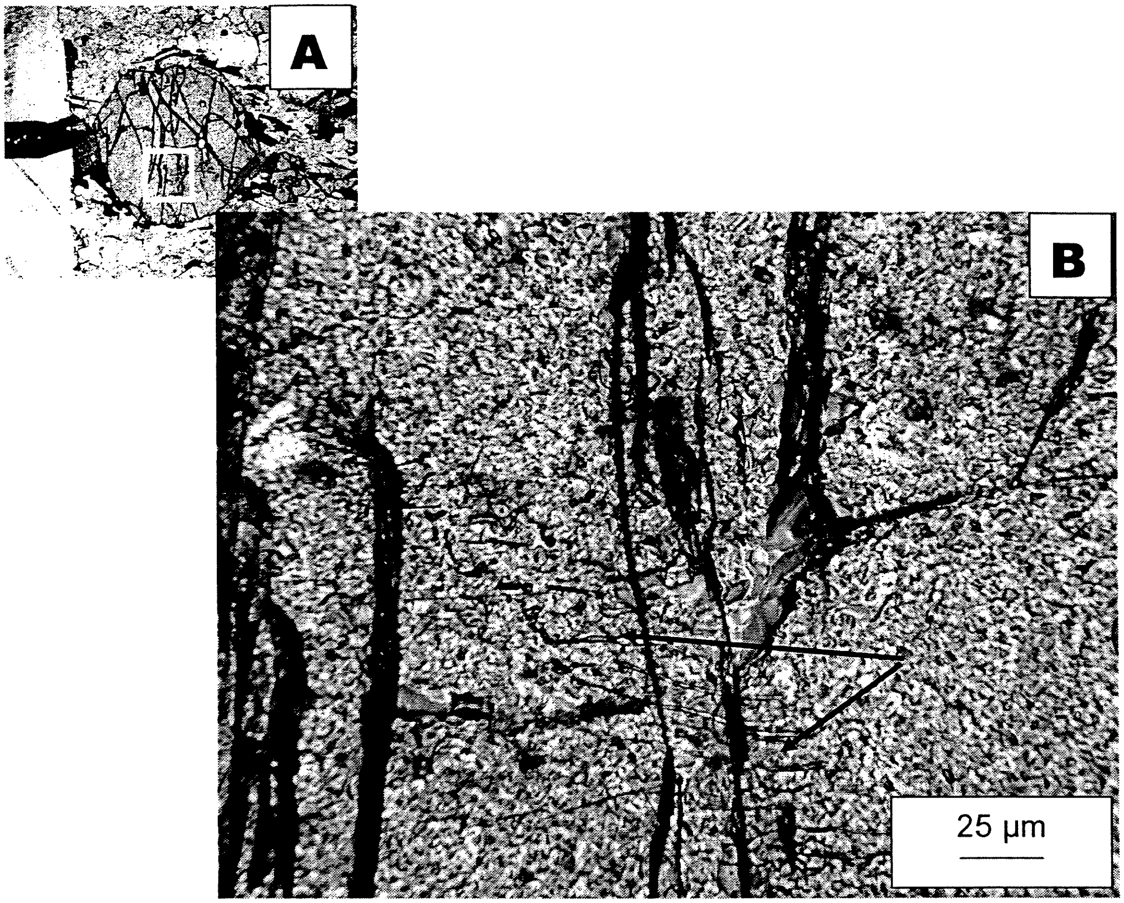

Figure H1. GSI-b type inclusions from sample MZ-1A. The host garnet crystal is shown (A), and is 2 mm across. The black mark to the left of the host garnet crystal is an ink mark used to relocate the grain; the white box indicates the area shown in (B). (B) Two-phase GSI-b inclusions in MZ-1A (indicated with arrows).

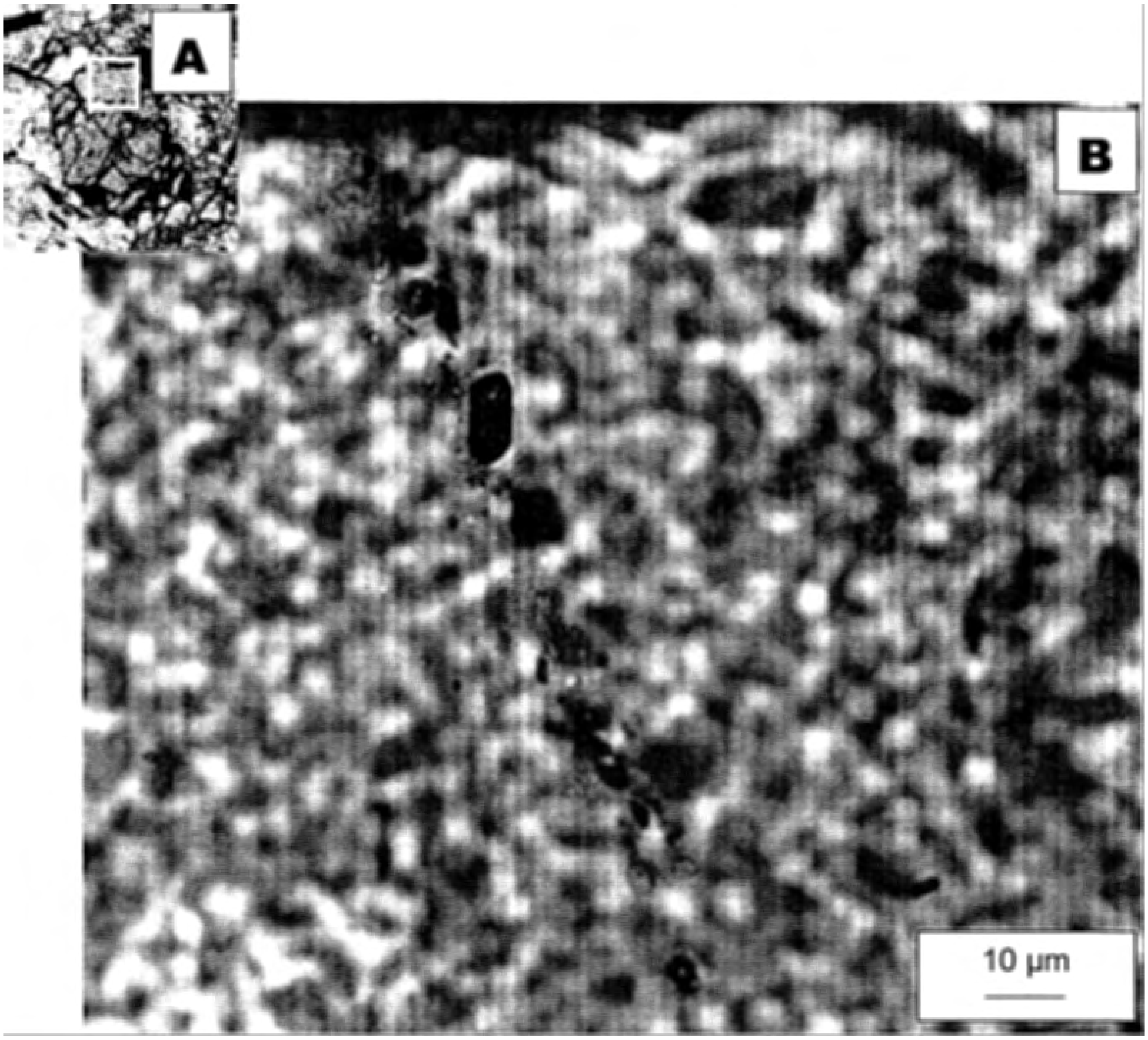

Figure H2. GSI-a type inclusions in MZ-1A. The host garnet crystal is shown in (A) and is 0.7mm across. The white box indicates the area shown in (B). (B) Monophase GSI-a inclusions in MZ-1A.

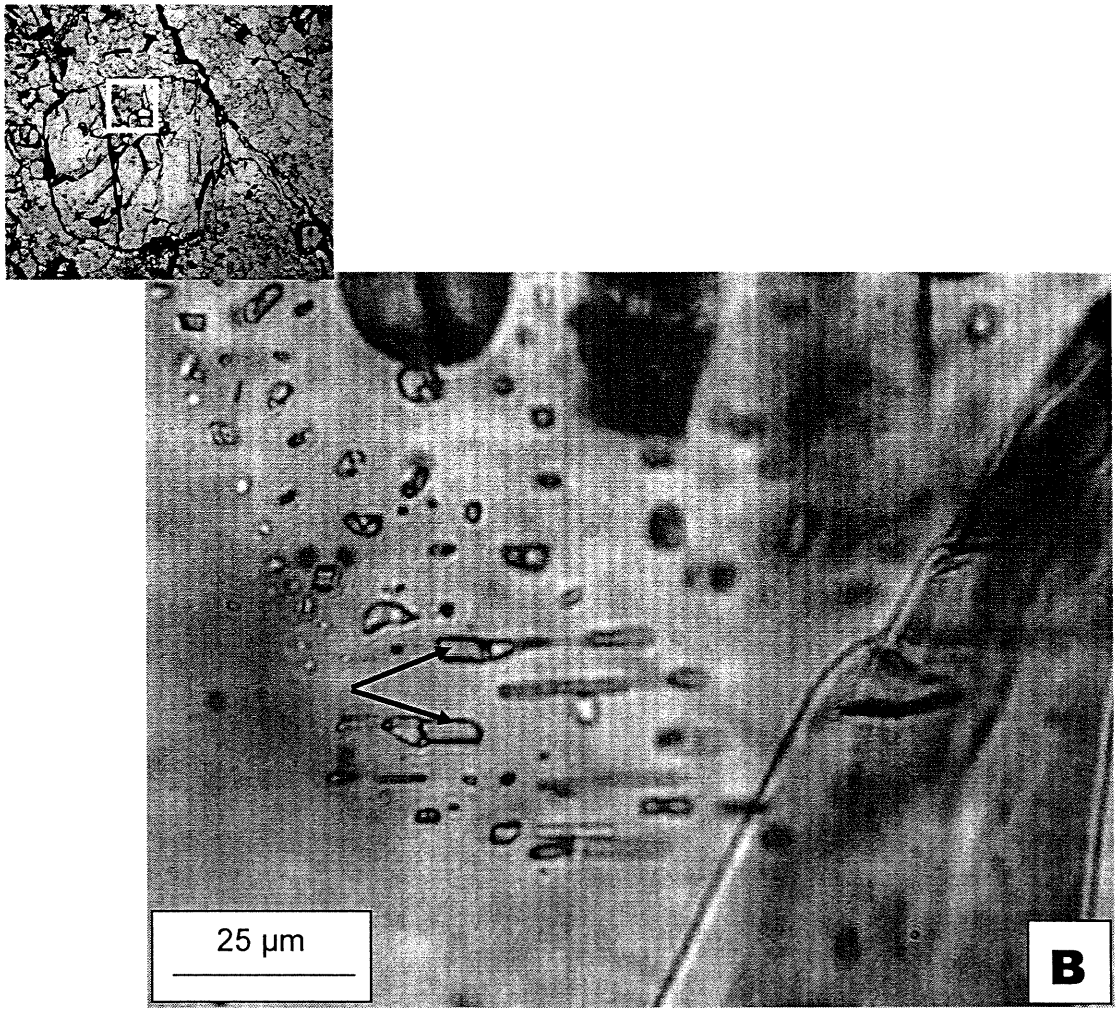

Figure H3. GSI-b inclusions from MZ-1B. The host garnet crystal is shown in (A), and is ~2 mm across. The white box indicates the area show in (B). (B) Two phase GSI-b inclusions in MZ-1B; ubiquitous solid phases included with fluid inclusions are indicated with arrows.

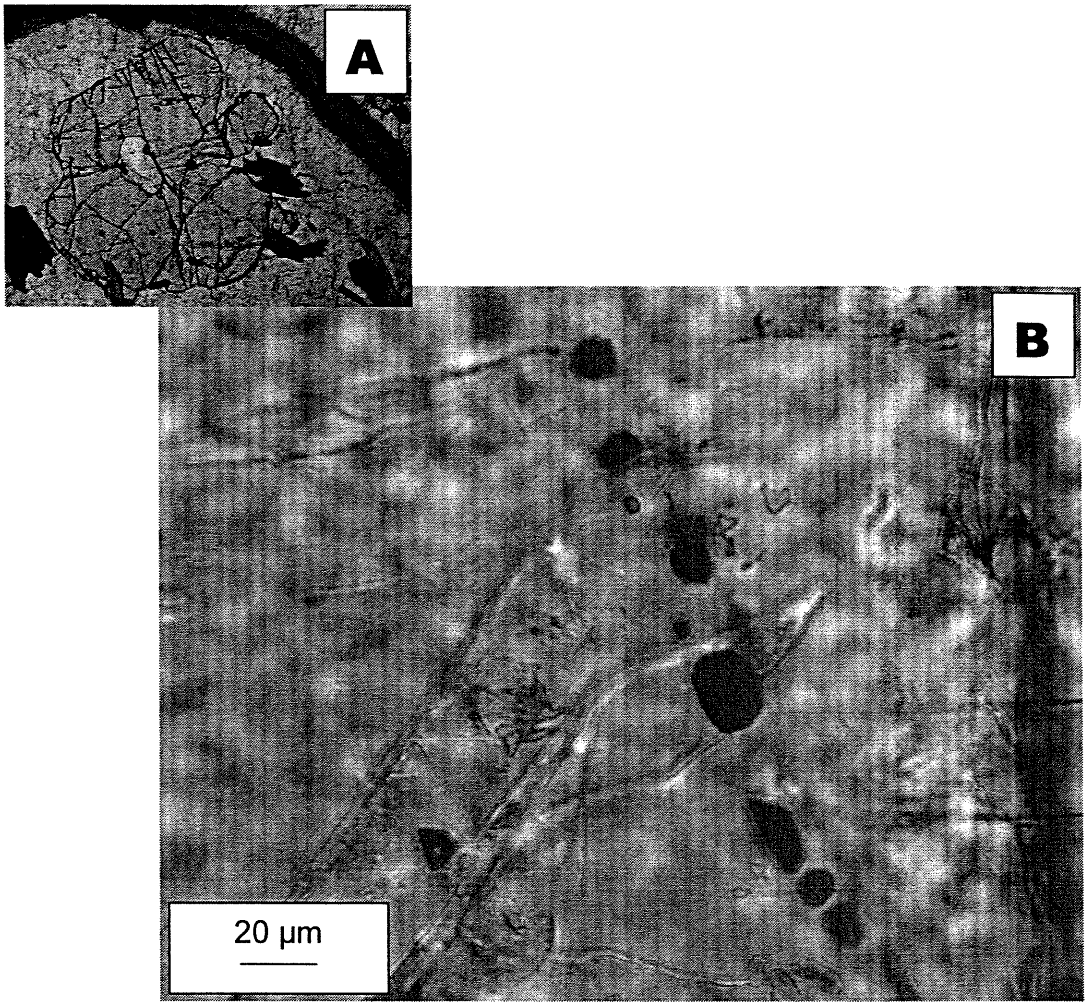

Figure H4. GSI-a type inclusions in MZ-2A. The host garnet crystal is shown in (A), and is ~2 mm across. The black band above the garnet grain is an ink mark used to relocate the grain. The white box indicates the area shown in (B). (B) Monophase GSI-a inclusions in MZ-2A.

References:

Bakker, R.J., Diamond, L.W., 2000. Determination of the composition and molar volume of H2O-CO2 fluid inclusions by microthermometry. *Geochimica et Cosmochimica Acta*, **64**, 1753-1764.

Berman, R.G., Aranovich, L.Y., 1996. Optimized standard state and solution properties of minerals: I. Model calibration for olivine, orthopyroxene, cordierite, garnet, and ilmenite in the system $FeO\text{-}MgO\text{-}CaO\text{-}Al_2O_3\text{-}TiO_2\text{-}SiO_2$. *Contributions to Mineralogy and Petrology*, **126**, 1-24.

Carr, S.D., Easton, R.M., Jamieson, R.A., Culshaw, N.G., 2000. Geologic transect across the Grenville orogen of Ontario and New York. *Canadian Journal of Earth Sciences*, **37**, 193-216.

Cliff, R.A., 1985. Isotopic dating in metamorphic belts. *Journal of the Geological Society of London*, **142**, 97-110.

Culshaw, N.G., Davidson, A., Nadeau, L., 1983. Structural subdivisions of the Grenville Province in the Parry Sound – Algonquin region, Ontario. *In: Current Research, Part B, Geological Survey of Canada, Paper* **83-1B**, 243-252.

Culshaw, N.G., Jamieson, R.A., Corrigan, D., Ketchum, J.W.F., Reynolds, P.H., Wodicka, N., Heaman, L., Krogh, T.E., 1990. History of the Central Gneiss Belt, Grenville Province, along Georgian Bay, Ontario. *Lithoprobe Abitibi-Grenville Project, Workshop Report* **3**, 73-76.

Culshaw, N.G., Ketchum, J.W.F., Wodicka, N., Wallace, P., 1994. Deep crustal ductile extension following thrusting in the southwestern Grenville Province, Ontario. *Canadian Journal of Earth Sciences*, **31**, 160-175.

Culshaw, N.G., Jamieson, R.A., Ketchum, J.W.F., Wodicka, N., Corrigan, D., Reynolds, P.H., 1997. Transect across the northwestern Grenville orogen, Georgian Bay, Ontario: polystage convergence and extension in the lower orogenic crust. *Tectonics*, **16**, 966-982.

Davidson, A., 1984. Tectonic boundaries within the Grenville Province of the Canadian Shield. *J. Geodynamics*, **1**, 433-444.

Davidson, A., Easton, R.M., 1998. From front to interior: an Ontario transect of the Grenville Province, Sudbury to the St. Lawrence. *GSA Annual Meeting, Toronto, Canada, 1998, Field Trip Guide Number 1.* Geological Society of America.

De Maesschalck, A. A., Touret, J.L.R., Maaskant, P., Dahanayake, K., 1991. Petrology and fluid inclusions in garnetiferous gneisses and charnokites from Weddagala (Ratnapura District, Sri Lanka). *Journal of Geology*, **99**, 443-456.

Diamond, L.W., 2001. Review of the systematics of CO2-H2O fluid inclusions. *Lithos*, **55**, 69-99.

Dodson, M.A., 1973. Closure temperature in cooling geochronological and petrological systems. *Contributions to Mineralogy and Petrology*, **40**, 259-274.

Easton, R.M., 1992. The Grenville Province and the Proterozoic history of central and southern Ontario. *Geology of Ontario*, edited by P.C. Thurston, H.R. Williams, R.H. Sutcliffe, G.M Stott. Ontario Geological Survey Special Volume 4, part **2**, 715-904.

Faul, H., 1966. *Nuclear clocks. Understanding the Atom*, United States Atomic Energy Commission, Division of Technical Information, Tennessee, USA.

Ferry, J.M., Spear, F.S., 1978. Experimental calibration of the partitioning of Fe and Mg between biotite and garnet. *Contributions to Mineralogy and Petrology*, **66**, 113-117.

Fowler, C.M.R., 1990. *The Solid Earth: an introduction to global geophysics.* Cambrigde University Press, Cambridge, England.

Ghent, E.D., 1976. Plagioclase-garnet-Al2SiO5-quartz; a potential geobarometer-geothermometer. *American Mineralogist*, **61**, 710-714.

Goldstein, R.H., Reynolds, T.J., 1994. *Systematics of fluid inclusions in diagenetic minerals. SEPM Short Course 31.* SEPM (Society for sedimentary geology), USA.

Kontak, D.J., 1998. A study of fluid inclusions in sulfde and nonsulfide mineral phases from a carbonate-hosted Zn-Pb deposit, Gays River, Nova Scotia, Canda. *Economic Geology*, **93**, 793-817.

Montel, J.-M., Foret, S., Veschambre, M., Nicollet, C., Provost, A., 1996. Electron microprobe dating of monazite. *Chemical Geology*, **131**, 37-53.

Nadeau, L., 1990. Tectonic, thermal, and magmatic evolution of the Central Gneiss Belt, Huntsville region, southwestern Grenville orogen. Unpublished Ph.D. thesis, Carleton University, Ottawa, Ontario.

Pan Y., Fleet, M.E., Longstaffe, F.J., 1999. Melt-related metasomatism in mafic granulites of the Quetico subprovince, Ontario: constraints from O-Sr-Nd isotopic and fluid inclusion data. *Canadian Journal of Earth Sciences*, **36**, 1449-1462.

Parrish, R.R., 1990. U-Pb dating of monazite and its application to geological problems. *Canadian Journal of Earth Sciences*, **27**, 1431-1450.

Rivers, T., Martignole, J., Gower, C.F., Davidson, A., 1989. New tectonic divisions of the Grenville Province, southeast Canadian Shield. *Tectonics*, **8**, 63-84.

Roeder, E., 1984. *Fluid Inclusions. Reviews in Mineralogy*, Vol. 12, Mineralogical Society of America.

Slagstad, T., 2003. Muskoka and Shawanaga domains, Central Gneiss Belt, Grenville Province, Ontario: Geochemical and geochronological constraints on pre-Grenvillian and Grenvillian geological evolution. *PhD. Thesis*, Dalhousie University, Halifax, Nova Scotia.

Spear, F.S., 1993. *Metamorphic Phase Equilibria and Pressure-Temperature-Time Paths*. Mineralogical Society of America Monograph, Mineralogical Society of America, Washinton D.C., USA.

Steiger, R.H., Wasserburg, G.J., 1966. Systematics in the ^{208}Pb-^{232}Th, ^{207}Pb-^{235}U, and ^{206}Pb-^{238}U systems. *Journal of Geophysical Research*, **71**, 6065-6090.

Timmermann, H., 1998. Geology, metamorphism, and U-Pb geochronology in the Central Gneiss Belt between Huntsville and Haliburton, southwestern Grenville Province, Ontario. *PhD. Thesis*, Dalhousie University, Halifax, Nova Scotia.

Timmermann, H., Jamieson, R.A., Parrish, R.R., Culshaw, N.G., 2002. Coeval migmatites and granulites, Muskoka domain, southwestern Grenville Province, Ontario. *Canadian Journal of Earth Sciences*, **39**, 239-258.

Touret, J.L.R., 2001. Fluids in metamorphic rocks. *Lithos*, **55**, 1-25.

Van Breemen, O., Hanmer, S., 1986. Zircon morphology and U-Pb geochronology in active shear zones: studies on syntectonic intrusions along the NW boundary of the Central Metasedimentary Belt, Grenville Province, Ontario. *Current Research, Geological Survey of Canada*, **Paper 86-1B**, 775-784.

Van der Berg, R., Huizenga, J.M., 2001. Fluids in granulites of the Southern Marginal Zone of the Limpopo Belt, South Africa. *Contributions to Mineralogy and Petrology*, **141**, 529-545.

White, D.J., Forsyth, D.A., Asudeh, I., Carr, S.D., Whu, H., Easton, R.M., Mereu, R.F., 2000. A seismic-based cross-section of the Grenville Orogen in sourthern Ontario and western Quebec. *Canadian Journal of Earth Sciences*, **37**, 183-192.

Williams, M.L., Jercinovic, M.J., 2002. Microprobe monazite geochronology: putting absolute time into microstructural analysis. *Journal of Structural Geology*, **24**, 1013-1028.

Windley, B.F., 1986. Comparative tectonics of the western Grenville and the western Himilayas. *The Grenville Province*, edited by J.M. Moore, A. Davidson, A.J. Baer. Geological Association of Canada, Special Paper **31**, 341-348.

Winter, J.D., 2001. *An introduction to igneous and metamorphic petrology.* Prentice-Hall, New Jersey, USA.

Wodicka, N., Ketchum, J.W.F., Jamieson, R.A., 2000. Grenvillian metamorphism of monocyclic rocks, Georgian Bay, Ontario, Canada: implications for convergence history. *The Canadian Mineralogist*, **38**, 471-510.

Wynne-Edwards, H.R., 1972. The Grenville Province. *Variations in Tectonic Styles in Canada*, edited by R.A. Price, R.J.W. Douglas. Geological Association of Canada, Special Paper **11**, 263-334.